

Immunomodulatory Effects of Intracranial Gene Therapy in Feline Sandhoff Disease

by

Allison Marie Bradbury

A dissertation submitted to the Graduate Faculty of
Auburn University
in partial fulfillment of the
requirements for the Degree of
Doctor of Philosophy

Auburn, Alabama
May 6, 2014

Keywords: Sandhoff disease, neurodegenerative disease, AAV gene therapy, immune response, neuroinflammation, biomarkers of disease

Copyright 2014 by Allison Marie Bradbury

Approved by

Douglas R. Martin, Chair, Associate Professor of Anatomy, Physiology, and Pharmacology
Elaine S. Coleman, Professor of Anatomy, Physiology, and Pharmacology
Nancy R. Cox, Professor of Pathobiology
Frederick W. van Ginkel, Associate Professor of Pathobiology
Bruce F. Smith, Professor of Pathobiology

ABSTRACT

Sandhoff disease (SD) is a lysosomal storage disorder characterized by absence of hydrolytic enzyme β -N-acetylhexosaminidase (Hex), which results in storage of GM2 ganglioside in neurons and unremitting neurodegeneration. Neuronal loss initially affects fine motor skills, but rapidly progresses to a vegetative state and death by the age of five in humans. A well-established feline model of SD has allowed disease characterization in a large animal model and provided necessary means to test safety and efficacy of therapeutic interventions before initiating human clinical trials.

When treated with intracranial adeno-associated viral (AAV) gene delivery of human Hex, two SD cats lived to 7.0 and 8.2 months of age, compared to an untreated life span of 4.5 ± 0.5 months. Due to a pronounced humoral immune response to both the AAV vector and human Hex, a feline cDNA for Hex was cloned into AAVrh8 vectors. Cats treated with vectors expressing the species-specific transgene produced enzymatic activity >75 fold normal at injection site, a substantially mitigated humoral immune response, and lived to 10.4 ± 3.7 months, or 2.3 times longer than untreated cats.

High levels of circulating antibodies did not preclude successful transduction of AAV or sustained Hex expression. Furthermore, sera antibody titers did not correlate with lifespan and were not an indicator of clinical outcome. Decreasing the dose of treatment lowered sera antibody titers; however, clinical symptoms were not as effectively attenuated. Furthermore, directly targeting the ventricular system did not increase sera antibody titers compared to

injecting the brain parenchyma. After intracranial injection, AAVrh8 demonstrated a surprisingly strong tissue tropism for the liver, sciatic nerve, and quadriceps, likely explaining the pronounced humoral immune response.

Intracranial delivery of AAV vectors expressing feline Hex also attenuated neuroinflammation, characterized in untreated SD cats by marked expansion and activation of microglia, upregulation of major compatibility complex II, and increased expression of macrophage inflammatory protein-1. The therapy also demonstrated a peripheral effect by normalizing blood, CSF, MRI and electro-diagnostic biomarkers of disease progression. These studies support the therapeutic potential of AAV mediated gene therapy for SD and provide highly translatable data in support of initiation of human clinical trials.

ACKNOWLEDGMENTS

I would like to express my sincerest gratitude to my mentor, committee chair, advisor, and teacher, Dr. Douglas R. Martin. Thank you for taking a chance on me, having faith in me, and allowing me to grow into the researcher and scientist I have become.

I would also like to thank my graduate committee, Dr. Elaine S. Coleman, Dr. Nancy R. Cox, Dr. Frederick W. van Ginkel, and Dr. Bruce F. Smith for your dedication to my research project, guidance throughout my PhD program, and careful revision of my dissertation.

Without the foresight of Dr. Henry J. Baker over 30 years ago to initiate the GM2 gangliosidosis cat colony, this research would not be possible. Your dedication to the development and maintenance of this research program has positively influenced the careers of countless people, including my own. Your guidance and wisdom have had an immense impact on my life.

A heartfelt thank you to my husband, David Bradbury, for your sacrifices and support while I focused on my career, and to my parents, Pam and John Baker, and sister and brother-in-law, Lauren and Raul Pou, for your unconditional support throughout this journey.

This work would not have been possible without financial support from the National Institute of Health grant U01NS064096, the National Tay-Sachs and Allied Diseases Foundation, and the Jewish Community Endowment Fund. Lastly, my most profound thank you to the children and families afflicted with these devastating diseases. Your strength is admirable and I vow to continue fighting for a cure.

TABLE OF CONTENTS

Abstract.....	ii
Acknowledgments.....	iv
List of Tables.....	vi
List of Figures.....	viii
Literature Review.....	1
Chapter 1. Therapeutic Response in Feline Sandhoff Disease Despite Immunity to Intracranial Gene Therapy.....	38
Chapter 2. AAV Mediated Gene Delivery Attenuates Neuroinflammation Associated with Feline Sandhoff Disease.....	73
Chapter 3. Systemic Effects after Intracranial Delivery of AAV in Feline Sandhoff Disease....	102
Chapter 4. Biomarkers for disease progression and AAV therapeutic efficacy in feline Sandhoff Disease.....	136
Chapter 5. Summary.....	168
References.....	175

LIST OF TABLES

Literature Review

Table 1. Transduction efficiency of AAV serotypes	35
---	----

Chapter 1

Table 1. AAV-Treated Cats and Corresponding Serum Antibody Titers to the Vectors.....	58
---	----

Table 2. Fold Normal Specific Activity in Heterozygote and SD Cat Cerebrum Post-AAV.....	64
--	----

Table 3. Summary of Immune-related and Histological Findings.....	68
---	----

Supplementary Table S1. In vitro functionality of AAVrh8 vectors expressing feline HEXA or HEXB cDNAs	69
--	----

Supplementary Table S2. AAV Vectors for Treatment of SD and Normal Cats.....	70
--	----

Supplementary Table S3. Correlation of Hex Activity with Neurons Containing Eosinophilic, Botryoid Inclusions.....	71
---	----

Supplementary Table S4. Primers used in the current study.....	72
--	----

Chapter 2

Supplementary Table S1. Enzyme activity in brain draining lymph node	101
--	-----

Chapter 3

Table 1. Enzyme activity in peripheral tissues 16 weeks post AAV treatment	123
--	-----

Table 2. Vector copies in peripheral tissues 16 weeks post AAV treatment.	124
--	-----

Table 3. Enzyme activity in peripheral tissues after long-term AAV treatment.	127
--	-----

Table 4. Enzyme activity and vector copies in liver after 1/10 th dose of AAV treatment.....	130
---	-----

Table 5. Enzyme activity in peripheral tissues 16 weeks post AAV treatment.....	131
---	-----

Table 6. Enzyme activity in peripheral tissues after bilateral thalamic and ICV injections of AAVrh8-fHEX.....134

Table 7. Serum antibody titers to AAVrh8-nhpHEX in treated healthy non-human primates...135

LIST OF FIGURES

Literature Review

Figure 1. Pathology of GM2 gangliosidosis	31
Figure 2. Ganglioside degradation pathway	32
Figure 3. Structure and function of hexosaminidase subunits	33
Figure 4. Pathology of GM2 gangliosidosis in a feline model.....	34
Figure 5. Production of recombinant AAV.....	36
Figure 6. Innate and adaptive immune responses to AAV vectors.....	37

Chapter 1

Figure 1. Therapeutic benefit of human Hex expressed from an AAV1 vector in SD cats.....	59
Figure 2. Serum antibody titers to human HexA in AAV-treated cats.....	61
Figure 3. HexA activity after expression of feline Hex α and β subunits.....	62
Figure 4. Therapeutic benefit in SD cats after intra-thalamic injection of AAVrh8 vectors expressing feline Hex.....	65
Figure 5. Histological findings after AAV injection in the normal and SD cat brain.....	66

Chapter 2

Figure 1. Activation of microglia in feline Sandhoff disease.....	90
Figure 2. MHCII expression associated with microglia but not astrocytes.....	92
Figure 3. AAV therapy attenuates microglia activation.....	93
Figure 4. Upregulation of MHCII in untreated SD cat brains and normalization with AAV- mediated gene delivery	94

Figure 5. AAV-fHEX successfully transduces neurons.....	96
Figure 6. Upregulation of MIP-1 α expression in untreated SD cat brain and normalization with intracranial injection of AAV.....	98
Supplementary Figure 1. Isolated areas of microglia activation and expansion in AAV-treated SD cats.....	99

Chapter 3

Figure 1. Serum antibody titers to AAVrh8-fHEX in treated SD cats	122
Figure 2. Survival in SD cats after bilateral thalamic and bilateral DCN injections of AAVrh8-fHEX.....	125
Figure 3. Serum antibody titers to AAVrh8-fHEX in long-term treated SD cats	126
Figure 4. Survival in SD cats after 1/10 th dose injection of AAVrh8-fHEX.....	128
Figure 5. Serum antibody titers to AAVrh8-fHEX in 1/10 th dose treated SD cats.....	129
Figure 6. Survival in SD cats after bilateral thalamic and ICV injections of AAVrh8-fHEX...	132
Figure 7. Serum antibody titers to AAVrh8-fHEX in treated SD cats.....	133

Chapter 4

Figure 1. Blood chemistry findings in normal, untreated SD, and SD cats 16 weeks after AAV gene therapy.....	158
Figure 2. CSF based biomarkers in normal, untreated SD, and SD cats 16 weeks after AAV gene therapy	160
Figure 3. LysoTracker quantification in peripheral blood mononuclear cells in SD and normal age-matched control cats	161
Figure 4. Echinocyte formation in normal, untreated SD cats, and AAV-treated SD cats.....	163
Figure 5. Brain and peripheral tissue enzyme activity in normal, untreated SD, and AAV-treated SD cats.....	164
Figure 6. MRI signal intensity in normal, untreated SD, and AAV-treated SD cats.....	165
Figure 7. Brainstem Auditory Evoked Responses in SD cats.....	167

LITERATURE REVIEW

1.1 GM2 Gangliosidosis

Lysosomal storage disorders (LSDs) encompass over forty individual diseases that result from defective hydrolysis of macromolecules and their subsequent accumulation within lysosomes. All LSDs are an effect of a single gene defect, and the vast majority are inherited in an autosomal recessive fashion. A retrospective case study conducted in Australia during the period of 1980-1996 found the combined prevalence of all LSDs to be 1 in 7700 live births (*1*). However, this report cautioned that the rate of LSDs was steadily increasing as biochemical and genetic characterization of these diseases continued to advance. Therefore, it is likely that the prevalence to date is higher than calculated 18 years ago. The first description of a LSD was in 1881 by ophthalmologist Warren Tay and was further depicted in 1887 by neurologist Bernard Sachs, defining the now well-known and characterized Tay-Sachs disease. Tay-Sachs along with Sandhoff disease comprise a category of LSDs known as monosialoganglioside 2 (GM2) gangliosidoses, which result from a deficiency of the hydrolytic lysosomal enzyme β -N-acetylhexosaminidase (Hex). Defective Hex fails to cleave the target substrate, GM2 ganglioside, which then accumulates in neurons throughout the central nervous system (CNS) leading to progressive and fatal neurodegeneration. The prevalence of Tay-Sachs disease is reported to be 1 in 222,000 and Sandhoff disease to be 1 in 422,000 live births with carrier frequencies at 1 in 224 and 1 in 310 respectively (*1*). Despite being characterized over 130 years ago, to date there remain no viable treatment options for these fatal diseases.

1.1.1 Clinical manifestations of GM2 gangliosidosis

Three forms of GM2 gangliosidosis are defined based on age of onset and subsequently disease severity: (1) infantile (classical) (2) juvenile and (3) adult-onset, with the latter two having a more heterogeneous disease progression. Infantile GM2 has a mean age at onset of 5.0 ± 3.3 months, age at diagnosis of 13.3 ± 5.3 months, and life span of 47 months. The most frequent initial symptoms reported are developmental arrest (83%), abnormal startle response (65%), and low muscle tone (60%), which progress to seizures (98%), blindness (68%), and ultimately a vegetative state (2). Despite the early onset of symptoms, GM2 gangliosidosis is not typically diagnosed until after a year of age (13.3 ± 5.3 months). In the majority of patients, discovery of a cherry red spot upon ophthalmic exam prompted the appropriate genetic testing. The cherry red macular spot is resultant of lipid storage in neuronal cells of the eye. Due to storage, the cells that normally cover the fovea centralis instead reveal the color of the choroidea behind the retina (Fig. 1A, (3)). To date this ophthalmic exam is the most common diagnostic tool, initiating further genetic testing in 67% of patients (2).

1.1.2 Pathology of GM2 gangliosidosis

Signs of neurodegeneration are visible upon gross examination of the brain at the time of autopsy. Namely, the ventricles are enlarged in accordance with macrocephaly and the gyri become broad and the sulci shortened due to cortical atrophy (Fig. 1B, (4)). Upon histological examination, the most apparent sign of pathology associated with GM2 gangliosidosis is the presence of swollen, edematous neurons. Neurons laden with storage of glycosphingolipid become enlarged, attributable to cytoplasmic distention by accumulation of foamy, vacuolated material. This material often displaces neuronal nuclei peripherally and obscures visualization of Nissl substance (Fig. 1C, (4)). Ultrastructure examination reveals the presence of electron-dense

lamellated material known as membranous cytoplasmic bodies (Fig. 1D, (4)) as well as transversely-stacked myelinoid membranes known as zebra bodies (not shown). Loss of neurons due to apoptosis, astrogliosis, and microgliosis are also notable on histological exam at end stage of disease. Many pathological signs of aberrant storage are also detectable in visceral organs, including the liver, heart, spleen, and skeletal system.

1.1.3 Biochemistry of ganglioside catabolism in gangliosidoses

Gangliosides were first described by German scientist Ernst Klenk in the 1930's when he isolated new lipids that had accumulated in brain tissue of patients suffering from "amaurotic idiocy", now known to be GM2 gangliosidosis (5). Gangliosides are glycosphingolipids (GSLs) that contain one or more sialic acid residue on a sugar chain. These GSLs comprise a significant part of cell surface and are oriented with a hydrophobic ceramide anchored in the lipid bilayer and hydrophilic carbohydrate including a sialic acid on the outer membrane surface. Degradation of gangliosides occurs in a stepwise manner, with each of the six catabolic steps removing a successive terminal residue (Fig. 2, (6)). Each step requires the coordinated effort of hydrolytic enzymes and activator proteins in the requisite acidic environment of the lysosome. Portions of the plasma membrane are endocytosed into vesicles that fuse with early endosomes, which mature to late endosomes. Late endosomes fuse with lysosomes, which house the hydrolytic enzymes, sphingolipid activator proteins, and have the obligatory pH of 4.8 at which the enzymes can function. The first ganglioside in the degradation pathway is GM1, with the "G" standing for ganglioside and "M" for monosialic. Hydrolytic enzyme β -galactosidase cleaves the terminal galactose residue from GM1 ganglioside and creates GM2, the next ganglioside in the pathway. Inherited defects in β -galactosidase cause lysosomal storage of GM1 ganglioside and

resultant neurodegenerative disease coined GM1 gangliosidosis. Hydrolysis of GM2 ganglioside is facilitated by β -N-acetylhexosaminidase, which functions to cleave the terminal N-acetylgalactosamine residue from GM2 to create GM3. Insufficient levels of β -N-acetylhexosaminidase result in accumulation of GM2 ganglioside within the lysosome and consequence in GM2 gangliosidosis.

The deficient enzyme, β -N-acetylhexosaminidase (Hex, EC 3.1.2.52), is comprised of two subunits, α and β , which dimerize to form three distinct isozymes with different physiological functions (Fig. 3, (7)). HexA is comprised of an α/β subunit heterodimer, HexB is a β/β homodimer, and a α/α homodimer leads to an unstable isozyme, Hex S, with no known physiological function. HexA cleaves charged substrates and is the isozyme responsible the hydrolytic cleavage of GM2 ganglioside. HexB cleaves neutral substrates and thus is not directly responsible for ganglioside cleavage (8). The action of HexA is also dependent on a non-hydrolytic protein known as GM2 Activator Protein (GM2AP). GM2AP is a small, 20kDa, glycolipid binding protein which functions to form water-soluble complexes with ganglioside GM2 and presents the lipid substrate to the water soluble HexA (9, 10). At an acidic pH, GM2AP contains two exposed hydrophobic loops that are capable of interacting with the membrane and extracting the ganglioside molecule (11). A HexA binding helix of the GM2AP facilitates the establishment of the Michaelis-Menten complex allowing for the degradation of GM2 ganglioside (12).

The α and β subunits and GM2AP are encoded by three different genes, *HEXA*, *HEXB*, and *GM2AP* respectively. A mutation in the *HEXA* gene (the α subunit) leads to a deficiency of HexA (α/β) and results in Tay-Sachs disease. A mutation in the *HEXB* gene (the β subunit) leads to a deficiency in both HexA (α/β) and HexB (β/β) since they both have β subunit involvement

and results in Sandhoff disease. Because HexB cleaves neutral substrates including oligosaccharides, HexB deficiency results in secondary oligosacchariduria, which in turn leads to visceral involvement. Absent in Tay-Sachs disease due to a functional HexB, many Sandhoff patients will experience visceromegaly and involvement of the skeletal and cardiac systems (13, 14). Similar to HexA deficiency, loss of GM2AP results in accumulation of GM2 ganglioside due to loss of transport of the glycolipid to the functionally active enzyme. The location and magnitude of the mutation within the gene determines the amount of residual enzyme activity, which in turn governs disease onset and severity. Individuals with mutations resulting in residual HexA activity as low as 10% of normal have remained asymptomatic (15). Therefore, therapeutically it is not necessary to fully restore HexA activity to normal levels to ameliorate clinical symptoms, but it will likely be critical to reach the 10% of normal activity threshold. Because different genes encode the α and β subunits, these diseases hold an additional challenge of concomitantly restoring the function of two gene products.

1.1.4 Treatment of human GM2 gangliosidosis

To date there are limited treatment options for patients with GM2 gangliosidosis. Peripheral delivery of the native enzyme, known as enzyme replacement therapy, is effective for lysosomal diseases without neurologic involvement, such as Gaucher's disease. The Food and Drug Administration (FDA) approved intravenous delivery of recombinant glucocerebrosidase for clinical use in the treatment of Gaucher's disease in 2010. However, the inability of Hex to cross the blood brain barrier renders this treatment option ineffective for GM2 gangliosidosis, which affects primarily the CNS.

1.1.4.1 Stem cell transplantation

In an attempt to provide a peripheral source of cells containing Hex, five patients with GM2 gangliosidosis (2 SD and 3 TSD patients) underwent hematopoietic stem cell transplantation. Combined, their average age of symptom onset was 3.8 ± 2.6 months, age at diagnosis 8.8 ± 5.0 months, and age at transplant 10.4 ± 5.8 months. After transplantation no milestones were gained and none of the recipients were able to sit without aid. All patients acquired classic clinical disease onset (previously described). At completion of the study, 4 of the 5 patients were deceased, one due to complications of the transplant and the remaining three from primary disease or disease related causes. The median life span of the 5 recipients was 64 months, which was not significantly different from the life span of untreated patients (47 months) (2). Due to the substantial risks and little apparent therapeutic benefit associated with hematopoietic stem cell transplantation, there is little justification for use of this treatment option.

1.1.4.2 Substrate reduction therapy

An alternative to the therapeutic approach of replacing the deficient enzyme is to reduce the synthesis of the substrate the enzyme is intended to degrade, known as substrate reduction therapy. *N*-butyldeoxynojirimycin (NB-DNJ) is an imino sugar that inhibits the enzyme glucosylceramide synthase, which is requisite for the synthesis of glycosphingolipids. Importantly, NB-DNJ is capable of crossing the blood brain barrier, and thus could reduce storage in the central nervous system (16). Substrate reduction therapy with NB-DNJ has been applied to other lysosomal storage diseases including Gaucher's disease (17, 18) and Niemann-Pick C disease (19). Substrate reduction with NB-DNJ was tested for therapeutic efficacy in two

infantile TSD patients. Despite significant concentration of the drug in the CSF and preclusion of macrocephaly, the therapy did not arrest clinical disease development (20). Two patients diagnosed with juvenile SD began treatment with NB-DNJ at 14 and 16 years of age and ≥ 2 years after initiation of therapy disease progression had slowed or even stabilized (21, 22). These results suggest that NB-DNJ may not be sufficient to halt substrate accumulation in the most aggressive forms of GM2 gangliosidosis associated with infantile onset; however, this simple compound may help stabilize symptoms associated with more mild disease presentation.

1.2 Animal models of GM2 gangliosidosis

1.2.1 Murine models of TSD and SD

Murine models of TSD and SD were created by targeted deletion of *HEXA* and *HEXB* genes, respectively. Surprisingly, disruption of the *HEXA* gene led to limited pathology and no signs of neurologic disease. In stark contrast, the *HEXB* knockout (*HEXB*^{-/-}) mouse model has progressive and profound neurologic disease and pathological findings that closely recapitulate human SD. Profound neuronal storage was noted throughout the CNS and some storage material was also observed in the liver and kidney. Membranous cytoplasmic bodies were also prominent within cells accumulating ganglioside storage (23). Similar to humans, *HEXB*^{-/-} mice appear healthy at birth; however, by 3 to 4 months of age animals present with spasticity, muscle weakness, rigidity, tremors, and ataxia and the disease is inevitably fatal within 6 weeks of the onset of symptoms (24). The disparity between human TSD and *HEXA* knockout (*HEXA*^{-/-}) mice has been explained by an alternative degradation pathway present in the mouse. In the absence of HexA, GM2 is converted to asialo-GM2 by murine sialidase, asialo-GM2 can in turn be further degraded to a ceramide by HexB. In contrast, human sialidase does not function to

catabolize GM2 and instead is reliant on degradation solely by HexA (23). Due to the subclinical manifestations of the HEXA^{-/-} mouse model, the HEXB^{-/-} mouse has been widely adapted as the murine model to study GM2 gangliosidosis.

1.2.2 Treatment of SD mouse

The establishment of an authentic animal model of human SD has allowed not only for detailed disease characterization but also an opportunity to test therapeutic interventions. Early experiments took a more generalized approach on introducing peripheral cells with functional Hex by bone marrow transplantation or neural stem cell transplantation. More targeted efforts focused on enzyme replacement therapy of recombinant Hex and substrate reduction therapy by impeding glycosphingolipid biosynthesis. Most recently, research has largely shifted towards the field of gene therapy, as development of a new generation of viral vectors has made this therapy safer and more effective.

1.2.2.1 Bone marrow transplantation

Bone marrow transplantation (BMT) in SD mice proved to significantly extend life span to 203-254 days, compared to humane endpoint of 101-139 days in untreated mice ($P < 0.0001$). Furthermore, SD mice had improved neurologic function after undergoing BMT. Hex was primarily detected in the spleen and liver, and was capable of reducing storage and correcting pathology in select peripheral organs. In contrast, the presence of Hex in the CNS was negligible and ganglioside storage was not reduced and pathology not prevented (25). Despite the inability to decrease GM2 ganglioside storage, BMT did decrease apoptosis and neuroinflammation (microgliosis) at 4 months of age (26). BMT failed to correct the primary source of the disease,

storage in the CNS, but did attenuate peripheral disease. This therapeutic approach is not sufficient in its own right; however, it may be beneficial in combination with targeted therapy of the CNS.

1.2.2.2 Stem cell transplantation

Mouse neural stem cells (mNSCs) implanted in the brain of newborn SD mice prolonged life up to 170 days and improved motor function. HexA activity was nearly 5% of wildtype levels in the cerebrum, and up to 28% of normal in the most densely engrafted regions and survival correlated with the level of enzyme restoration in the brain. Engrafted cells proved capable of cleaving GM2 ganglioside, as storage levels were 40% lower in transplanted mice than untreated mice and neuroinflammation was also reduced. Transplantation experiments were repeated with NSCs isolated from human origin and had comparable effects (27).

Substrate reduction therapy with imino sugars NB-DNJ or N-butyldeoxygalactonojirimycin (NB-DGJ) starting at 6 weeks of age in combination with mNSC transplant had a synergistic effect. Survival was prolonged as long as 215 days, the onset of symptoms was significantly delayed compared to mice that received mNSC transplant alone, and GM2 ganglioside storage was reduced by an additional 50%. Substrate reduction therapy alone had little benefit. The major limitation of this experiment was the differentiation pattern of the engrafted neural stem cells. Only 4% of engrafted mNSCs were found to differentiate into neurons, which is likely not enough of the population to correct the resident neurons (27). As realized with BMT, this data suggests that stem cell transplantation may best be applied in combination with other therapies.

1.2.2.3 Enzyme replacement with modified Hex

Matsuoka et al. created a genetically engineered *HEXB* encoding chimeric human beta subunit containing partial amino acid sequence of the alpha subunit so that it had catabolic activity towards GM2 and binding ability to GM2AP. The modified HexB was delivered by intracerebroventricular (ICV) injection to the lateral ventricle of 10-week old SD mice. One week after injection, Hex activity was 40% of normal levels but decreased to 15% of normal three weeks post injection, which remained greater than delivery of unmodified HexA. The modified Hex proved to have catabolic function, as three weeks after treatment notable reductions of GM2 ganglioside were observed in the thalamus and cerebral cortex, but to a lesser degree in the cerebellum. Storage in the liver was also significantly reduced three weeks after therapy, proving peripheral effects of the modified Hex after ICV injection. Longevity and neurologic behavior were not assessed in this study (28).

Recombinant human HexA was also modified with increased mannose 6-phosphate content in attempt to increase the amount of Hex binding to mannose 6-phosphate receptors. The modified HexA was administered by ICV injection to SD mice 12-13 weeks of age at 2 different doses. Hex activity was present in most brain regions; however, levels decreased to just 10% of normal activity by 1 week post-injection. The modified Hex proved functional; although, the ability of modified Hex to reduce ganglioside storage was dependent on the dose administered. SD mice treated with modified HexA showed significantly improved motor performance and lifespan was prolonged from 116 ± 3 days up to 131 ± 7 days, or a 12.9% increase (29).

1.2.2.4 Substrate reduction therapy

SD mice received substrate reduction therapy with NB-DNJ or NB-DGJ at two different doses starting at 6 weeks of age until they reached humane endpoint. The lower dose of NB-DNJ resulted in extension of lifespan from 124 ± 1 days to 161 ± 3 days, or a 30% increase above untreated, and 162 ± 2 day days or a 31% increase above untreated for NB-DGJ. The higher dose of NB-DNJ did not further increase survival and resulted in more severe weight loss. The higher dose of NB-DGJ did further increase survival to 185 ± 3 days, or a 49% increase above untreated and did not significantly affect weight loss. Motor behavior was improved after treatment, with the high dose group retaining skills for a longer duration. Mice treated with the low dose and sacrificed after 6 weeks of treatment showed a $10 \pm 5\%$ decrease in GM2 ganglioside with NB-DGJ and $6 \pm 2\%$ decrease after NB-DNJ treatment when compared to untreated SD mice. However, at humane endpoint mice treated with lower dose NB-DGJ showed a $26 \pm 0.8\%$ increase in GM2 ganglioside and the higher dose showed a $31 \pm 9\%$ increase compared to younger untreated controls. In the liver, at humane endpoint GM2 was decreased by $44 \pm 9\%$ after low dose of NB-DNJ, $39 \pm 3\%$ after low dose NB-DGJ, and $36 \pm 6\%$ after high dose NB-DGJ (30).

SD mice treated with nonsteroidal anti-inflammatory drugs (NSAIDs) starting at 8-9 weeks of age or 12-13 weeks of age showed slightly increased survival to 126 ± 5 days and 128 ± 5 days respectively, compared to untreated SD mice (113 ± 6 days). Antioxidative therapy with vitamin E starting at 7-8 weeks of age also resulted in a moderate increase of life span to 127 ± 6 days and treatment with vitamin C to 138 ± 5 days. SD mice that started substrate reduction therapy with NB-DNJ at 6 weeks of age showed a much greater increase in survival to 169 ± 4 days, or a 50% increase. Furthermore, when NSAID and substrate reduction therapy were combined, there was a synergistic effect and life span was extended to 187 ± 5 days. Clinically,

treatment with NSAIDs delayed the failure of motor function tests by approximately 20 days, vitamins C and E by 17-19 days, NB-DNJ delayed test failure by 35 days, and combination NSAID and NB-DNJ resulted in the longest, a 48 day delay. Neuroinflammation, measured by MHCII+ cells in the brainstem, was significantly reduced in SD mice after treatment with NSAIDs (31).

1.2.2.5 Gene Therapy

1.2.2.5.1 Retroviral vectors

Many initial gene therapy studies were conducted with retroviral vectors. Neonatal SD mice were treated by intraperitoneal administration of feline immunodeficiency virus (FIV) vectors encoding hexosaminidase (FIV-HEX). In the CNS, Hex expressing cells were largely found in the periventricular areas of the cerebrum and cerebellum, namely localized in ependymal, glial, and Purkinje cells. HexB subunit enzyme activity was partially restored to 22% of wildtype levels in the brain and 4 months after treatment, immunostaining demonstrated reduction in GM2 ganglioside, MHCII+ microglia, and GFAP+ astrocytes. Hex activity was also detectable in the liver, with the majority of transduced cells localized to portal triads. Furthermore neuromuscular function and locomotive behavior were improved when compared to untreated HexB^{-/-} mice. The effects of therapy on survival were not analyzed in this study (32).

In contrast to FIV vectors, intraperitoneal administration of human immunodeficiency virus (HIV) vectors encoding HEX resulted in an accelerated neurological phenotype in SD mice. Mice that were treated on postnatal day 4 showed loss of neuromuscular functions at an earlier age and required euthanasia earlier than untreated SD mice due to significant weight loss. HIV-HEX treated HEXB^{-/-} mice showed an even greater increase in numerous pro-

inflammatory genes and a significantly increased number of infiltrating CD45+ peripheral immune cells and activated MCHII+ microglia when compared to untreated HEXB^{-/-} mice. Treated mice showed a 20% decrease in GM2 ganglioside storage despite largely accelerated brain pro-inflammatory response secondary to treatment (33).

1.2.2.5.2 Adenoviral vectors

Safety concerns regarding the use of retroviral vectors as therapeutic agents accelerated the development of safer alternatives. An adenoviral vector encoding human HEXB (Ad-HEXB) was injected intracerebrally into SD mice. The brains were analyzed for Hex activity 13 days post-injection and treated mice had greater activity than normal control mice. However, Hex-positive cells were restricted primarily to the region surrounding the needle track, with a few cells present in the striatum and cortex further from the needle track. Hex expressing cells were also present in the ventricular region of the cerebral hemispheres and the cerebellum. In an attempt to further distribute the therapeutic enzyme, Ad-HEXB was coinjected with mannitol, an osmotherapy used to disrupt the blood–brain barrier to facilitate diffusion. Adjunction of mannitol to Ad-HEXB significantly increased the extent of hexosaminidase staining, with the whole striatum, the internal and external capsules, and the thalamus establishing intense activity. The ventricular area of distribution within the contralateral hemisphere suggests vector diffusion via spinal fluid, likely generated by the crossing of the lateral ventricle by the needle during the injection. Coinjection with mannitol showed a significant increase in enzyme distribution; however, the increased number of Hex expressing cells may have been transduced by less viral particles, as similar enzyme activities resulted from the overall brain homogenates.

In spite of partial restoration of enzyme, intracerebral injection of adenovirus had potentially deleterious side effects, especially with the highest dosage tested. Just two days after injection, nuclear fragments derived from cellular necrosis were apparent. By 13 days post-injection, vascular cuffing and microglia activation, indicative of an inflammatory response, as well as spongiosis, were seen and severe demyelination and reactive hypercellularity were established. Mice injected with lower doses showed fewer and less diffuse lesions. Therapeutic efficacy of intracranial delivery of Ad-HEXB was not established in this study (34).

1.2.2.5.3 Adeno-associated viral vectors

Due to the immune response produced by adenoviral vectors, less immunogenic adeno-associated viral (AAV) vectors were designed for therapeutic use. One month old HEXB^{-/-} mice were treated with single striatal injection of recombinant AAV serotype 1 encoding HEX (AAV1-HEX). At 4 months of age, treated mice retained relative normal neuronal density in the thalamus, compared to untreated mice in which over half of the neurons had died. However the single injection to the striatum failed to prevent neuronal loss at more distal sites. Clinically, AAV1-HEX treated SD mice did not display overt signs of disease. Three additional treated mice were allowed to reach humane endpoint, which occurred between 151-258 days, and showed variable neuronal loss in the thalamus, which directly correlated with survival. Despite bilateral thalamic neuron rescue in the animal that lived 258 days, it nevertheless developed characteristic signs of SD disease. A transient and localized immune response to the vector and/or transgene was noted and characterized by cellular infiltrate and inflammatory markers near the striatal injection site. In this experiment, partial rescue of disease was likely due to incomplete distribution of the vector and enzyme (35).

To improve upon limited distribution seen with single striatal injections, numerous injection routes were compared including: unilateral injection of the striatum, bilateral injection of striatum, bilateral injection of striatum and cerebellum, and bilateral injection of hippocampus and cerebellum. The best outcome for survival was bilateral striatum and cerebellum (681 days) and bilateral hippocampus and cerebellum (609 days) injections, with no statistical difference between the two routes, compared to 131 days for untreated HEXB^{-/-} animals. Along with increased survival, an absence of neuronal storage in the brains and spinal cords and greatly reduced neuroinflammation were observed. Of treated mice surviving > 1 year with little to no overt neurological disease, more than half developed acute and fatal illnesses. Illnesses were most commonly due to bladder and intestinal dysfunction, which can be attributed to autonomic neuropathy. Some treated mice did remain healthy for at least 2 years of age. Improved survival with these combined injection routes is attributed to widespread enzymatic distribution throughout the brain (36).

In addition to the location of injections, the timing of treatment is also crucial. In contrast to untreated SD mice which live to ~131 days, treatment with AAV1-HEX bilaterally in to the striatum and cerebellum at 4 weeks resulted in survival of 615 days ($p < 0.0001$), injection at 8 weeks a survival of 233 days ($p < 0.001$), treatment at 10 weeks resulted in an average of 292 days ($p < 0.0001$), and at 12 weeks lifespan was just 126 days ($p > 0.05$). Despite the differences in survival, widespread distribution of virus and enzyme was present in all age groups. Furthermore, all treatment groups showed undetectable or small discrete areas of ganglioside storage at humane endpoint. Neuroinflammation, as measured by CD68 immunohistochemistry, revealed SD mice injected at 4 weeks had microglia numbers and morphology similar to normal control mice. SD mice injected at 12 weeks also had largely attenuated inflammation except for

a few scattered cells in the thalamus and white matter of the spinal cord. Animals treated at 4 weeks of age had a neuron cell density not significantly different from normal. In contrast, in the brain of SD mice treated at 12 weeks of age the neuronal density was not different from untreated SD mice. Mice treated at 8 and 10 weeks were intermediate, with 10 and 19% loss of neurons, respectively. These results suggest that despite widespread distribution of enzyme, effective clearance of ganglioside, and attenuation of neuroinflammation, late stage therapy does not preclude neuronal loss and does not improve survival (37).

1.2.3 Feline GM2 gangliosidosis

Feline GM2 gangliosidosis results from a mutation in the *HEXB* gene (the β subunit) causing a deficiency in both HexA (α/β) and HexB (β/β) enzymes, and thus is a true model of Sandhoff disease. The GM2 gangliosidosis cat model was first described in 1977 (38), has been extremely well-characterized in the intervening years (39, 40), and presents an unparalleled opportunity to test therapeutic options for translation to human clinical trials. Although mouse models are popular and valuable, the mouse brain is 1000-2000 times smaller and much less complex than the human infant brain. The cat brain, 75 times larger and more complex than the mouse brain, is a much better model of therapeutic barriers to be overcome in human treatments. In addition, mice possess an alternative metabolic pathway for gangliosides that is much less active in cats and insignificant in humans. Finally, most mouse models are “knockouts,” meaning that expression of the relevant protein has been completely eliminated, unlike varying levels of residual enzyme activity seen in large animal models and human patients.

1.2.3.1 Pathology of SD cat

There are four known mutations in the hexosaminidase β -subunit gene (*HEXB*) that result in feline SD: a 25 base pair inversion at the 3' terminus (39), a single base deletion in exon 1 (41), a nonsense mutation in exon 7 (42), and a 15 base pair deletion encompassing the splice acceptor site of intron 11 (40). Premature termination of the coding sequence results in < 3% of normal Hex enzyme activity in the brain and peripheral tissues. Interestingly, *HEXB* mRNA levels in the brain are actually elevated above normal, likely due to a compensatory feedback mechanism resultant from the deficient enzyme. Cats homozygous for the 25 base pair inversion mutation have progressive neurologic disease similar to human patients. Disease onset occurs at ~1.7 months of age with slight intention tremors of the head and tail. Symptoms gradually progresses to ataxia, hind limb weakness, overt whole body tremors, and inability to stand (humane endpoint) by 4.5 ± 0.5 months (n=11). The pathological presentation of feline GM2 gangliosidosis is very similar to that seen in human disease and includes distended neurons and membranous cytoplasmic bodies in the CNS and storage inclusions resulting in vacuolation of cells in the viscera (Fig. 4, (38)).

1.2.4 Sheep as a model of TSD

Ovine GM2 gangliosidosis results from a homozygous recessive mutation in the *HEXA* gene and thus is a reliable animal model of TSD. Specifically, a missense (G to C transition) mutation at nucleotide position 1330, results in an amino acid change from Gly444 to Arg. Subsequently, HexA activity in the brain of TSD sheep is reduced to 29% of normal and 6% of normal in the liver. GM2 ganglioside in the brain was established to be elevated ~ 3-fold over normal levels (43). The pathology is remarkably similar to human TSD, with characteristics including swollen neurons, astrogliosis, microgliosis, loss of myelin, scattered spheroids

(swollen axonal segments), and membranous cytoplasmic bodies prominent in the CNS. Clinical disease onset in Tay-Sachs disease sheep (43, 44) occurs at ~1.5 months of age with a proprioceptive deficit termed “knuckling”, followed by ataxia at 3.5 – 6.0 months and a diminished menace reflex at 4.5 – 6.0 months. Subsequent clinical signs are mostly neuromuscular and include hind limb weakness, wide-based stance and difficulty rising. Urinary incontinence is variably present at ~8 months of age. The inability to stand on 2 consecutive days constitutes the humane endpoint, which occurs between 8 – 10 months of age.

2.0 Gene therapy with adeno-associated viral vectors

2.1.1 Adeno-associated virus

The adeno-associated virus (AAV) belongs to the *Parvoviridae* family and *Dependovirus* genus. Consistent with other parvoviruses, AAV is a non-enveloped, single-stranded DNA virus. The genome is approximately 4.7 kb and consists only of two genes flanked by inverted terminal repeats (ITR). The 5' end gene is the *rep* (replication) gene, which encodes for non-structural, regulatory proteins. Due to the presence of two promoters and internal splice sites, the *rep* transcript is spliced into four proteins named for their molecular weights: Rep40, Rep52, Rep68 and Rep78. These proteins are utilized in site-specific binding, helicase activity, regulation of gene expression, and additional regulatory functions. The *cap* (capsid) gene is located immediately downstream from the *rep* gene and encodes for structural proteins. With one promoter and alternative splicing, the *cap* transcript produces 3 proteins: VP1, VP2, and VP3. Together, these proteins form the capsid, icosahedral in shape and approximately 25nm in size (45, 46). The discovery of the atomic structure of AAV in 2002 revealed that the capsid consists largely of β -barrel motifs, interspaced by loops that are capable of interacting with cellular

receptors and antibodies (47). Flanking the *trans-acting rep* and *cap* genes are 145 nucleotide-long, *cis-acting*, inverted terminal repeats that contain palindromic regions. Base pairing between palindromic regions leads to the creation of T-shaped hairpin loops. This secondary structure at the 3' terminal repeat offers a free hydroxyl group which now serves as a primer for DNA synthesis. The AAV *rep* gene does not encode a polymerase and thus the virus must rely on host polymerase for replication to occur (48, 49).

As defined by its genus, AAV lacks the ability to replicate, and thus establish infection, without the assistance of a helper virus, usually the adenovirus. In the absence of the helper virus, AAV establishes latent infection by site-specific integration into host chromosome, or by persisting in episomal forms. Integration into the genome allows the virus to be perpetuated through host cell divisions. This site-specific recombination requires the AAV inverted terminal repeats as well as Rep68 or Rep78 (50). Once a host becomes inundated with an appropriate helper virus, AAV gene expression is activated and AAV is excised from the host chromosome by a Rep mediated mechanism. AAV then undergoes replication and packaging of the viral genome. The helper virus induces cell lysis, releasing the newly constructed AAV to infect cells and propagate (46, 48). While wildtype AAV is capable of entering the lytic cycle and establishing infection, it is non-pathogenic in nature and is not known to be associated with any disease (51). This lack of pathogenicity is one of the characteristics that first made AAV appealing as a potential vector for use in gene therapy. In addition, AAV is able to infect a wide range of tissues due to a large number of serotypes. Presently, there are 11 AAV serotypes and over 100 AAV variants that have been isolated. A serotype by definition is “a newly isolated virus that does not efficiently cross-react with neutralizing sera specific for all other existing and characterized serotypes” (46). A variant is simply an isolate with an unknown serology.

Serotypes differ in their tropism, immune response, and transfer efficiency. Because of these differences, basic knowledge of vector serotype is critical when designing gene therapy experiments. For example, AAV1 and 7 are optimal serotypes for transducing skeletal muscle, while AAV9 has the highest transduction efficiency in lung tissue, compared to the other serotypes. Table 1 below depicts the hierarchy of transduction efficiency of AAV serotype vectors in some major tissue types (46).

2.1.2 Recombinant AAV

Because of its lack of pathogenicity and ability to infect a diversity of tissues, a variety of wildtype AAV serotypes have been isolated, made into recombinant vectors, and purified. By removing the *trans-acting rep* and *cap* genes from between the *cis-acting* terminal repeats, the AAV is now a genetic cassette that can contain a transgene of ≤ 4.7 kilobases in length packaged in to virions and delivered to specific host cells (52). Originally, a plasmid was constructed containing the recombinant AAV (rAAV) genome flanked by the wildtype ITRs, instead of the *rep* and *cap* genes, and co-transfected into a cell along with a Rep and Cap expression plasmid. However, since a helper virus is required for AAV activation, the rep and cap packaging cells were infected directly with wild-type adenovirus (48). This protocol raised obvious contamination and safety concerns and today superior methods have evolved.

Instead of using wild-type adenovirus during the recombination process, current protocols utilize plasmids containing the necessary helper virus genes and transfection in 293 cells (Fig. 5) (46, 48). A cloning vector utilizes a multiple cloning site to position a gene of interest into an expression cassette that is flanked by restriction sites. Upon digestion with an appropriate restriction enzyme, the insert-containing expression cassette is removed from the cloning vector

and cloned into the complementary restriction site of a replication-deficient AAV vector, containing the AAV ITR sequences. The AAV vector is digested with a restriction enzyme for removal of the original cassette and insertion of the expression cassette. This vector is accompanied by two additional vectors; one vector carries the genes required for replication (*rep*) and packaging (*cap*), while the other vector carries helper genes E2A and E4, which are essential for generating sufficient titers of AAV in HEK293 cells. The AAV- ITR-containing plasmid and the *rep/cap* containing plasmid, lack homologous regions, avoiding recombination that could produce wildtype AAV. These three plasmids are cotransfected into a HEK293 cell line, which contributes the remaining required adenovirus proteins essential for packaging virions, E1A and E1B. Through this cotransfection, recombinant AAV virions are produced, that can then be used to infect target cells (46, 53).

2.1.3 Immune response to AAV

In order to understand how best to evade the immune system when utilizing viral vectors for therapy both innate and adaptive immune responses to viruses must be considered. The innate immune system recognizes pathogens by pathogen associated molecular patterns (PAMPs). The receptors that recognize PAMPs are pattern recognition receptors (PRRs), the most significant of which are toll-like receptors (TLRs). Once innate immune response is activated by antigen recognition, cytokines such as type 1 interferons (IFN) are activated, secreted, and induce potent antiviral effects. Concurrently, the inflammatory response by the innate immune system leads to migration of phagocytes and other antiviral cells by extravasation and chemotaxis. One major bridge between the innate and adaptive immune response is the dendritic cell. Immature dendritic cells, a type of antigen presenting cell (APC), use PRRs, mainly TLRs, to recognize pathogens,

which leads to activation and maturation of the cell. Mature dendritic cells express major histocompatibility complex (MHC) class II molecules, as well as their required costimulatory molecules. Dendritic cells migrate to the lymphoid tissue and present antigen to T cells in two different manners. Endogenous antigens are degraded by proteasomes, assembled with class I MHC molecules in the RER, and then presented on the membrane of the dendritic cell to cytotoxic T lymphocytes (CTLs). Exogenous antigens are degraded in the endocytic compartment, combined with class II MHC molecules and presented to T helper (TH) cells and B cells. However, a mechanism known as cross-presentation allows exogenous antigens to interact with class I MHC molecules and thus activate CTLs (54). Studies have found this process of cross-presentation to play a significant role in the immune response to rAAV (55). Once a T cell has been presented an antigen to which it is specific, it is now activated and leaves the lymph node and enters circulation to act as an effector molecule: either as a CD4⁺ T cell (T helper cell), which assists in B and T cell activation, or a CD8⁺ T cell (CTL) which locates and kills cells presenting antigen. The T cell response to an antigen is termed cell mediated immunity. While B cells can recognize antigen by an APC, it is not required for B cell activation, as they have antibody molecules for antigen recognition on their surface. Once activated by presentation of an antigen to which it is specific, the B cell leaves the lymph node, and enters circulation to act as an effector plasma cell by secreting antibodies which locate and eradicate cells presenting antigen. The B cell response to an antigen is termed humoral immunity. Both B and T cells create and leave behind memory cells to create a stronger and quicker immune response upon subsequent exposure to the same antigen (54).

The brain has largely been thought to be an “immune privileged” organ and not subject to many of the immune processes experienced by the rest of the body. In reality both innate and

adaptive immune responses can be initiated in the brain; however, the type and extent of the reaction are largely dependent on what part of the CNS the antigen is presented to. The brain parenchyma is isolated from the lymphatic system by the blood-brain-barrier, made up of tight cellular junctions. Because of this, delivery of viral particles exclusively into the brain parenchyma can instigate an innate inflammatory response but fails to initiate a systemic adaptive immune response (56-59). Outside of the parenchyma, however, a much more complex system of the CNS exists. The ventricular system (including CSF), meninges, choroid plexus, and brain draining lymph node (BDLN) are all highly integrated in to the vascular and lymphatic system, and thus are capable of initiating systemic immune responses. Either targeted delivery to the ventricular system or accidental leakage of antigen out of the brain parenchyma can simultaneously stimulate an innate and adaptive immune response (56). The major reason for the differences in the ventricular system is the presence of dendritic cells, which can travel to the BDLN, and as previously mentioned act as APCs and activate T cells and initiate an adaptive immune response. In light of this, careful consideration must be made when considering intracranial injection routes for AAV. Even intended parenchymal injections may traverse ventricular or vascular components and inadvertently initiate systemic immunity.

2.1.3.1 Innate immune response to rAAV

It was initially believed that innate immune response to AAV vectors was inconsequential. It was reported that AAV vectors lacked the ability to engage PRRS, including TLRs, and failed to induce type I IFNs (60). One explanation was that AAV vectors failed to reach the immunogenicity threshold for CTL induction due to an inability to effectively transduce dendritic cells (52). However, more recent studies have provided convincing evidence

that innate immune signaling through TLRs can have a detrimental outcome on transgene expression. Specifically, Zhu et al. demonstrated in vivo and in vitro that the PAMP on AAV2 is recognized by TLR9 receptors expressed on dendritic cells. The activated dendritic cells then produce type I IFNs and mediate CD8+ T cell responses (Fig. 6, (61)). This immune response ultimately leads to the loss of transgene expression and the formation of antibodies, which would hinder subsequent attempts at utilizing the vector for therapy (62). This finding demonstrates that AAV does interact with TLRs, activates dendritic cells, initiates an innate immune response, and induces secretion of potentially detrimental cytokines, such as type I IFN. This discovery of an activation pathway of the innate immune system not only provides insight to the generation of the disadvantageous adaptive immune response, but also presents a potential pathway to deliberately impede in order to enhance therapeutic gene expression.

In addition to peripheral injection of AAV, this vector type is being explored widely for use in neurologic diseases. As will be discussed below, multiple clinical trials have already been initiated for intracranial delivery of AAV. Due to the compartmentalization of the brain previously mentioned, careful injection of non-soluble diffusible antigens into the brain parenchyma of naïve animals results in minimal innate immune response (63-65). However, increasing the dosage of rAAV vector ($\sim 4 \times 10^{10}$ particles) delivered by intrastriatal injection in the rat brain resulted in a substantial, but transient, inflammatory response marked by astrogliosis and microgliosis (66). This suggests that there may be an innate immune response in the brain once a threshold of titer is reached.

2.1.3.2 Adaptive immune response to rAAV

2.1.3.2.1 Cell mediated immune response

In one of the first human clinical trials to utilize AAV, Manno et al. used recombinant AAV2 expressing human factor IX (F.IX) to treat patients with severe Hemophilia B. This study followed successful long-term expression of therapeutic levels of canine F.IX in dogs with severe Hemophilia B by utilizing AAV in a single portal vein infusion (67). The clinical trials were carried out in seven subjects with dose escalation of rAAV2-F.IX infused through the hepatic artery. As in the canine study, therapeutic levels of factor IX were achieved; however, contrary to the long lasting levels seen in canines, therapeutic levels in human patients were limited to 8 weeks. Concurrent with the decline in factor IX, elevated levels of liver transaminases were detected. Upon further investigation it was determined that AAV capsid specific T cells were responsible for the decline in F.IX and the elevated transaminase levels (68). While successful transduction of rAAV in human hepatocytes was noteworthy, the subsequent destruction of these hepatocytes by cell-mediated immunity was somewhat unexpected and has since presented the scientific community with a new impediment in utilizing rAAV as a therapeutic vector.

2.1.3.2.2 Humoral immune response

The 2006 Manno et al. study determined that capsid specific T cells were responsible for the decline in transgene expression after successful transduction. However, one subject also lacked effective transduction, with factor IX levels only reaching 3% of normal and declining to baseline by 4 weeks post injection, despite receiving the same vector dose as another subject with successful transduction. The disparity was attributed to the presence of neutralizing antibodies at a titer of 1:17 in the patient that failed to reach therapeutic levels of factor IX (68). In contrast to the cell mediated immune response previously described, in this case AAV therapy

was not efficacious due to the humoral immune response with antibodies created and stored from previous exposure to the capsid.

The presence of naturally occurring neutralizing antibodies is thought to be high in humans and non-human primates, who are the natural hosts for AAV. In order to look at the prevalence of AAV-specific memory T cells in the general human population, Mingozi et al. tested 46 adults for AAV2 neutralizing antibodies and for frequencies of circulating capsid-specific T cells. They found that approximately half of the subjects (25/46) had readily detectable serum titers of AAV2 neutralizing antibodies (69). In rhesus macaques, which are natural hosts for AAV8, it was observed that with titers as low as 1:5, the presence of neutralizing antibodies prevented successful transduction of rAAV8 and expression of F.IX. In contrast, those macaques with undetectable levels of antibodies were successfully transduced by rAAV8 expressing F.IX (70). Most recently, data on neutralizing antibodies to AAV1, AAV2, AAV7, and AAV8 in 888 serum samples of healthy subjects dispersed in 10 countries was collected. This data revealed that neutralizing antibodies to AAV2 were considerably the most prevalent, followed distantly by serotypes 1 and 7, with AAV8 having the least amount of serum antibodies (71).

Since most rodents are not normally infected by AAV, experiments in animals without preimmunization may not accurately portray potential immune responses in humans since a significant portion of the population has experienced prior exposure to the virus. Two studies conducted in rats showed that peripheral preimmunization with wildtype AAV2 or rAAV2 completely blocked brain transduction of rAAV2, but not rAAV5, after intrastriatal delivery (72, 73). Furthermore, upon readministration of rAAV2, preimmunized animals had a further enhanced immune response, including markers of a cell-mediated immune response (73).

Especially in light of this new data, the high level of neutralizing antibodies in the human population should be of major concern when designing human clinical trials, even those proposing intraparenchymal injections. In depth screening assays on neutralizing antibodies and CD8+ T cells should be implemented as selection criteria in human trials utilizing AAV, as the adaptive immune response has proven capable of detrimental effects on therapeutic success.

2.1.4 Clinical applications of recombinant AAV

2.1.4.1 Approved clinical use of recombinant AAV

AAV gene therapy has been approved for treatment of the metabolic disorder lipoprotein lipase deficiency (LPLD). Like TSD and SD, LPLD is a rare autosomal recessive disorder. Lipoprotein lipase (LPL) is required for plasma triglyceride hydrolysis and its deficiency can result in hypertriglyceridemia, pancreatitis, cardiovascular disease, and even diabetes. Recombinant AAV serotype 1 encoding a functional copy of LPL, now referred to as aliopogene tiparvovec (Glybera[®]), delivered by intramuscular injection demonstrated safety and efficacy in phase I/II and phase II/III clinical trials and is now commercially available for use in Europe. Aliopogene tiparvovec significantly lowers plasma triglycerides and increases LPL activity, reducing complications including pancreatitis (74). Five patients treated with intramuscular injection of aliopogene tiparvovec were analyzed for immune response to the therapy. All patients were administered immune suppression prior to and for 12 weeks after injection. Cell mediated immune response were demonstrated in 4 of 5 patients and consisted of CD8+ T cells that lacked cytotoxic potential as well as regulatory CD4+ T cells. A stable humoral immune response against the AAV1 capsid protein was also documented. Immune responses did not compromise transgene expression, as LPL activity was present long-term (75).

2.1.4.2 Clinical trials utilizing AAV

The use of rAAV vectors has already been approved for clinical trial use in neurodegenerative diseases including Parkinson's disease and Alzheimer's disease. Patients with Parkinson's disease received bilateral intraputaminial infusion of AAV2-hAADC vector (AAV serotype 2 encoding human aromatic L-amino acid decarboxylase) at two doses. Improvements in motor scores were reported, with more significant corrections occurring after treatment with the higher dose. PET scans using a fluorescent tracer for gene expression showed a 30% increase of putamen uptake in the low-dose cohort and a 75% increase in the high-dose cohort 6 months after surgery. Adverse events included asymptomatic hemorrhage, identified by postoperative MRI, in 2 subjects. Modest increases in serum antibody titers (2- to 8-fold) were seen in 4 subjects, no increase in 1 subject, and pronounced increase in another patient. Antibody titers reached a maximum within the first 6 months post-treatment and did not correlate with clinical outcome (76). Recombinant AAV serotype 2 encoding nerve growth factor has been developed by the company Ceregene Inc. for use in Alzheimer's disease. Injections were targeted to the nucleus basalis of Meynert in a total of 4 or 6 injections of 12 human subjects. The recombinant vector has passed phase 1 safety trials and is currently underway in phase II clinical trials (77).

AAV-mediated gene therapy has also been approved and is currently recruiting patients for a phase I/II clinical trial for a non-neurologic lysosomal storage disorder known as Pompe disease. In this study recombinant AAV serotype 1 encodes the gene GAA, responsible for the deficient enzyme acid alpha-glucosidase. The vector will be delivered via intramuscular injection into the diaphragm of children with ventilator dependent Pompe disease. In this study patients

will receive either 1.0×10^{12} or 5.0×10^{12} vector genomes, and will be followed with a number of measures including pulmonary function on days 14, 90, 180, 270, and 365 post injection.

A clinical trial is also underway for a neurodegenerative lysosomal storage disorder similar to TSD and SD known as Batten's disease, or Neuronal Ceroid Lipofuscinoses. Recombinant AAVrh10 encoding CLN2 cDNA, which is responsible for the deficient enzyme tripeptidyl peptidase 1 (TPP-I), will be delivered intracranially among 12 locations delivered through 6 burr holes (2 locations at 2 depths through each hole), 3 burr holes per hemisphere. The vector will be delivered at 2 different doses, 9.0×10^{11} or 2.85×10^{11} genome copies/subject. Treated children will undergo extensive neurological assessment at predetermined intervals to determine if the AAV transfer is safe and if it slows the rate of disease progression.

This is the same study design that was previously implemented in a clinical trial of 10 children affected with Batten's disease; however, in the initial study AAV serotype 2 was used. One of the patients developed status epilepticus from which she did not recover and died 49 days after the procedure. There were no signs of inflammation in the CNS or signs of infection. Since Batten's disease commonly presents with seizures, doctors were unable to delineate whether disease processes or the therapeutic agent resulted in this event. EEG monitoring was conducted on all subsequent patients for 14 days post-surgery with no sign of seizure activity. A second subject developed pneumonia approximately 520 days after surgery and died 704 days after vector administration. Respiratory dysfunction and resultant pneumonia are common secondary effects and causes of death with these diseases and thus was not related to the procedure. While no patients had detectable neutralizing serum antibodies prior to treatment, 4 of the 10 patients developed a humoral immune response to vector, which reached a maximum titer of 1:270 within the first 6 months of surgery. For 3 of the 4 patients, titers returned to baseline by 18

months post-surgery. Grey matter volume, ventricular volume, and cortical apparent diffusion coefficient were quantitatively assessed by MRI imaging. For all three parameters, a decline in the rate of change was noted for treated patients; however, the sample size was too small for statistical significance. Assessment of 8 treated subjects with a neurologic rating scale showed a significantly reduced rate of decline in the treated subjects compared to untreated control patients. Overall, the primary outcome measure of improved neurologic function was achieved; however, adverse events and immune response also ensued. These mixed results merited a second phase 1 safety study utilizing AAV serotype rh10, which was described above and is currently underway (78).

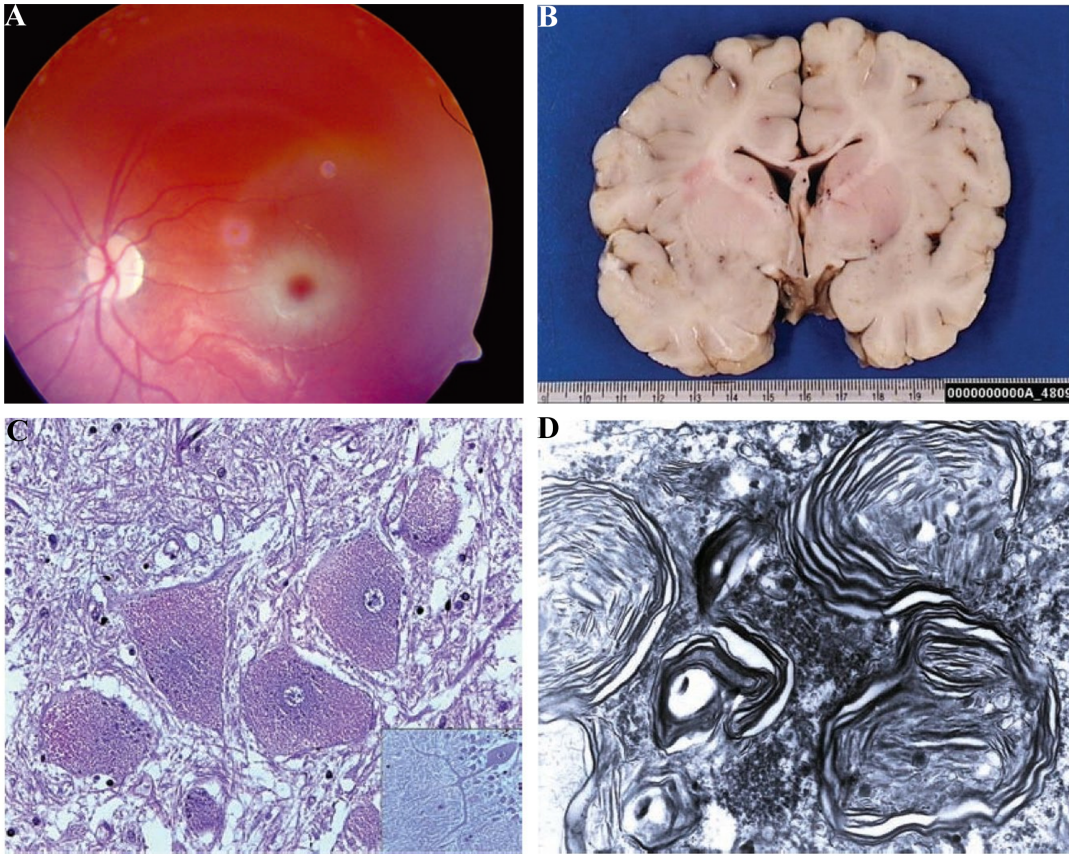


Figure 1. Pathology of GM2 gangliosidosis. A) Photograph of a fundus showing “cherry red spot” in the eye. B) Gross photograph of a coronal section with evidence of brain atrophy. C) Routine hematoxylin and eosin staining showing enlarged neurons and a meganeurite (inset). D) Electron microscopy photograph of lamellar “membranous cytoplasmic body”. Figure adapted from (3, 4).

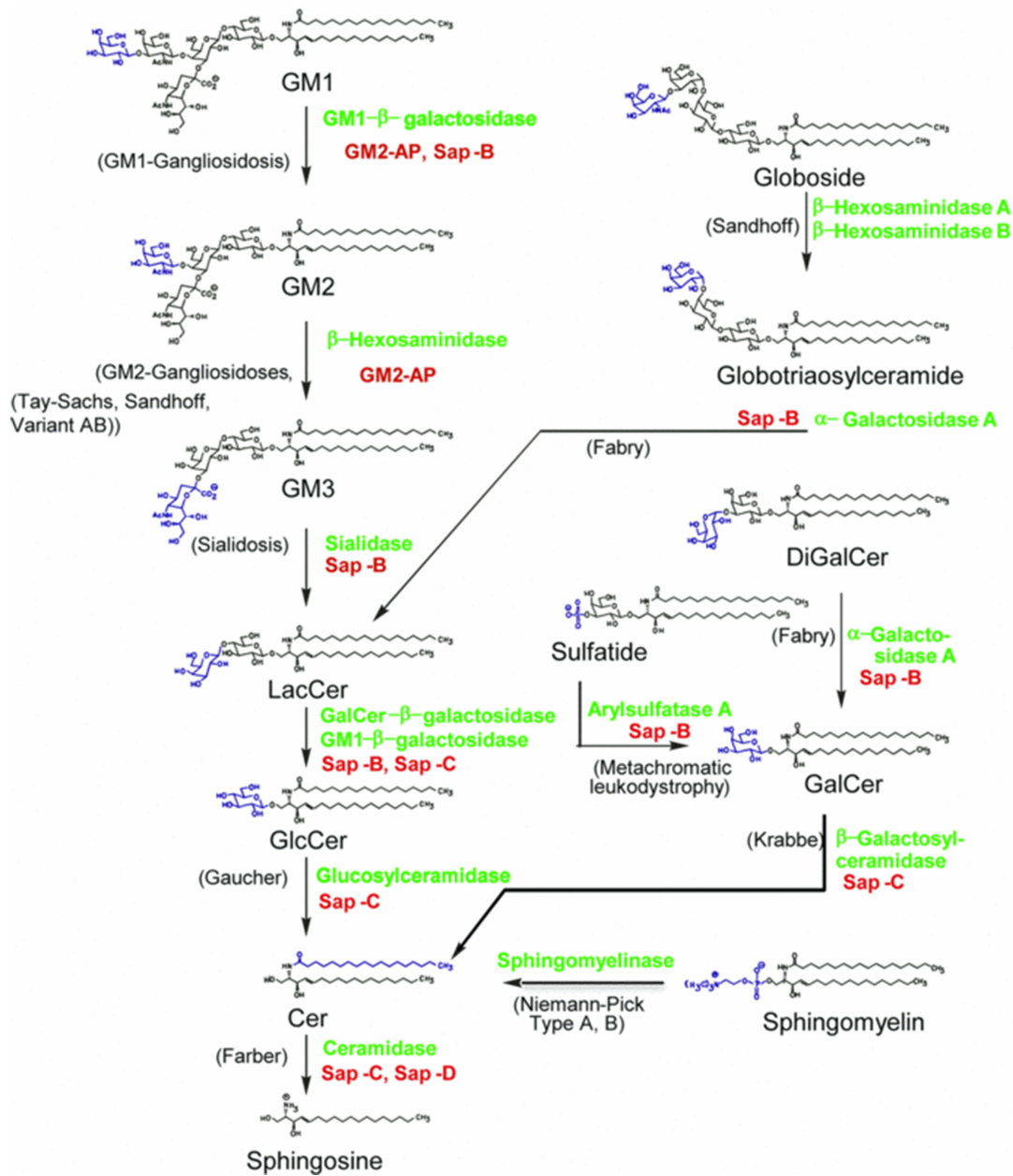


Figure 2. Ganglioside degradation pathway (6). Hydrolytic enzymes are indicated in green, sphingolipid activator proteins in red, and known metabolic disorders resulting from protein deficiency at each step in parenthesis. GM2AP, GM2 Activator Protein. Figure adapted from (6).

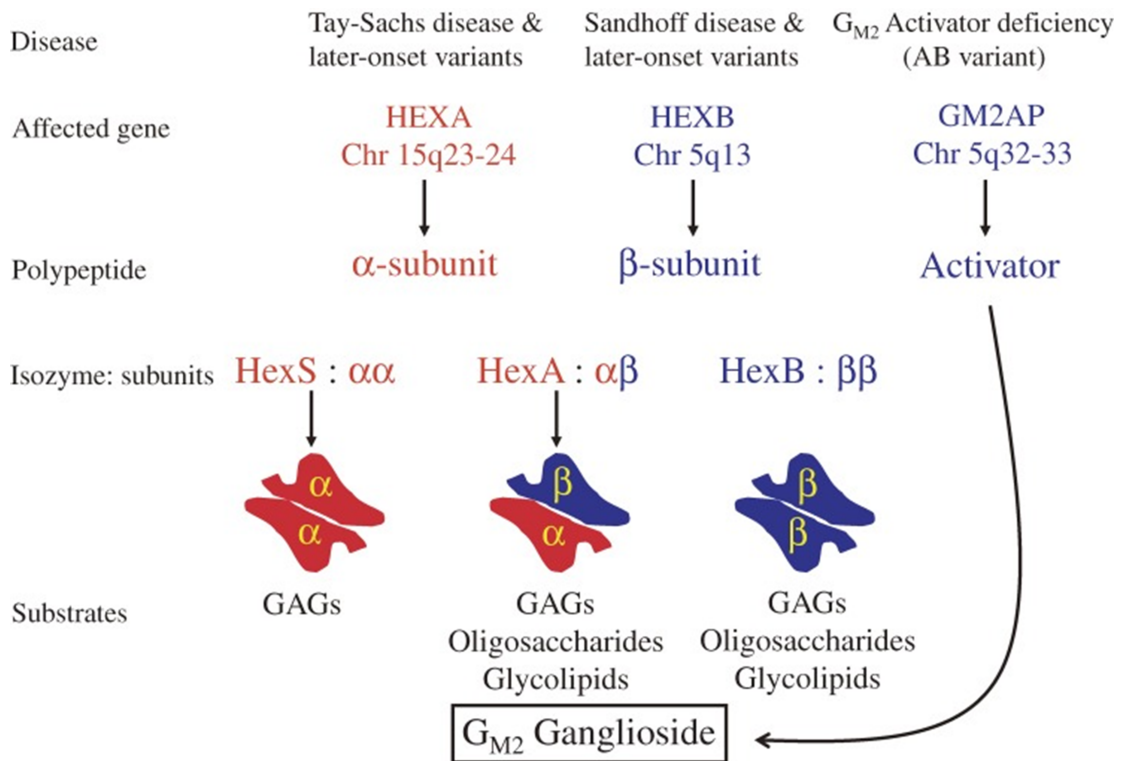


Figure 3. Structure and function of hexosaminidase subunits (7). Different genes encode each hexosaminidase subunit and the GM2 Activator Protein (GM2AP). The α - and β -subunit of the HexA isozyme and GM2AP, which binds the ganglioside and presents it to the enzyme, are needed for GM2 ganglioside degradation. GAGs, glycosaminoglycans. Figure adapted from (7).

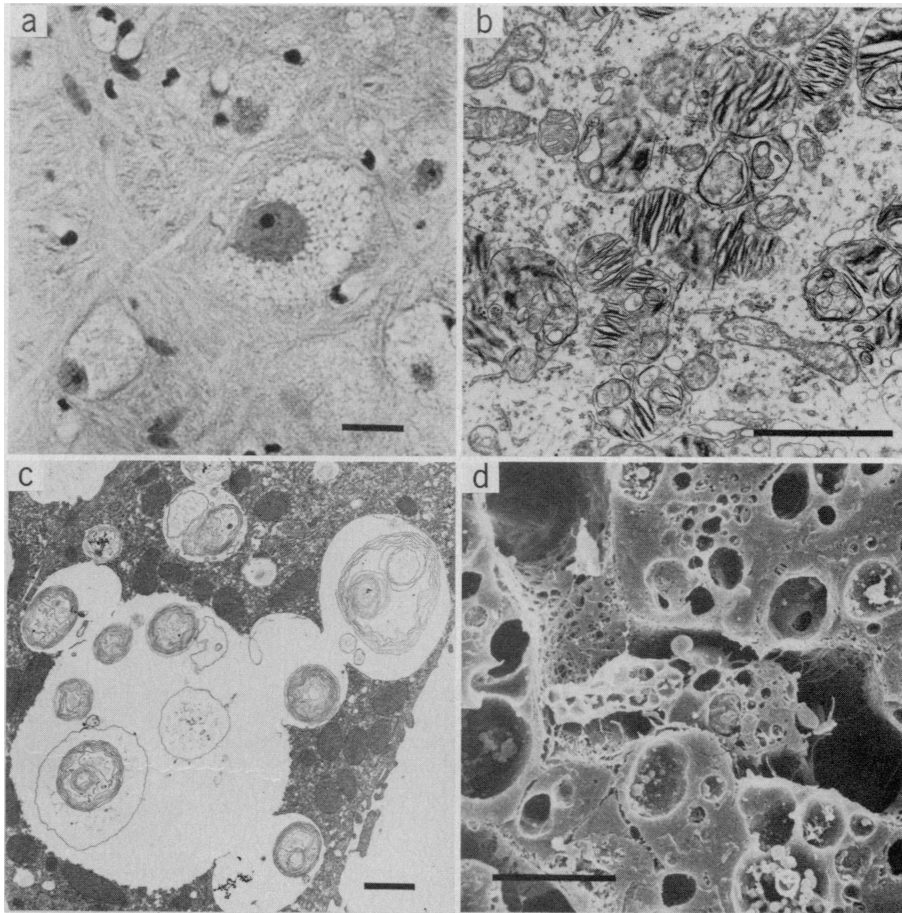


Figure 4. Pathology of GM2 gangliosidosis in a feline model (38). A) An enlarged neuron with vacuolated material in the cytoplasm and peripherally displaced nuclei. B) Electron micrograph of lamellar “membranous cytoplasmic body”. C) Hepatocyte containing vacuolated storage material. D) Electron micrograph of vacuoles in hepatocytes and Kupffer cell of the liver. Figure from (38).

Table 1. Transduction efficiency of AAV serotypes (46).

Tissue	Serotype
Liver	AAV8, AAV9
Skeletal muscle	AAV1, AAV7, AAV6, AAV8, AAV9
CNS	AAV5, AAV1, AAV4
Lung	AAV9
Heart	AAV8
Pancreas	AAV8
Kidney	AAV2

Table adapted from (46).

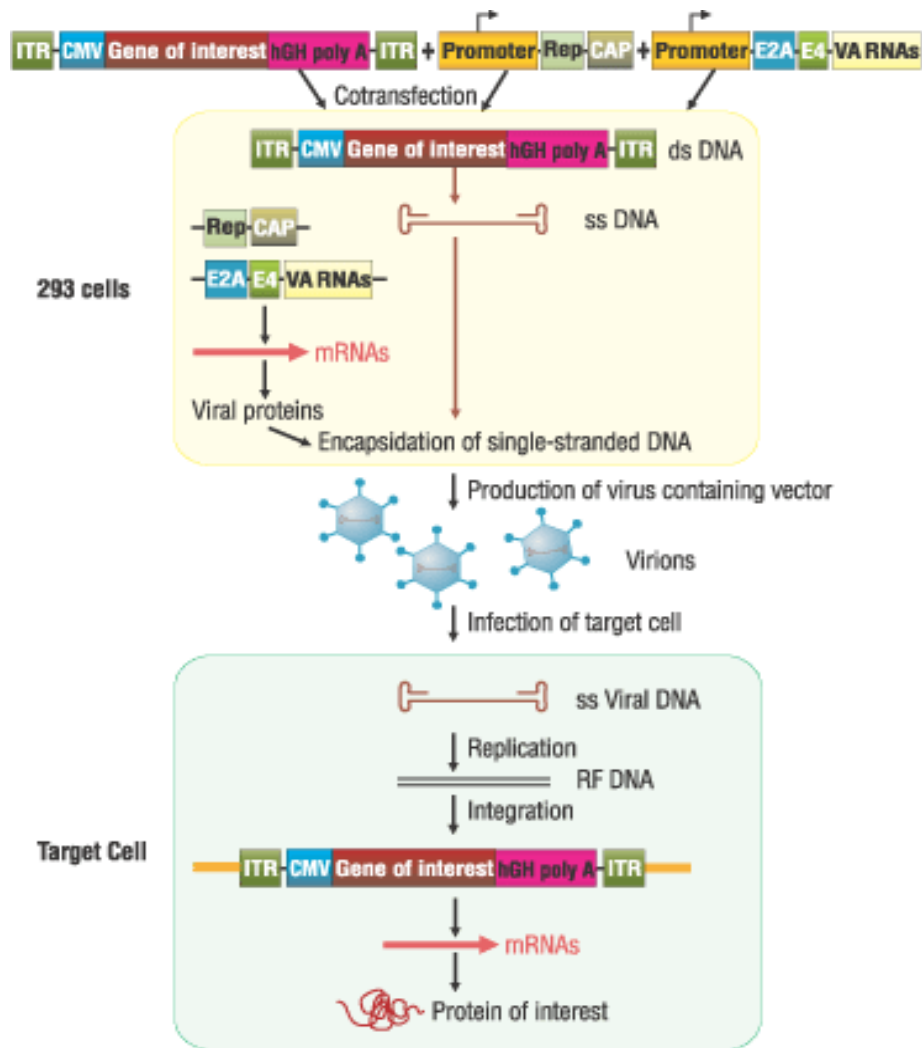


Figure 5. Production of recombinant AAV (53). The vector encoding the gene of interest is cotransfected with two additional vectors; one vector carries the genes required for replication (rep) and packaging (cap), while the other vector carries helper genes E2A and E4; into a HEK293 cell line. Encapsidation of single-stranded (ss) DNA occurs and recombinant AAV virions are produced. Target cells are then infected with the recombinant virions, which are replicated and produce the protein of interest. Figure from (53).

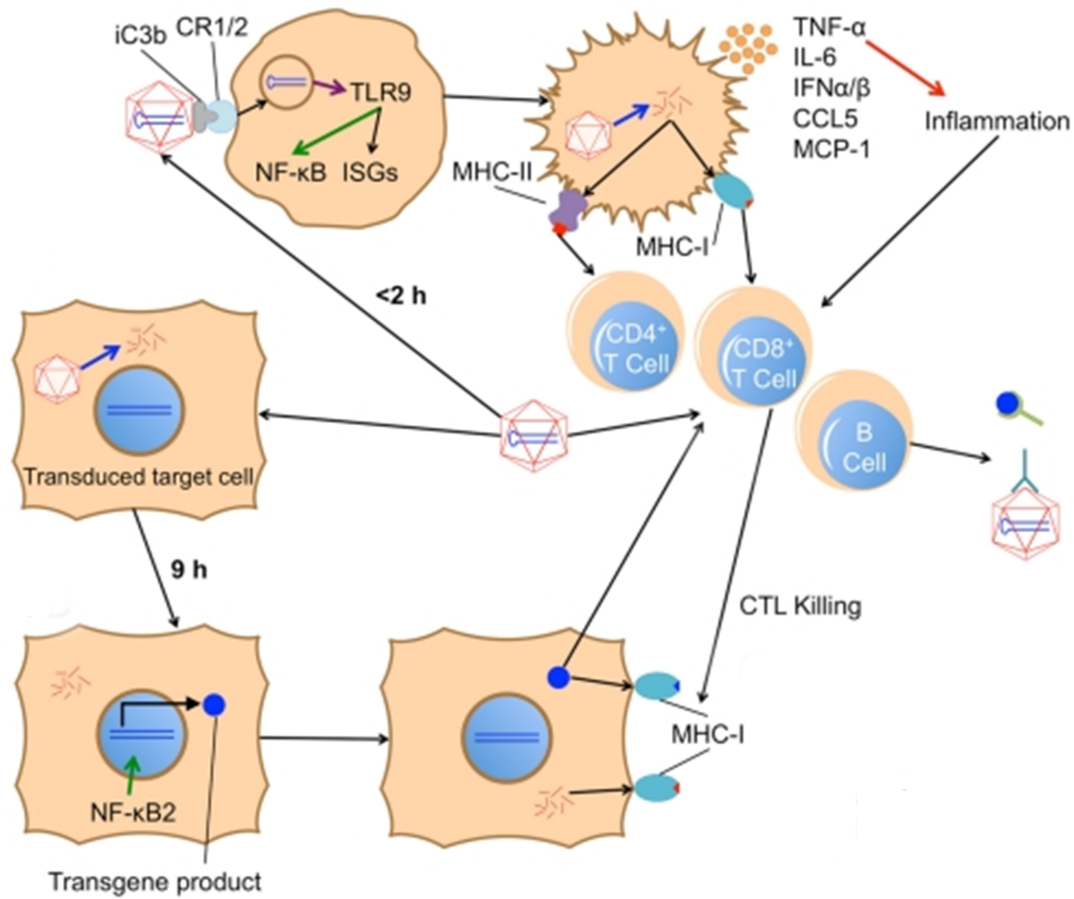


Figure 6. Innate and adaptive immune responses to AAV vectors. Within 2 hours of vector injection, the innate immune response is initiated when AAV is phagocytosed by an APC, detected by TLR9, and activates the classical NF-κB pathway. Maturation of the APC then occurs, including up-regulation costimulatory molecules and production of pro-inflammatory cytokines including TNF-α, IL-6, CCL5, MCP-1, and type I IFNs. Additionally, cross-presentation of the antigen by APCs, initiate an adaptive response, including B cells, CD4⁺ T cells, and CD8⁺ T cells. B cells produce antibodies against the capsid and transgene product while CD8⁺ T cells induce a CTL response and kill transduced cells. MHC, major histocompatibility complex; TLR, toll like receptor; CTL cytotoxic T lymphocyte. Figure adapted from (61).

CHAPTER 1

Therapeutic Response in Feline Sandhoff Disease Despite Immunity to Intracranial Gene Therapy

Allison M Bradbury^{1,2}, J Nicholas Cochran¹, Victoria J McCurdy^{1,2}, Aime K Johnson³, Brandon L Brunson², Heather Gray-Edwards¹, Stanley G Leroy⁴, Misako Hwang¹, Ashley N Randle¹, Laura S Jackson¹, Nancy E Morrison¹, Rena C Baek⁵, Thomas N Seyfried⁵, Seng H Cheng⁶, Nancy R Cox^{1,7}, Henry J Baker¹, M Begona Cachón-González⁸, Timothy M Cox⁸, Miguel Sena-Esteves⁴ and Douglas R Martin^{1,2}

¹*Scott-Ritchey Research Center, ²Department of Anatomy, Physiology & Pharmacology,*

³*Department of Clinical Sciences and ⁷Department of Pathobiology; College of Veterinary Medicine, Auburn University, Auburn, AL 36849, USA*

⁴*Department of Neurology and Gene Therapy Center, University of Massachusetts Medical School, 381 Plantation Street Suite 250, Worcester, MA 01605, USA*

⁵*Biology Department, Boston College, Chestnut Hill, MA 02467, USA*

⁶*Genzyme Corporation, 49 New York Avenue, Framingham, MA 01701-9322 USA*

⁸*Department of Medicine, University of Cambridge, Level 5, Box 157, Addenbrooke's Hospital, Hills Road, Cambridge CB2 2QQ, United Kingdom*

Abstract

Salutary responses to adeno-associated viral gene therapy have been reported in the mouse model of Sandhoff disease, a neurodegenerative lysosomal storage disease caused by deficiency of β -N-acetylhexosaminidase. While untreated mice reach the humane endpoint by 4.1 months of age, mice treated by a single intracranial injection of vectors expressing human hexosaminidase may live a normal life span of 2 years. When treated with the same therapeutic vectors used in mice, two cats with Sandhoff disease lived to 7.0 and 8.2 months of age, compared to an untreated life span of 4.5 ± 0.5 months (n=11). Because a pronounced humoral immune response to both the AAV1 vectors and human hexosaminidase was documented, feline cDNAs for the hexosaminidase α and β subunits were cloned into AAVrh8 vectors. Cats treated with vectors expressing feline hexosaminidase produced enzymatic activity >75 fold normal at the brain injection site with little evidence of an immune infiltrate. Affected cats treated with feline-specific vectors by bilateral injection of the thalamus lived to 10.4 ± 3.7 months of age (n=3), or 2.3 times as long as untreated cats. These studies support the therapeutic potential of adeno-associated viral vectors for Sandhoff disease and underscore the importance of species-specific cDNAs for translational research.

Introduction

The GM2 gangliosidoses are a class of lysosomal storage disorders that include Tay-Sachs disease (TSD) and Sandhoff disease (SD), both causing rapid and fatal neurodegeneration in children by ~ 5 years of age (79). Although the pathogenic mechanism is incompletely understood, the underlying cause is catalytic deficiency of β -N-acetylhexosaminidase (Hex, EC 3.1.2.52), a lysosomal enzyme that initiates the stepwise catabolism of GM2 ganglioside by

removing its terminal N-acetylgalactosamine (GalNAc) residue. Functional Hex activity requires the coordinated action of 3 distinct proteins, a nonhydrolytic GM2 activator protein and the 2 hydrolytic subunits, α and β . Subunits combine in the endoplasmic reticulum to form the 2 major Hex isozymes, each with different substrate specificities: HexB ($\beta\beta$) or HexA ($\alpha\beta$), the isozyme responsible for degradation of GM2 ganglioside in humans. Therefore, GM2 gangliosidosis may be caused by a defect in either the Hex α (TSD) or β (SD) subunit, or by a deficiency of the GM2 activator protein. First described in 1881 (80), the GM2 gangliosidoses remain incurable today.

Hope for effective treatment of GM2 gangliosidosis arises from several recently developed experimental therapies, including adeno-associated virus (AAV) gene therapy. Because optimal production of HexA is suggested to require co-expression of both Hex subunits (81-83), SD mice were treated by bilateral injections of the striatum and deep cerebellar nuclei (DCN) with monocistronic vectors expressing human Hex α and β subunits, both with carboxyl terminal fusions to the HIV Tat protein transduction domain (84). Treated mice routinely survived to 2 years, the maximum age permitted by institutional animal welfare mandates (85, 86). Hence we contend that AAV gene therapy holds promise for successful translation to clinical trials for human GM2 gangliosidosis.

The feline model of SD, first discovered and reported in the 1970's (87), has been continuously maintained as a research colony to the present day. With stereotypical disease progression that has been characterized thoroughly in the intervening years (88-95), the feline model presents an excellent opportunity to test AAV gene therapy and address important issues to be resolved prior to initiating human clinical trials. For example, the cat brain is >50 times larger than the mouse brain and is more complex and anatomically similar to humans, thus presenting a better approximation of the challenges posed to widespread vector delivery in a

large brain with global disease. Moreover, the human storage profiles of GM2 ganglioside, asialo-GM2 ganglioside and myelin-enriched lipids are more effectively modeled by SD cats than SD mice, suggesting that ganglioside metabolism in cats is more similar to that in humans than in mice (96). For these reasons, the feline SD model was chosen to test AAV gene therapy as an intermediate step between mouse experiments and human clinical trials.

Results

Initial tests of AAV vector function were performed in SD cat 7-532 by injection of the right thalamus with the same AAV1 vectors expressing human Hex α or β subunits used to effectively treat SD mice in previous experiments (85) (Table 1). Six weeks post-injection, the brain was analyzed for Hex expression and therapeutic effect. Injection of vector through a single needle tract produced substantial Hex activity spanning the entire anterior-posterior axis of the ipsilateral cerebrum, over a distance of ~ 2.5 cm. Fluorogenic enzyme assays with an α -subunit selective substrate (4-methylumbelliferyl 6-sulfo-2-acetamido-2-deoxy- β -D-glucopyranoside, MUGS) measured HexA activity ranging from 236.7% of normal at the injection site to 91.4% of normal 1 cm anterior to the injection site. MUGS activity in contralateral blocks ranged from 5.0-10.4% normal. Untreated SD cats express $0.8 \pm 1.4\%$ (mean \pm s.d., n=7) of normal MUGS activity in the cerebral cortex. Furthermore, high performance thin layer chromatography (HPTLC) demonstrated a reduction of GM2 ganglioside storage at the injection site in cat 7-532. In agreement with previous studies (96), GM2 comprised $\sim 72\%$ of all ganglioside in the untreated SD cat brain but only 23% of total ganglioside at the injection site of the treated SD cat brain (Fig. 1a). Correction was not complete, however, since the normal cat brain has undetectable levels of GM2 ganglioside.

After demonstrating functionality of AAV vectors expressing human Hex in the SD cat brain, long-term therapeutic experiments were conducted in 2 SD cats (7-588, 7-589) using bilateral thalamic injection of a 1:1 ratio of vectors AAV1-hHEXA/B-Tat (Table 1, Table S1). To minimize an anticipated immune response to the human Hex subunit-Tat fusion proteins, both cats were immunosuppressed with 10 mg/kg cyclosporine administered orally twice per day for the duration of the experiment. To further minimize immunity to the therapeutic proteins and to treat non-CNS (central nervous system) organs, a peripheral tolerization protocol reported previously for Niemann-Pick disease mice (97) was employed in one of the SD cats (7-589). Cat 7-589 was treated first by intravenous injection of 5.0×10^{12} genome equivalents (g.e.)/vector/kg of AAV8 vectors expressing the human Hex subunit-Tat fusion proteins from a liver-restricted enhancer/promoter (DC172 (98)). Two weeks following intravenous treatment, cat 7-589 was treated identically to cat 7-588. Due to the limited availability of SD cats, control treatments of cyclosporine or peripheral tolerization alone were not performed.

AAV-treated cats 7-588 and 7-589 lived to 7.0 and 8.2 months, respectively, compared to a humane endpoint of 4.5 ± 0.5 months for untreated SD cats (n=11). Although treated animals progressed through disease stages typical of untreated SD cats, they acquired symptoms at older ages (Figure 1b). At end point, both AAV-treated cats expressed brain MUGS activity between 25-30% normal at the injection site, which diminished to 5-13% normal at 1 cm anterior to the injection site. In addition, HPTLC documented mild to moderate decreases in GM2 ganglioside storage (16.3% - 32.9%) at the injection site with increased GM2 storage (19.5% - 36.3%) in adjacent brain blocks, compared to an untreated SD cat. Similarly, GA2 ganglioside levels decreased by up to 55.1% at the injection site or increased slightly in adjacent blocks (Figure 1c).

Though routine histopathology with H&E staining revealed no clear evidence of a

cellular infiltrate in the brain of cats 7-588 and 7-589 (not shown), both animals demonstrated pronounced serum antibody titers against the AAV1 vectors (Table 1) and purified human HexA enzyme (Fig. 2). While undetectable in pre-treatment samples, serum antibody titers against the AAV1 vectors were 1:65,536 and 1:24,576 at the humane endpoint for cats 7-588 and 7-589, respectively. Also, serum titers against semi-purified human HexA were 1:8,192 and 1:27,307 for cats 7-588 and 7-589, respectively, demonstrating a pronounced immune response to the human transgene product. To further investigate the immune response after AAV gene therapy in the cat brain, 4 additional SD cats and 4 normal cats were injected with vectors expressing the human Hex subunits with or without C-terminal Tat fusions (Table 1). For all SD cats and 2 normal cats, brain and other tissues were collected 1.4 - 2.1 months post-injection and analyzed for enzymatic activity and evidence of an immune response. The 2 remaining normal cats (9-1252, 9-1253) were observed for behavioral signs of vector toxicity for 14.3 and 12.2 months, respectively, before tissues were collected. No treated cats in this study, including those followed for over 1 year, demonstrated any clinical signs of vector toxicity.

As with cats 7-588 and 7-589, subsequent AAV1-treated cats had pronounced serum antibody titers to the vector and to human HexA (Table 1 and Fig. 2, respectively). In AAV-treated normal cats, serum titers to vector ranged from 1:16,384 – 1:262,144 while in AAV-treated SD cats, anti-vector serum titers ranged from 1:65,536 – 1:196,608. The difference in serum titers to the vector between AAV-treated normal and SD cats did not achieve statistical significance ($p=0.051$). In contrast, serum antibodies against the human HexA enzyme were statistically lower in AAV-treated SD versus normal cats ($p=0.011$; range, 1:1,024 – 1:5,120 v. 1:8,192 – 1:87,381). When cat 7-589 was omitted from the SD group (because it was pre-treated by IV injection of vector as described above), significance of the lower serum titers to HexA in

SD cats increased slightly ($p = 0.009$).

After high serum antibody titers to human HexA were documented in AAV-treated cats, feline HEXA and HEXB cDNAs were cloned for use in future therapeutic experiments and have been assigned GenBank accession numbers JF899596 and JF899597, respectively. Because high serum titers were also documented to the AAV1 vectors (presumably the capsid protein), feline Hex vectors were produced using a different serotype (AAVrh8). As demonstrated in Fig. 3a and Table S2, feline Hex α and β subunit cDNAs were functional in immortalized fibroblasts from a SD cat (89) transduced with AAVrh8-fHEXA/B vectors at 3 different doses. For all doses tested, activity with the HexA-selective MUGS substrate was highest after co-expression of both α and β subunits and ranged from 97.7 – 3,817.8 nmol/mg/hr (0.8 – 30.3 fold normal, $p=0.043$ when compare to the β subunit alone). MUGS activity for untreated SD cells or immortalized fibroblasts from a normal cat was 4.9 ± 4.2 or 125.9 ± 28.8 nmol/mg/hr, respectively. Because MUGS substrate can be cleaved at low levels by HexB (in cats) and HexS, ion exchange chromatography was used to calculate the relative production of each isozyme. The ratio of HexA:HexB was 0.14 after expression of the β subunit alone and 1.57 when α and β subunits were co-expressed (Fig. 3b, $p=0.002$). No HexS was detected after either treatment.

Having demonstrated in vitro functionality of the feline HEXA and HEXB cDNAs, a 1:1 formulation of AAVrh8-fHEXA/B vectors was injected into 4 heterozygote cats to test functionality and immunogenicity in the brain (Table 1). Because therapeutic benefit in SD mice was most dramatic after treatment of the thalamus and DCN, (85, 86) heterozygote cats were treated by the same routes in preparation for eventual experiments in SD cats. Three of the cats received bilateral injections of the thalamus and DCN and were euthanized 1.1 months post-treatment (7-705, 7-710) or 21 months post-treatment (7-708). Because it was reasoned that

behavioral evidence of vector toxicity would be most apparent after a unilateral injection, 1 cat (7-707) was injected singly in the right thalamus, and tissues were collected 4.1 months post-surgery.

AAVrh8-fHEXA/B vectors generated high levels of enzymatic activity after injection into the SD heterozygote cat brain (Table 2). In the cerebrum, mean MUGS activity was 71.3 fold normal at the thalamic injection site, ranging from 39.8 to 127.4 fold normal in 4 individual cats. Over the ~2.5 cm length of the cat cerebrum, mean MUGS activity diminished with increasing distance from the injection site, yet remained > 3-fold normal at the frontal pole of the brain (1.8 cm anterior to the injection site) and > 10-fold normal in the posterior most block (occipital lobe, 0.6 cm posterior to the injection site). MUGS activity in the cerebellum mimicked that in the cerebrum, with a mean activity of 40.4 fold normal at the DCN injection site, decreasing to 10.7 fold normal in the anterior-most cerebellar block (0.6 cm from injection, data not shown).

After in vivo functionality was demonstrated in heterozygote cat brains, AAVrh8 vectors expressing feline Hex were used to treat 3 SD cats by bilateral thalamic injections. To maximize therapeutic benefit, SD cats were injected pre-symptomatically at ~ 4 weeks of age with a total dose of 3.2×10^{12} g.e. (Table 1). As shown in Fig. 4a, mean life span for SD cats treated with the feline Hex subunits more than doubled (10.4 ± 3.7 months) and was significantly increased compared to untreated controls (4.5 ± 0.5 months, $p=0.0064$, log-rank test). Perhaps the best evidence of therapeutic effect is that the clinical rating scale developed for untreated SD cats (Fig. 1b) was not applicable to AAV-treated SD cats. For example, AAV-treated cats did not acquire fine or whole body tremors, and their initial and primary disease symptom was hind limb weakness, which had not been appreciated fully in untreated SD cats. In fact, 2 of the treated SD

cats were euthanized due to hind limb weakness so pronounced that they were unable to stand, thus triggering the predetermined humane endpoint. The third SD cat was quite ambulatory at endpoint but was euthanized due to substantial weight loss (>20% maximal body weight), and at necropsy was found to have gross distension of the urinary bladder and fecal impaction. Soft-tissue compression of the spinal cord in the caudal cervical/rostral thoracic region was documented at necropsy in the 2 cats with pronounced hind limb weakness (7-856, 7-879), but not in the third SD cat with substantial weight loss (7-885).

In SD cats treated bilaterally in the thalamus, Hex activity detected by postmortem histochemical staining spanned the entire cerebrum from occipital to frontal poles, though distribution was not uniform and appeared as gradients of staining intensity that diminished with distance from the injection site (Fig 4b-d). Mean MUGS activity was 8.6 ± 1.5 fold normal at the thalamic injection site and decreased to 0.8 ± 0.3 fold normal at the frontal pole (1.8 cm anterior to injection site, Table 2).

No clinical evidence of vector toxicity was observed in any cat treated with intracranial AAV gene therapy, even those living beyond 1 year post-treatment. However, profound vascular cuffing was observed in the brains of normal cats treated with AAV1 vectors expressing human Hex subunits (both Tat fusions and wild-types, Fig. 5a). The cellular infiltrate consisted primarily of CD20+ B lymphocytes, with CD4+ T helper cells comprising less than 2% of the infiltrate and dispersed at low levels throughout the brain parenchyma (not shown). A reliable antibody to feline CD8 was not available, so potential infiltrates of cytotoxic T cells were not evaluated. None of the 7 cats injected with AAVrh8 vectors expressing feline Hex subunits demonstrated any behavioral or histological evidence of toxicity. Specifically, no vascular cuffing was apparent in cats treated with AAVrh8-fHEX vectors. When humoral immunity was

evaluated, heterozygote and SD cats treated with AAVrh8-fHEX vectors had notable serum antibody titers to the vectors (1:4,096 - 1:32,768 and 1:1,024 - 1:3,072, respectively; Table 1). While anti-vector serum titers appear lower after treatment with AAVrh8 vectors than with AAV1 vectors, statistical significance cannot be evaluated with current cohorts and animal numbers. Though purified feline HexA was unavailable, no antibody titers were documented when sera from AAVrh8-treated heterozygotes were tested against human HexA or a feline β subunit-specific 14-mer peptide (fHEXB 240 (89)).

The only consistent histological abnormality in cats treated with AAVrh8-fHEX vectors was the presence of strongly eosinophilic neurons with granular to botryoid intracytoplasmic inclusions (Fig 5b). Eosinophilic neurons usually appeared in discrete locations within the dorsal thalamus/hippocampus and/or cerebellar Purkinje cells, and the density of such neurons correlated with Hex specific activity (i.e., brain blocks with the highest Hex activity generally had the highest numbers of botryoid neurons, Table S3). Immunofluorescence confirmed that the strongly eosinophilic neurons expressed high levels of Hex, which appeared to be vesiculated within the neurons (Fig 5c). Endogenous Hex levels in normal cat brain were below the limit of detection of the immunofluorescence assay (data not shown). Table 3 summarizes the immune-related and histological findings for each treatment group in the current study.

Discussion

This study documents extraordinary levels of serum antibodies to both AAV1 and AAVrh8 vectors in normal and SD cats after direct brain injection, though pretreatment titers were $\leq 1:32$ in all cats tested. Maximum titers to AAV1 were at or above $\sim 1:200,000$ in both SD and normal cats, while the highest titer to AAVrh8 was $\sim 1:33,000$. Differences in humoral and

cellular immune responses were detected between phenotypically normal and SD cats. Though both groups clearly generated serum antibodies to human HexA after AAV1 treatment, titers in normal cats (mean = 1:45,739) were statistically higher than those in SD cats (mean = 1:3,584; $P = 0.009$). Also, brains of normal cats treated with vectors expressing human Hex had marked cellular infiltrates apparent as vascular cuffs consisting primarily of B lymphocytes, while SD cats treated with the same vectors demonstrated little or no infiltrate. A differential immune response to the same AAV vectors may result from immune defects in affected animals, such as premature thymic involution caused in part by a ganglioside-mediated apoptotic cascade, as reported in cats with GM1 gangliosidosis (99-101) and in SD mice (102, 103) and cats (unpublished data). Though decreased thymus size is measurable only in late-stage disease, increased thymocyte apoptosis and other changes are present in early to middle disease stages, perhaps contributing to the diminished immune response of AAV-treated SD cats. It is possible that immune deficiencies in feline SD facilitate treatment response due to a reduced immune reaction to the therapeutic agent, and therefore it will be important to evaluate whether AAV treatment normalizes immune function through central or peripheral mechanisms. AAV vector and AAV-generated lysosomal enzyme have been detected in peripheral tissues after intracerebral treatment in animal models, (104, 105) demonstrating that AAV injected into the brain may also have peripheral effects.

Despite strong humoral immunity to both the AAV1 vectors and human HexA protein, therapeutic benefit was demonstrated in 2 SD cats treated by bilateral thalamic injection, with an extension of lifespan from 4.5 months (untreated) to 7.0 and 8.2 months. Though treated in the early post-symptomatic period, both cats demonstrated delayed disease progression (Fig. 1b) and improved quality of life. It is well accepted that treatment of lysosomal storage diseases is most

beneficial when performed early, preferably before the onset of disease (106). Though rare, reports of symptom reversal post-treatment have been published, as in the feline model of α -mannosidosis (107). Similarly, demonstration of substantive therapeutic benefit in post-symptomatic SD cats in the current study is encouraging for the treatment of children with GM2 gangliosidosis, most of whom are diagnosed after the onset of clinical disease.

Because initial experiments demonstrated high serum titers to the AAV1 vectors and purified human HexA, second-generation vectors incorporated the AAVrh8 capsid and feline HEXA/B cDNAs. AAVrh8 vectors used to transduce fibroblasts from a SD cat demonstrated that maximal Hex activity is achieved by co-expression of both subunits versus replacement of a single subunit alone, at 3 different doses over a 16-fold range. MUGS activity in cells expressing both subunits was 4.2-fold higher than with the β subunit alone. Also, the ratio of HexA to HexB after co-expression of both subunits was ~11-fold higher than with expression of the β subunit alone. Since HexA is solely responsible for degradation of GM2 ganglioside in humans, the findings are an important consideration when designing human clinical trials to be minimally invasive yet achieve the widest possible distribution of HexA throughout the brain. If optimal production of HexA is achieved at target sites chosen to provide maximal neuronal interconnectivity between brain regions (e.g., the thalamus), fewer brain injections should be required for therapeutic effect. On the other hand, supranormal HexA levels after subunit co-expression from a strong promoter (CBA) must not be toxic to the cells that express it.

When phenotypically normal cats were injected with AAVrh8 vectors expressing feline Hex, MUGS activity was >3-fold normal throughout the cerebrum (Table 2) and >10-fold normal throughout the cerebellum (not shown). Cats were followed for ~ 1, 4 and 21 months post-treatment, and none showed any clinical evidence of surgery- or vector-related toxicity.

Unlike AAV1-hHEX vectors, perivascular cuffing in the brain was absent after AAVrh8-fHEX treatment. Since the choice of AAV capsid can alter the immune response to the same transgene product (reviewed in (108)), reduced immunity in cats expressing feline Hex may have resulted from a combination of species-specific enzyme and rh8 capsid. Though evidence of a cellular immune response was minimal, discrete regions of strongly eosinophilic neurons were found to express extraordinary levels of Hex in intracellular vesiculated bodies, and the density of these bodies correlated generally with brain blocks having the highest Hex activity. Other studies have documented brain toxicity after AAV-mediated overexpression of proteins such as green fluorescent protein (GFP) or tau (109, 110), manifested by neuron loss and clinical symptoms. However, no evidence of neuron loss or clinical neurological signs was found in treated cats in the current study, even those living >1 year post-injection.

This is the first report of clear therapeutic benefit from any treatment modality in a non-rodent model of GM2 gangliosidosis, with cats having a brain that is intermediate to mice and humans in complexity and size (~20-fold smaller than the brain of a human infant). In the >35-year history of the feline SD breeding colony, no experimental treatment has shown unequivocal therapeutic benefit, as reported herein for AAVrh8-fHEX vectors delivered in a surgery requiring only 2 injection sites and ~90 minutes to perform. In the past decade, the longest-lived untreated SD cat was 5.3 months at humane endpoint, so the average 10.4-month life span of treated cats in the current study is a significant advance ($p=0.0064$) and provides real hope for future human therapy. In addition to increased longevity, quality of life was dramatically improved for animals treated with feline Hex, as demonstrated by the absence of debilitating, whole-body tremors. In many respects, AAV treatment converted the severe, infantile-onset phenotype in SD cats to a later-onset form of the disease described in humans, both of which

exhibit muscle wasting, limb weakness and intestinal dysfunction (*III*). It is hypothesized that partial restoration of enzyme activity in treated cats mimics the residual Hex activity of late-onset human patients, moderating CNS dysfunction and permitting the emergence of otherwise subclinical peripheral disease. These results encourage further optimization of therapy, including development of a bicistronic vector encoding Hex α and β in the same construct to ensure optimal HexA expression distal to the injection site, where co-transduction of cells with monocistronic vectors may not occur due to reduced vector concentration. In addition, improved enzyme distribution throughout the brain is needed. Though normal or above normal in most brain regions after thalamic infusion of vector, Hex activity was minimal in the temporal lobe and cerebellum (Fig. 4d). Therefore, additional injection sites are expected to provide enhanced therapeutic benefit, as is being borne out in ongoing experiments.

Materials and methods

Cloning of feline Hex α and β subunit cDNAs Sequences for the feline Hex α subunit (HEXA) and β subunit (HEXB) open reading frames have been deposited in the GenBank database and assigned accession numbers JF899596 and JF899597, respectively.

With cDNA prepared from cat cerebral cortex, feline HEXA cDNA was amplified using primers ORFc1 and ORFn1 (Table S4) according to standard protocols with Taq DNA polymerase. The fHEXA PCR product was purified with the QIAquick PCR purification kit (Qiagen, Valencia, CA), polished for 30 minutes at 72°C with 2.5 units of Taq and 0.5mM each dNTP, then cloned into plasmid pcDNA3.3-TOPO (Invitrogen, Grand Island, NY). The fHEXA insert was ~1.8 kb.

A previously published feline HEXB cDNA (GenBank no. S70340(*II2*)) is truncated at

the 5' end by only 4 base pairs. From S70340, gene assembly primers 5.1 – 5.6 (Table S4) were designed using DNAWorks (<http://helixweb.nih.gov/dnaworks>)(113) to generate the appropriate amino acid sequence of the 5' end using codons chosen to reduce the GC content of the fragment. The gene assembled product was amplified with primers 5.7 (coding strand) and 5.8 (noncoding strand), which contain flanking *Nhe*I and *Bsm*BI restriction sites, respectively. The remainder of the feline HEXB sequence was amplified from plasmid fHEXB#2 (89), containing a clone truncated at the 5' end by ~95 bp, using primers fHEXB-3 and fHEXB2-NotI, which contain *Bsm*BI and *Not*I restriction sites, respectively. The gene assembled 5' end of fHEXB was joined to the remainder of the fHEXB cDNA by restriction digestion with *Bsm*BI.

AAV vectors AAV vectors and their abbreviations are listed in Table S1. AAV1 vectors containing human HEXA/B cDNAs with 3' Tat fusions have been described previously (85). For liver targeted expression in cat 7-589, the vectors referenced above were modified by substituting the AAV8 capsid in place of AAV1 and the DC172 promoter (114) in place of the CAG promoter. Vectors containing wild-type (without Tat) cDNAs were constructed as follows. Human HEXA and HEXB cDNAs were PCR amplified from Mammalian Gene Collection (MGC) clones 14125 (IMAGE ID: 3353424; Genbank ID: BC018927) and 1725 (IMAGE ID: 2967035; Genbank ID: BC017378) obtained from the American Type Culture Collection (Manassas, VA) using primer pairs hHexA-1+hHexA-2 and hHexB-1+hHexB-2, respectively, which introduce *Spe* I and *Xho* I sites flanking the coding region. The feline HEXA cDNA was amplified with primers fHexA-1 and fHexA-4 that introduce *Nhe* I and *Not* I sites flanking the coding region. The feline HEXB cDNA was amplified in two fragments as indicated above. All PCR products were cloned into pAAV-CBA-MBG-W (115) in place of the mouse β gal cDNA.

Transgene expression in these vectors is mediated by the hybrid CBA promoter (comprised of the CMV immediate-early enhancer fused to the chicken beta-actin promoter (116)) and the woodchuck hepatitis virus post-transcriptional regulatory element (WPRE). AAV1 and AAVrh8 vector stocks encoding wild-type human or feline HEX subunits were produced as previously described (117).

Animals and surgeries All animal procedures were approved by the Auburn University Institutional Animal Care and Use Committee. Table 1 summarizes all AAV-treated cats. In untreated SD cats, neurological disease onset occurs at 1.7 months of age with a slight head tremor that progresses to an inability to stand (humane endpoint) by 4.5 ± 0.5 months (mean \pm standard deviation, n=11). Disease progression was scored from 10 (normal) to 1 (lateral recumbency) according to a clinical rating scale developed for untreated SD cats (Fig. 1b). Animals at an intermediate stage of disease progression were assigned a half-integer score (e.g., 5.5). Affected animals express 9.2 – 22.1% of normal levels of the Hex β subunit protein, which contains 3 amino acid substitutions at the carboxyl terminus of the protein and a translational stop that is 8 amino acids premature (89).

Cats were anesthetized with ketamine (10 mg/kg) and dexmedetomidine (0.04 mg/kg) using an intravenous catheter and maintained with isoflurane (0.5-1.5%) in oxygen delivered through an endotracheal tube. Stereotaxic delivery of vector was performed using a Horsley-Clark stereotaxic apparatus (David Kopf Instruments). Coordinates (in cm) for the thalamus relative to bregma were AP -0.7, ML \pm 0.4, DV -1.6, and for the deep cerebellar nuclei (DCN) relative to lambda were AP 0.0, ML \pm 0.4, DV -1.25. The DV zero point was marked at meninges. The thalamus was injected either unilaterally or bilaterally with or without bilateral

injection of the DCN. Single entry sites above each thalamus were made through the skull and dura with a 20G hypodermic needle. For DCN injections, craniotomy was performed directly above the target by inserting the needle vertically (i.e., at an angle perpendicular to the base of the stereotaxic apparatus) through the skull and then through the cerebellar tentorium, passing just caudal to the occipital pole of the cerebrum.

Vector was delivered using a Hamilton syringe (Harvard Apparatus, Holliston, MA) with a non-coring needle (22-25G). In each thalamus, 70 μ l was delivered in 10-20 μ l aliquots at a rate of 2 μ l/min. Between each aliquot, the injection needle was raised 0.15 cm, so that the final needle position was 1.15 cm ventral to meninges (~ 2.5mm ventral to the lateral ventricle). For each DCN, a total of 20 μ l was injected at a single site at a rate of 2 μ l/min.

Tissue and serum analysis After euthanasia by pentobarbital overdose (100 mg/kg), animals were transcardially perfused with cold, heparinized saline. Each brain was divided into coronal blocks of ~0.5cm from the frontal pole through the cerebellum. Tissues were processed as appropriate for each type of downstream analysis.

Prior to immunostaining on 6 μ m paraffin sections, antigen unmasking was performed by heat treatment in Tris-EDTA buffer (10 mM Tris, 1 mM EDTA, 0.05% Tween 20, pH 9.0), and sections were blocked for 1 hour with 5% normal donkey serum in PBS containing 0.05% Tween 20. Sections were stained with a monoclonal antibody to the feline Hex β subunit (89) (1:1,000) followed by 488-conjugated donkey anti-mouse IgG (Jackson Immuno Research, West Grove, PA, 1:100).

For serum antibody titers, 100 ng of AAV vectors or purified human HexA (Sigma, St. Louis, MO) were coated onto ELISA plates (Nunc, Rochester, NY) and incubated overnight at

4°C. Plates were washed and then blocked with 5% nonfat powdered milk in PBS for 90 minutes at room temperature. One hundred microliters of two-fold serial dilutions of feline serum samples were added. Goat anti-feline IgG:HRP (Jackson ImmunoResearch, West Grove, PA, 1:20,000) was used for color development with tetramethylbenzidine (Pierce, Rockford, IL).

Brain lipid analysis As described in greater detail previously, (96) total lipids were extracted with chloroform (CHCl₃) and methanol (MeOH) 1:1 by volume and purified from the lyophilized brain tissue (118-120). Neutral and acidic lipids were separated using DEAE-Sephadex (A-25, Pharmacia Biotech, Upsala, Sweden) column chromatography (121). The total lipid extract was applied to a DEAE-Sephadex column after suspension in solvent A (CHCl₃:CH₃OH:dH₂O, 30:60:8 by volume), which also was used to collect the neutral lipid fraction containing sphingomyelin and neutral GSLs to include asialo-GM2 (GA2). Next, acidic lipids were eluted from the column with CHCl₃:CH₃OH: 0.8 M Na acetate (30:60:8 by volume), dried by rotary evaporation and then partitioned so that acidic lipids were in the lower organic phase and gangliosides were in the upper aqueous phase (122-124). The resorcinol assay was used to measure the amount of sialic acid in the ganglioside fraction, which then was further purified with base treatment and desalting. Neutral lipids were dried by rotary evaporation and resuspended in CHCl₃:CH₃OH (2:1 by volume). To further purify GA2, an aliquot of the neutral lipid fraction was evaporated under a stream of nitrogen, treated with 1 N NaOH, and Folch partitioned (120).

All lipids were analyzed qualitatively by high-performance thin-layer chromatography (HPTLC) with an internal standard (oleoyl alcohol) added to the neutral and acidic lipids to enhance precision (120-122, 125). Purified lipid standards were either purchased from Matreya

Inc. (Pleasant Gap, PA), Sigma (St. Louis, MO), or were a gift from Dr. Robert Yu (Medical College of Georgia, Augusta, GA). HPTLC plates were developed, visualized and quantitated as described (96) (120). The total brain ganglioside distribution was normalized to 100% and the percentage distribution used to calculate sialic acid concentration of individual gangliosides (119). The density value for GA2 was fit to a standard curve of known lipid to calculate concentration.

Cell culture and transfection Fibroblasts immortalized with the Simian Virus 40 large T antigen were generated using primary skin cultures from SD (GM2/SV3 cells) or normal cats (N/SV3 cells) and have been described elsewhere (89, 126). Transfection was performed in 6-well plates or 25 cm² flasks with cells at 25-50% confluency using AAVrh8 vectors expressing feline HEXA or HEXB cDNAs. Doses in genome equivalents (g.e.)/ vector/cell were calculated based on cell count, and vector was incubated for 3-5 days with cells in standard growth media (Dulbecco's modified Eagle medium, 4.5 g/L glucose; 10% fetal bovine serum; 100 units/ml penicillin, 0.1 mg/ml streptomycin and 0.25 µg/ml amphotericin B).

Enzyme assays and staining Lysosomal enzyme activity was determined according to a previously published protocol(40) with the appropriate 4-methylumbelliferyl (4MU) substrates: β-galactosidase (βgal), 0.5 mM 4MU-N-acetyl-β-D-glucosaminide, pH 3.8; HexA, 1mM 4-MU 6-sulfo-2-acetamido-2-deoxy-β-D-glucopyranoside (MUGS), pH 4.2; and total Hex, 1mM 4MU-N-acetyl-β-D-glucosaminide (MUG), pH 4.3. Fluorescence of the samples was measured on a BioTek Synergy HT plate reader with excitation at 360nm and emission at 450nm. Protein concentrations were measured by the method of Lowry, and specific activity was expressed as

nmol 4MU cleaved/mg protein/ hour. Qualitative detection of Hex activity in the brain was performed on 40 μ m cryosections with 0.25 mM naphthol AS-BI-N-acetyl- β -D-glucosaminide (Sigma, St. Louis, MO) in the presence of hexazotized pararosaniline (127).

DEAE cellulose anion exchange chromatography Lysosomal enzymes were isolated from frozen brain tissue in a 10 mM sodium phosphate buffer (pH 6.0) containing 0.1% Triton-X 100. Tissue homogenate was centrifuged at 15,000G for 20 minutes at 4°C and filtered at 0.2 μ m. Supernatant was applied to a DEAE cellulose column (Sigma, St. Louis, MO) and fractions 1-3 were collected (0.5 ml each). A total of 26 fractions (0.5 ml each) were collected by washing the column with buffer (above) containing sodium chloride at increasing concentrations ranging from 0-400 mM, as follows: fractions 4-8 (0 mM), 9 (10 mM), 10 (20 mM), 11-24 (increasing concentrations of 20 mM each, from 40-300 mM), 25-26 (350 and 400 mM, respectively). Lysosomal enzyme activity of the fractions was determined as described above.

Statistical analysis Serum antibody titers to vector or human HexA protein were analyzed for significance by Wilcoxon Two-Sample Test and survival data was created using the Lifetest procedure and Log-Rank Test with SAS software. Significance of HexA activity and HexA:HexB ratios was determined with a 2-tailed T test.

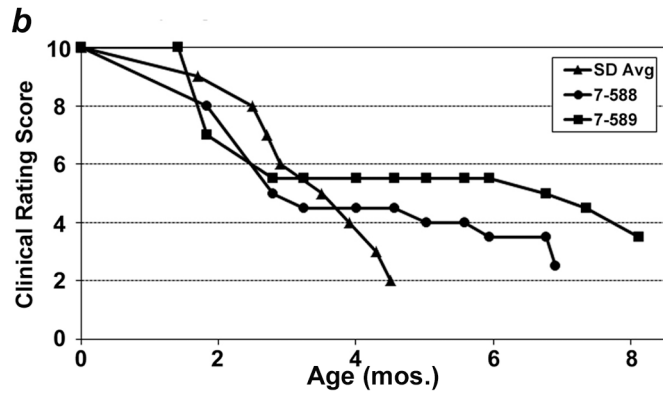
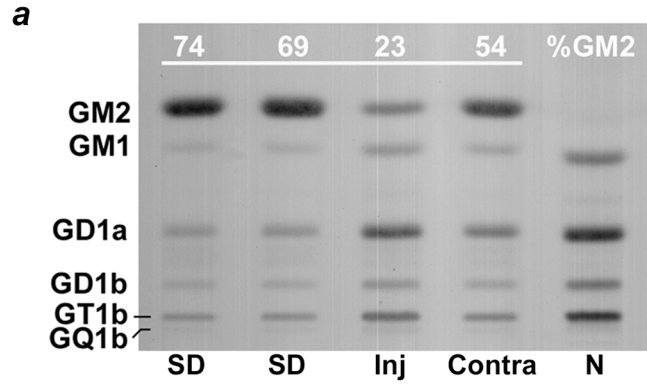
Figures and Tables

Table 1. AAV-Treated Cats and Corresponding Serum Antibody Titers to the Vectors

Cat	Tx Age (mos.)	Duration (mos.)	Tat (+/-)	Genotype	Total dose ^a (both vectors)	Serum titer (vector)
HUMAN HEX VECTORS (AAV1)						
7-532	1.0	1.5	+	SD	3.0×10^{11}	1:98,304
7-588	1.8	5.2	+	SD	1.3×10^{12}	1:65,536
7-589 ^b	1.8	6.7	+	SD	1.3×10^{12}	1:24,576
7-632	1.8	1.5	+	SD	5.4×10^{11}	1:65,536
7-635	2.6	1.4	+	SD	5.4×10^{11}	1:196,608
7-633	1.9	1.4	-	SD	5.4×10^{11}	1:196,608
7-634	2.5	1.4	-	SD	1.3×10^{12}	1:196,608
9-1252	3.1	14.3	+	Normal	7.6×10^{11}	1:196,608
9-1255	3.8	1.8	+	Normal	7.6×10^{11}	1:24,576
9-1253	3.5	12.2	+	Normal	7.6×10^{11}	1:262,144
9-1254	3.5	2.1	+	Normal	7.6×10^{11}	1:16,384
FELINE HEX VECTORS (AAVrh8)						
7-705	1.5	1.1	-	Carrier	4.2×10^{12}	1:32,768
7-710	1.6	1.1	-	Carrier	4.2×10^{12}	1:32,768
7-707	1.8	4.1	-	Carrier	1.6×10^{12}	1:4,096
7-708	1.6	21.0	-	Carrier	4.2×10^{12}	1:4,096
7-856	0.9	6.2	-	SD	3.2×10^{12}	1:3,072
7-885	1.0	11.8	-	SD	3.2×10^{12}	1:1,024
7-879	1.1	13.2	-	SD	3.2×10^{12}	1:2,048

^a Monocistronic vectors were combined and injected in a 1:1 ratio, except for 7-532, which received a 1:2 ratio (A:B). Vector designations: Tat (+), AAV2/1-hHEXA (or hHEXB)-Tat; Tat (-), AAV2/1-hHEXA (or hHEXB). All cats treated by injection of the right thalamus except for 7-588, 7-589, 7-856, 7-885, 7-879 (bilateral thalamic injection) and 7-705, 7-710 and 7-708 (bilateral injection of thalamus and DCN).

^b Pretreated by IV injection at 6.1 weeks with AAV2/8-DC172-hHEXA(or hHEXB)-Tat-WPRE (5×10^{12} g.e./vector/kg). The DC172 liver-targeted promoter has been described previously²⁰.



Score	Clinical Status	Age (mos.)
10	Normal	<1.6
9	Slight head tremor	1.7
8	Overt body tremor	2.5
7	Wide stance	2.7
6	Instability/falling	2.9
5	Can stand but not walk	3.5
4	Loss of hind limb weight bearing	3.9
3	Cannot enter litter box	4.3
2	Loss of fore limb weight bearing	4.5
1	Lateral recumbency	>4.5

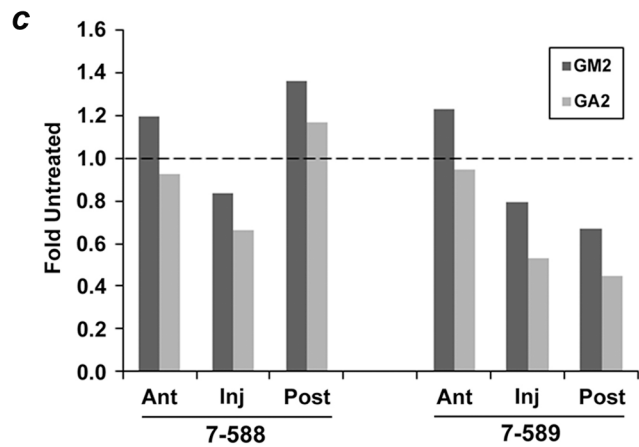


Figure. 1 Therapeutic benefit of human Hex expressed from an AAV1 vector in SD cats. (a)

Cat 7-532 was injected in the right thalamus with a 1:2 ratio of AAV1-CAG-hHEXA/B-Tat-WPRE (A:B = 1×10^{11} g.e.: 2×10^{11} g.e., Table 1). Tissue was collected 6 weeks post-injection, and GM2 storage was analyzed by high performance thin layer chromatography. Shown are samples from the injected thalamus (Inj), the contralateral thalamus (Contra), and corresponding sections from untreated SD and normal (N) cats. GM2 levels were quantitated densitometrically and expressed as a percentage of total ganglioside on the plate (%GM2). Gangliosides were identified by comparison to known standards and labeled accordingly. The absence of a prominent GM2 band in the normal control lane caused a slight migration shift for GM1 and other bands. (b) Two SD cats treated for long-term follow-up (7-588, 7-589) had delayed disease progression and increased life span (7.0, 8.2 months, respectively). Prior to intracranial injection, cat 7-589 was treated by intravenous injection of AAV8 vectors with a liver-targeted promoter. Disease progression was scored according to a clinical rating scale developed for untreated SD cats, with average age of symptom acquisition compiled from 9 separate animals (SD Avg). (c) Total brain lipids were analyzed as in panel (a) from the injection site (Inj) and the adjacent anterior (Ant) and posterior (Post) blocks from AAV-treated cats 7-588 and 7-589 at humane endpoint. GM2 (dark bar) and GA2 (light bar) levels were compared to corresponding blocks of an untreated SD cat at its humane endpoint (4.3 months of age). Data for AAV-treated cats is expressed as “fold untreated”, with the untreated level indicated by a dashed line.

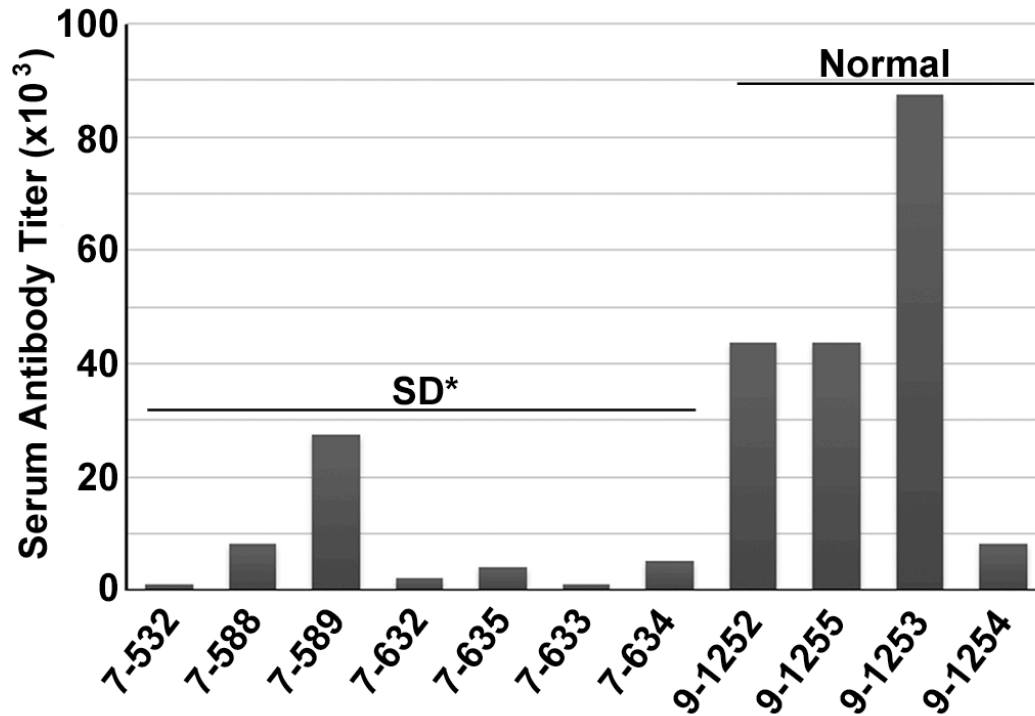


Figure. 2 Serum antibody titers to human HexA in AAV-treated cats. SD or Normal cats treated by intracranial injection of AAV vectors expressing human Hex were assayed at experimental or humane endpoint for serum antibodies to human HexA. AAV-treated SD cats had significantly lower titers compared to AAV-treated normal cats (* $p = 0.011$ with the inclusion of 7-589, or $p = 0.009$ with omission of 7-589, which was pretreated by IV injection prior to intracranial injection). Average titers of at least two assays are shown.

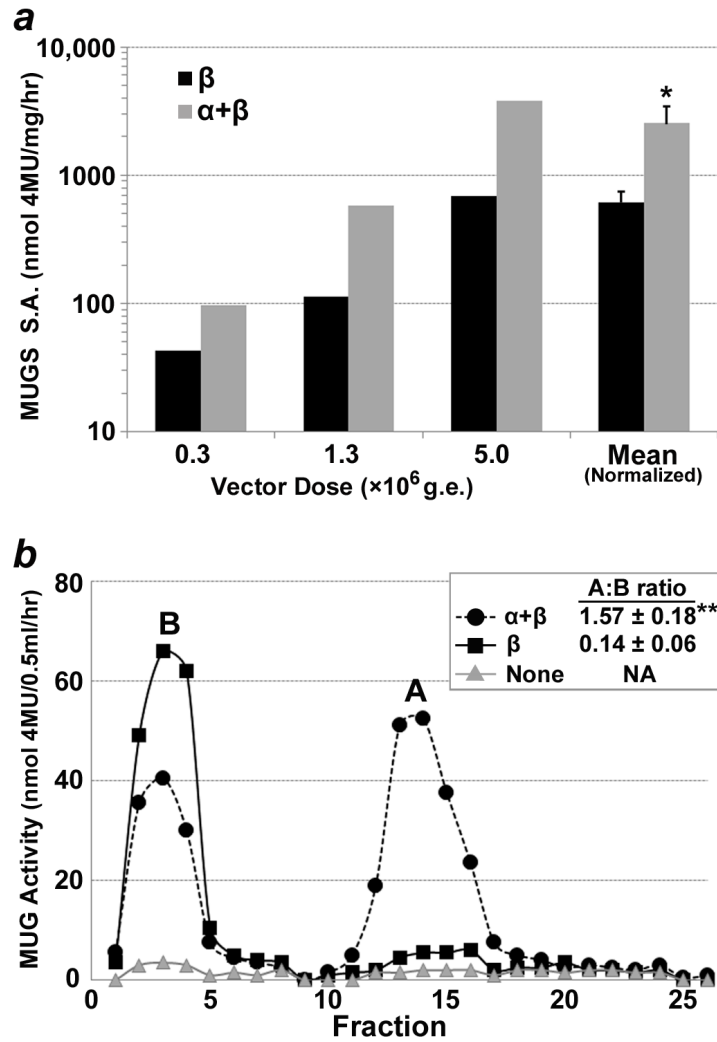


Figure. 3 HexA activity after expression of feline Hex α and β subunits. Immortalized skin fibroblasts from a SD cat were transduced with AAVrh8 vectors expressing the feline Hex subunits: α subunit alone, β subunit alone (β), or α and β subunits combined ($\alpha+\beta$). The vector dose per subunit remained constant, and 3 doses were tested: 0.3, 1.3 or 5.0×10^6 g.e./cell. (a) Specific activity was calculated for the MUGS (HexA preferred) substrate at each dose and plotted on a logarithmic scale. After normalization to vector dose, specific activities were averaged (Mean-Normalized) and found to be 4.2-fold higher after $\alpha+\beta$ co-expression than after β subunit expression alone (* $p = 0.043$). (b) DEAE cellulose anion exchange chromatography was used to separate HexA (A) and HexB (B) isozymes. Fractions of 0.5 ml eluates were

collected using a 0-400 mM NaCl gradient, and MUG substrate (cleaved by all Hex isozymes) was used to measure enzyme activity (nmol 4MU/0.5ml/hr). The total activity per isozyme was calculated by summing activities from fractions 1-8 (B) or 10-20 (A) and ratios of A:B were calculated for $\alpha+\beta$ (black circles) or β (black squares)(n=3 each). MUG activity was measured in untreated cells as a control (None, gray triangles). A:B ratios were statistically higher in cells treated with $\alpha+\beta$ (1.57) than with β alone (0.14) (**p = 0.002). HexS was not detected in any sample but generally elutes after fraction 20.

Table 2. Fold Normal Specific Activity in Heterozygote and SD Cat Cerebrum Post-AAV

Enzyme (Substrate)	Cats ^b	Brain Block, Distance From Injection Site (cm) ^a									
		A, +1.8		B, +1.2		C, +0.6		D, 0.0		E, -0.6	
HexA (MUGS)	Het.	3.2	(1.7)	3.2	(1.6)	4.8	(2.6)	71.3	(38.7)	10.2	(12.1)
	SD	0.8	(0.3)	0.8	(0.6)	2.8	(3.8)	8.6	(1.5)	ND^c	
Hex Total (MUG)	Het.	2.7	(1.3)	2.7	(1.2)	4.2	(2.5)	27.8	(9.6)	8.7	(9.5)
	SD	0.6	(0.2)	0.6	(0.4)	2.4	(3.2)	7.8	(1.2)	ND^c	
β Gal (MUGal)	Het.	0.6	(0.3)	1.1	(0.4)	1.1	(0.4)	2.0	(1.7)	1.5	(1.5)
	SD	1.0	(0.4)	1.1	(0.1)	1.2	(0.3)	1.3	(0.1)	ND^c	

^a Coronal brain blocks were collected at distances anterior (+) or posterior (-) to the thalamic injection site, and letter designations correspond to Fig. 4b. For each block, specific activities were calculated for HexA (MUGS), total Hex (MUG), and β -galactosidase (Bgal) and compared to untreated, normal cats to calculate the “fold normal” activity (\pm standard deviation). Normal cat specific activity in brain was as follows: HexA, 38.4 ± 10.0 ; total Hex, 670.9 ± 109.0 ; Bgal, 32.5 ± 11.4 nmol 4MU/mg/hr.

^b AAV-treated cats were either phenotypically normal heterozygotes (Het., n=4) or affected SD (n=3).

^c ND: Block was formalin fixed and not available for enzyme assay.

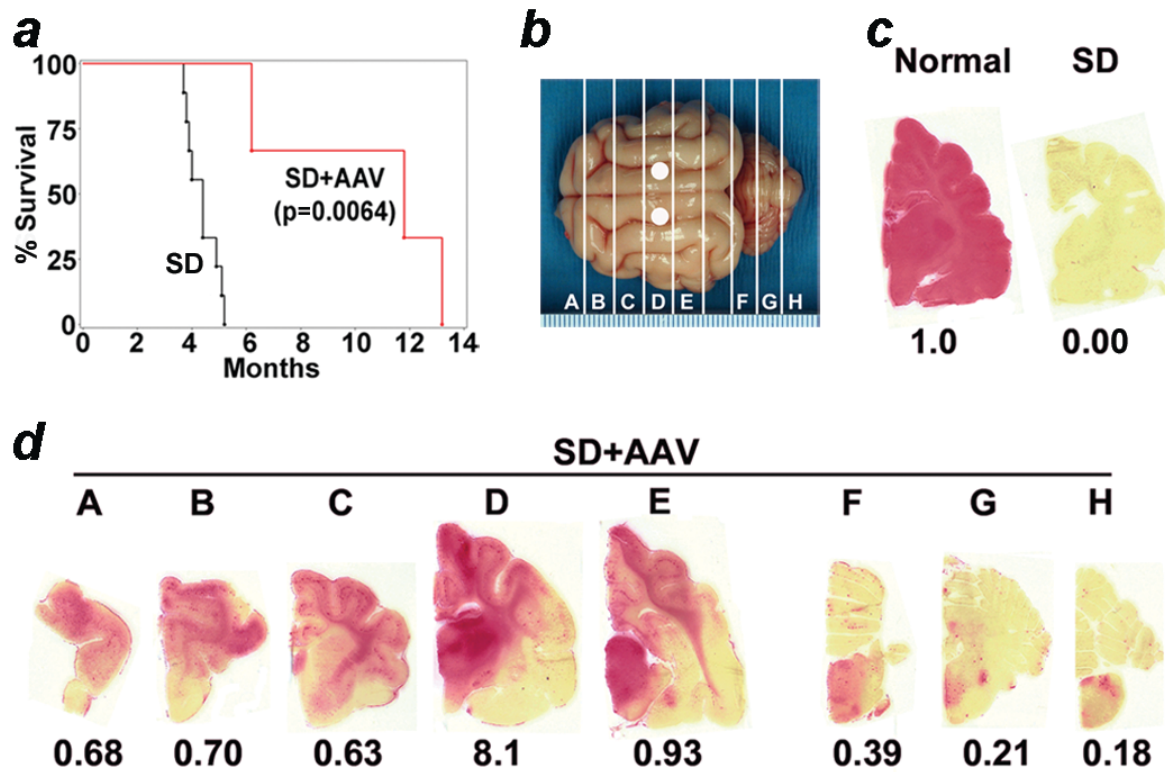


Figure. 4 Therapeutic benefit in SD cats after intra-thalamic injection of AAVrh8 vectors expressing feline Hex. SD cats (n=3) were followed to the humane endpoint after bilateral thalamic injection of AAVrh8-fHEX vectors (1:1 ratio of α : β ; total dose = 3.2×10^{12} g.e.). (a) Mean survival of treated SD cats (SD+AAV) was 10.4 months, a statistically significant increase compared to 9 untreated cats (SD; $p = 0.0064$, log-rank test). (b) Injection sites (white circles) and 0.6 cm coronal brain blocks (A-H) are shown. (c) Naphthol staining for Hex activity (red) is shown for untreated Normal and SD cat brains. The fold-normal Hex activity (measured by MUGS substrate) is listed below each brain block. (d) Naphthol staining for 1 representative AAV-treated SD cat (SD+AAV, 7-856) demonstrates Hex activity throughout the cerebrum (A-E) with minor activity in brainstem and cerebellum (F-H). MUGS activity ranged from 0.18- to 8.1-fold normal. Letter designations correspond to panel (b).

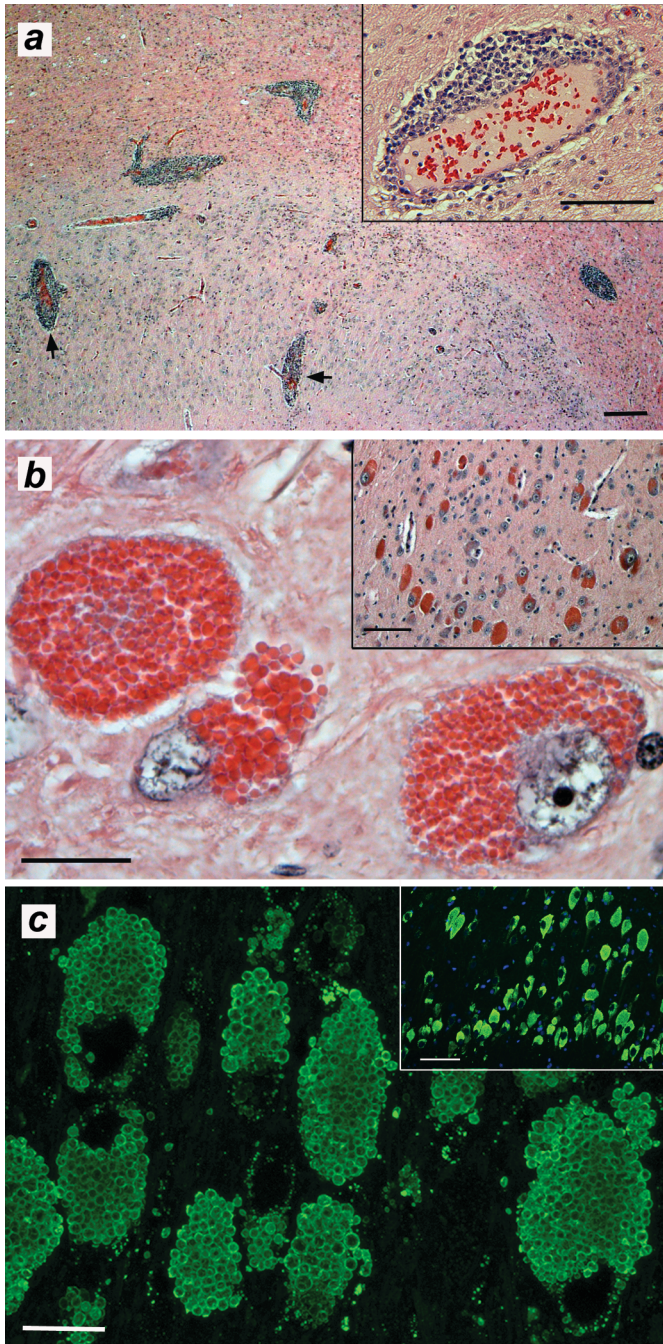


Figure. 5 Histological findings after AAV injection in the normal and SD cat brain. (a) Perivascular cuffing (black arrows) was apparent in the brains of normal cats expressing human Hex from AAV1 vectors, with greatest concentrations near the thalamic injection site. One representative cat (9-1254) is shown. Scale bar = 200 μm (inset = 100 μm). (b) Strongly eosinophilic neurons were observed in discrete areas of the brain (inset), corresponding to areas

of highest Hex activity. At high magnification, granular to botryoid intracellular inclusions were apparent. Scale bar = 20 μm (inset = 100 μm). The region of the dorsal thalamic nuclei from cat 7-708 is shown. (c) Immunofluorescence with a monoclonal antibody to the feline β subunit demonstrated that botryoid inclusions contained high levels of Hex (green). Dorsal thalamic nuclei of cat 7-708 were stained. Inset was taken with a standard fluorescence microscope with DAPI nuclear counterstain (scale bar = 100 μm). Main panel is a merged stack of 20 layers (6 μm total) from a confocal microscope (scale bar = 20 μm).

Table 3. Summary of Immune-related and Histological Findings

Vector	Genotype	Serum Antibodies		Vascular Cuffing	Eosinophilic, Botryoid Neurons
		Vector	Hex		
AAV1-hHex	Normal	+	+	+	-
	SD	+	+	+/- ^a	-
AAVrh8-fHex	Het.	+	ND	-	+
	SD	+	ND	-	+

* After AAV treatment, serum antibody titers against human Hex were lower in SD v. normal cats ($p = 0.009$).

^a +/-, Vascular cuffs were very rare and ≤ 5 cell layers thick.

ND = no data due to lack of purified feline Hex.

Table S1. AAV Vectors for Treatment of SD and Normal Cats

Vector^a	Abbreviation
AAV2/1-CAG-hHEXA-Tat-WPRE	AAV1-hHEXA-Tat
AAV2/1-CAG-hHEXB-Tat-WPRE	AAV1-hHEXB-Tat
AAV2/1-CBA-hHEXA-WPRE	AAV1-hHEXA
AAV2/1-CBA-hHEXB-WPRE	AAV1-hHEXB
AAV2/rh8-CBA-fHEXA-WPRE	AAVrh8-fHEXA
AAV2/rh8-CBA-fHEXB-WPRE	AAVrh8-fHEXB

^a Vector elements include the following: AAV2/1 or AAV2/rh8, HEXA or HEXB cDNAs were inserted into AAV2-based plasmids and pseudotyped with AAV1 or AAVrh8 capsids; CAG, human cytomegalovirus immediate-early enhancer and modified chicken β -actin promoter (and first intron) from plasmid pDRIVE-CAG (InvivoGen, San Diego, CA); CBA, similar to CAG, contains a CMV enhancer/chicken β -actin promoter derived from plasmid pTRUF12.1 (Matalon et al., *Mol Ther* 7:580-7, 2003); h, human; f, feline; Tat, protein transduction domain from human immunodeficiency virus-1; WPRE, woodchuck hepatitis virus post-transcriptional regulatory element.

Table S2. In vitro functionality of AAVrh8 vectors expressing feline HEXA or HEXB cDNAs

Sample/dose ^a	HexA			Total Hex			βgal		
	0.31	1.25	5.0	0.31	1.25	5.0	0.31	1.25	5.0
A	22.1	200.0	153.0	65.8	481.9	682.0	456.2	340.7	643.7
B	42.5	113.1	684.8	1716.6	5065.7	18,468.4	436.6	371.7	588.5
A+B	97.7	578.0	3,817.8	1724.4	5821.6	20,207.7	396.2	371.1	648.3
(-)	3.9	9.5	1.2	18.8	28.6	7.5	418.7	411.7	285.6
Normal	92.9	146.2	138.6	2588.3	2829.7	3,633.0	248.1	325.6	246.6
(A+B):B	2.3	5.1	5.6	1.0	1.1	1.1	0.9	1.0	1.1

^a Immortalized skin fibroblasts from a SD cat were transfected with AAVrh8 vectors at doses increasing by consecutive factors of 4 (0.31, 1.25 or 5.0×10⁶ g.e./vector/cell). Cells were transfected with vectors expressing fHEXA alone (A), fHEXB alone (B) or fHEXA+fHEXB (A+B). Three to five days later, cells were harvested for analysis of HexA (MUGS substrate), Total Hex (MUG substrate) or β-galactosidase (βgal) activity. Untreated SD (-) and untreated Normal immortalized fibroblasts were included as controls. Specific activity of each enzyme was compared after expression of fHEXA+fHEXB or fHEXB alone and the ratio expressed as (A+B):B.

Table S3. Correlation of Hex Activity with Neurons Containing Eosinophilic, Botryoid Inclusions^a

Block ^b	7-708		7-879		7-885		7-856	
	Eos. Neur ^c	MUGS ^d	Eos. Neur.	MUGS	Eos. Neur.	MUGS	Eos. Neur.	MUGS
B	+/-	3.8	+/-	0.3	-	1.4	-	0.7
C	+/-	5.3	+/-	0.5	-	7.2	+/-	0.6
D	++	53.5	++	7.5	+	10.3	++	8.1
E	++	24.1	+/-	ND	+/-	ND	-	0.9
G	+	68.1	+/-	0.5	+/-	2.7	-	0.2

^a -, negative; +/-, rare and scattered; +, regular but dispersed; ++, regular, discrete areas; +++, widespread

^b Block designations as in Fig. 4

^c Eos. Neur. = Eosinophilic Neurons

^d MUGS activity expressed as fold-normal specific activity

Table S4. Primers used in the current study

Gene*	Method	Primer	Sequence (5'→3')
fHEXA	PCR Cloning	ORFc1	GTC ACG TGG CAC GCC GAT A
		ORFn1	AAC ACT GGC CTC CTT CTC T
fHEXA	AAV Vector Cloning	fHexA-1	AAAGCTAGCGGAGCACCATGGCGGGCTGCGGGCTCTG
		fHexA-4	AAAAGCGGCCGCTCAGGTTTGTTCAAATTCCTGTTAC
fHEXB	PCR Cloning, Truncated Clone	3UB	GGT TTT GTC CCC TCC TCT T
		ORFu	ATG CCG CTC TCG GTG AAG A
		3L	TGT CCC CTC CTC TTC TTT GTT TAG
fHEXB	Gene Assembly, 5' End	5.1	ATGGCACCCGCAAGGCCCGCTA
		5.2	GCCAGGCCGAGGCCCTGTGCCTCATAGCGGGCCTTGCGG
		5.3	GGCCTCGGCCTGGCAGCCCTCCTGGCCCTGCTCGCCGAG
		5.4	GCAGCGGCGCTGCTCCTGGGGGCGACTGCGGCGAGCAGGG
		5.5	AGCAGCGCCGCTGCCGAGCCCCACTCTGGCCCATGCCCC
		5.6	CTTCACGCTCAGGGGCATGGGCCAGAG
fHEXB	AAV Vector Cloning	5.7	AAAGCTAGCGGAGCACCATGGCACCCGCAAGGCCCGCTATG
		5.8	GCAGGCGCGGAGACGTCTTCACGCTCAGGGGCATGGGCCA
		fHEXB-3	AAGACGTCTCCGCGCCTGCTGCACCTC
		fHEXB2-NotI	AAAAGCGGCCGCTTATGTTTTGTATTCATAGTCACAATA
hHEXA	AAV Vector Cloning	hHexA-1	ATCCACTAGTGGAGCACCATGACAAGTTCCAGGCTTTGGT
		hHexA-2	AATTCTCGAGTCAGGTCTGTTCAAACCTCCTGCTCAC
hHEXB	AAV Vector Cloning	hHexB-1	ATCCACTAGTGGAGCACCATGGAGCTGTGCGGGCTGG
		hHexB-2	AATTCTCGAGTTACATGTTCTCATGGTTACAATATC

* f = feline; h = human

CHAPTER 2

AAV Mediated Gene Delivery Attenuates Neuroinflammation Associated with Feline Sandhoff Disease

Allison M Bradbury^{1,2}, Tiffany A Peterson¹, Stephen Z Wells³, Victoria J McCurdy^{1,2}, Karen G Wolfe², John C Dennis², Brandon L Brunson², Heather Gray-Edwards¹, Ashley N Randle¹, Edward E Morrison², Nancy R Cox^{1,3}, Henry J Baker¹, Miguel Sena-Esteves⁴, Douglas R Martin^{1,2}

¹Scott-Ritchey Research Center, College of Veterinary Medicine, Auburn University, Auburn, Alabama, USA; ²Department of Anatomy, Physiology & Pharmacology, College of Veterinary Medicine, Auburn University, Auburn, Alabama, USA; ³Department of Pathobiology; College of Veterinary Medicine, Auburn University, Auburn, Alabama, USA; ⁴Department of Neurology and Gene Therapy Center

Abstract

Sandhoff disease (SD) is a lysosomal storage disorder characterized by the absence of hydrolytic enzyme β -N-acetylhexosaminidase (Hex), which results in storage of GM2 ganglioside in neurons and unremitting neurodegeneration. Neuronal loss initially affects fine motor skills, but rapidly progresses to loss of all body faculties, a vegetative state, and death by the age of five in humans. A well-established feline model of SD has allowed characterization of the disease in a large animal model and provided a necessary means to test the safety and efficacy of therapeutic interventions before initiating human clinical trials. For the first time in a large animal model of SD, we have demonstrated neuroinflammatory processes marked by expansion and activation of microglia, upregulation of major histocompatibility complex II (MHCII), and increased expression of macrophage inflammatory protein-1 alpha (MIP-1 α). Intracranial delivery of adeno-associated viral (AAV) vectors expressing feline Hex attenuated neuroinflammation and ameliorated disease phenotype 16-weeks post injection. This data reiterates the profound role that inflammation plays in the pathogenesis of SD and suggests that AAV-mediated gene delivery is able to correct the underlying storage disorder and preclude neuroinflammation.

Introduction

GM2 gangliosidosis is an inherited metabolic disorder resulting from a mutation in the gene encoding β -N-acetylhexosaminidase (Hex, EC 3.1.2.52), a lysosomal hydrolase. Deficiency in Hex activity leads to accumulation of GM2 ganglioside in neurons, which in turn causes unrelenting neurodegeneration and fatality by approximately 5 years of age. The GM2 gangliosidoses include Sandhoff disease (SD) and Tay-Sachs disease (TSD), both the consequence of a deficiency in Hex, an enzyme comprised of two hydrolytic subunits, α and β .

TSD results from a mutation in the gene encoding the α subunit (*HEXA*) while SD is the outcome of a mutation in the gene encoding the β subunit (*HEXB*). Despite being characterized over 100 years ago, the pathogenic nature of the GM gangliosidoses has not been fully elucidated and these diseases remain incurable today. The milieu of neuronal death is complex, involving numerous cell types such as microglia and astrocytes, and a myriad of signaling molecules including cytokines and chemokines. Having a more complete understanding of the events involved in neuronal death could provide therapeutic targets and allow for more comprehensive intervention in the disease process.

The *HEXB*^{-/-} mouse model has progressive, profound neurologic disease and pathological findings that closely recapitulate human Sandhoff disease (23). *HEXB*^{-/-} mice appear healthy at birth; however, by 3 to 4 months of age animals present with spasticity, muscle weakness, rigidity, tremors, and ataxia and the disease is inevitably fatal within 6 weeks of the onset of symptoms (24). It is evident in *HEXB*^{-/-} mice and human TSD and SD patients, that neuronal death results from activation of the apoptosis cascade by storage material (128). Apoptotic neurons were not detectable during the first two months, but rapidly and drastically increased at the end stage of disease in the SD mice. Despite the lack of apoptotic neurons early in disease, activated microglia were detectable by 2 months of age in select areas of the CNS, indicating that neuroinflammation precedes, and potentially exacerbates, apoptosis (26). Cortical sections from human Tay-Sachs and Sandhoff patients also revealed a significantly increased number of activated microglia, while the population of astrocytes remained within normal limits (129).

It has been shown that blood monocytes contribute to the expansion of the microglia population by crossing the endothelium and migrating to the parenchyma of the brain (130).

MIP-1 α , a chemokine responsible for recruitment of monocytes from the blood, was found to be increased throughout the brain and spinal cord of SD mice, even at the neonatal stage (130-132). This suggests that MIP-1 α is largely responsible for the recruitment of blood monocytes and thus expansion of the brain microglia population. MIP-1 α has been shown to co-localize with glial fibrillary acidic protein (GFAP)-positive astrocytes (130, 131) and ionized calcium binding protein 1 (Iba1)-positive microglia, but not GM2 containing neurons, suggesting that activated resident glial cells, but not neurons, produce MIP-1 α (131). Remarkably, knocking out MIP-1 α in the SD mouse resulted in diminished pathology, decreased apoptotic neuronal death and increase in body weight, behavior testing, and survival (130). The C-C chemokine receptor type 2 (CCR2) receptor is also implicated in the recruitment of peripheral blood mononuclear cells (PBMCs) and knockout of this receptor led to a significant reduction of MHCII, CD45, and tumor necrosis factor alpha (TNF- α) positive cells (but not GFAP positive cells) in the HEXB-/- mouse brain. The CCR2-/- HEXB-/- double knockout did not decrease pro-apoptotic activity or levels of GM2 ganglioside storage; however, significant improvement in locomotive behavior and a modest extension in life span were seen (132). This data further supports that a portion of the reactive microglia in the brain of SD mice are recruited from PBMCs and partial yet noteworthy amelioration of neuroinflammation can be attained by reduction of PBMC infiltration itself.

In the last five decades valiant efforts have been made to treat this devastating family of neurodegenerative lysosomal storage disorders. Great progress has been made in recent years with further characterization of the disease process in animal models and the evolution of therapeutic approaches. The challenge remains to treat both the underlying neurodegenerative disease and the secondary neuroinflammatory process. Bone marrow transplant in SD mice

significantly decreased apoptotic death and activation of microglia; however, failed to reduce the principal ganglioside storage (26). Gene therapy has emerged as the most promising therapy for this monogenic family of neurodegenerative diseases; however, in earlier attempts, SD mice treated with HIV-1 based lentiviral vectors expressing Hex showed an exacerbated, rather than attenuated, inflammatory response. Furthermore, the therapy had a negative impact on neurologic phenotype, resulting in euthanasia earlier than untreated SD mice (33). SD mice injected with newest generation adeno-associated virus serotype 1 (AAV1) encoding human Hex A and B intracranially (bilaterally into the striatum and cerebellum) precluded the activation and expansion of microglial cells. Early intervention (4 weeks of age) resulted in significant extension of the lifespan; however, delaying treatment until 12 weeks of age was ineffective despite only minor differences in neuroinflammatory properties between the groups (37). These studies reveal the necessity of effectively preventing neurodegeneration through both the interruption of cell death cascades and preclusion of the secondary inflammatory response.

Feline GM2 gangliosidosis results from a mutation in the *HEXB* gene (the β subunit) causing a deficiency in both HexA (α/β) and HexB (β/β) enzymes, and thus is a true model of Sandhoff disease. The SD cat model was first described in 1977 (38), has been extremely well-characterized in the intervening years (39, 40) and presents an unparalleled opportunity to test therapeutic options for translation to human clinical trials. Therefore, after success in the SD mice, the same AAV1 vectors encoding human hexosaminidase were tested in the feline model of SD. Two SD cats treated by bilateral thalamic injection lived to 7.0 and 8.2 months of age, compared with an untreated life span of 4.5 ± 0.5 months ($n = 11$). However, due to a robust humoral immune response to both the AAV1 vectors and human Hex protein, feline cDNAs for the α and β hexosaminidase subunits were cloned into AAV serotype rh8 vectors. Cats treated

with the species-specific vectors by bilateral injection of the thalamus had a less severe immune response and lived to 10.4 ± 3.7 months of age ($n = 3$), or > 2 times that of untreated cats (133). A study in SD mice found that combined injection to the cerebrum (striatum or hippocampus) and cerebellum was necessary to reach maximal survival (36). We therefore have adapted our injection route in the feline model of SD to directly treat the cerebellum by injection to the deep cerebellar nuclei (DCN) or indirectly by intracerebroventricular (ICV) injection via the left lateral ventricle.

In this study, we demonstrated that a robust CNS inflammatory response in feline SD, primarily marked by expansion and activation of the microglial cell population, occurred in concurrence with neurodegeneration. Activation of microglia, demonstrated by morphological changes and upregulation of MHCII, leads to further recruitment of monocytes from the blood and increased expression of the leukocyte chemokine MIP-1 α . Though widespread throughout the CNS, areas rich in white matter appeared to be more severely affected by microgliosis. AAV-mediated gene delivery repressed the expansion and activation of microglia and normalized MCHII and MIP-1 α levels 16 weeks after intracranial injection. The results reiterate the profound role of the inflammatory response in neurodegenerative diseases. For the first time in a large animal model, a therapeutic approach appears to correct the underlying storage disorder, prevent neuroinflammation, and ameliorate disease phenotype.

Results

Analysis of microglia activation in the SD cat was performed at humane endpoint (4.5 ± 0.5 months) with an antibody against Iba1, a microglia/macrophage-specific protein that stains both activated and resting microglia. The SD cat brain displayed a microglia cell population

consisting almost entirely of an amoeboid morphology, designated by enlarged cell body and shortened processes (Fig. 1 A). The amoeboid morphology is associated with an activated state, allowing microglia to phagocytize pathogens or cellular debris. Furthermore, SD cats showed a marked increase in staining for major histocompatibility complex II (MHCII), a marker of antigen presentation (Fig. 1 B). Results were consistent throughout the cerebrum (Fig. 1 A-B), cerebellum (Fig. 1 E-F), and spinal cord (not shown) of SD cats. In contrast, normal, age-matched control cats presented microglia with a ramified morphology designated by a small cell body and elongated, branching processes (Fig. 1 C, G). The ramified morphology is associated with a resting state, supporting the microglia's main function of surveying the brain for pathogens. In addition, the control cat lacked positive staining with MHCII (Fig. 1 D), indicating an absence of activation. The staining profile was comparable in the cerebellum (Fig. 1 G-H) and spinal cord (not shown).

To confirm that activated microglia were primarily responsible for the expression of MHCII, brain sections of untreated SD cats were co-labeled with Iba1 (red) and MCHII (green). As seen in Fig. 2 A, activated microglia of amoeboid morphology highly express MHCII, while microglia retaining the ramified nature of a resting cell do not. Additionally, microglia with the highest expression of MHCII were found in or near vessels (Fig. 2 B). To ensure that astrocytes were not a major source of MHCII expression, colocalization with glial fibrillary acidic protein (GFAP) (red), a marker for astrocytes, and MCHII (green) was also completed. As visualized in Fig 2 C, MHCII does not colocalize with astrocytes. While MHCII remained visible in vessels, astrocytes did not appear to be exiting the brain in large quantities (Fig. 2 D) as shown with microglia.

Seven SD cats were treated with monocistronic AAVrh8 vectors encoding feline HEX α and β subunits (AAVrh8-fHEXA/B) between 4-7 weeks of age. SD cats were divided into two treatment cohorts based on injection route: bilateral thalamic and DCN injection (n=3) or bilateral thalamic and ICV injection (n=3), at a dose in the range of 1.1×10^{12} . Sixteen weeks after injection, comparable to the humane endpoint of untreated SD cats, treated SD cats were euthanized for short-term analysis. As shown by Iba1 staining, microglia retained a ramified, resting morphology and largely lacked expression of MHCII at the level of the thalamus (Fig. 3 A-B) and DCN (Fig. 3 C-D), comparable to normal control cats shown in Figure 1. One treated cat had an isolated, discrete population of MHCII positive cells in the reticular thalamic nuclei (Supp. Fig. 1 A, indicated by black arrows) and a modest number of sporadic positively stained cells throughout the cerebellum. Interestingly, this cat was the oldest of all at the time of treatment, with injection occurring at 7.1 weeks of age. This may suggest that age of treatment and maturity of the immune system could contribute to the ability of AAV to completely attenuate neuroinflammation. Despite an absence of MHCII staining in the remaining cats, there does appear to be an increase in the number of microglia as seen by Iba1 staining, most notably in the thalamus (Supp. Fig. 1 B, indicated by black arrows) and DCN. The discrete location and shape of the infiltration suggest this could be a response to the injection site itself as the areas closely resemble the needle tract.

Activation of microglial cells was quantified by measuring the area of positive MHCII staining in select brain regions of SD, normal, and AAV treated SD cats. Measurements were taken in the cerebrum at the level of the thalamus (Fig. 4 A) and in the cerebellum at the level of the deep cerebellar nuclei (DCN) (Fig. 4 B). In untreated SD cats, MHCII was significantly upregulated in the cerebral white matter ($p = 0.0079$), cortical grey matter ($p = 0.0452$), and

thalamus ($p = 0.0251$) when compared to normal, age-matched control cats (Fig. 4 C-E). MHCII also was significantly increased in cerebellar white matter ($p = 0.009$), grey matter ($p = 0.0159$), and in the DCN ($p < 0.0001$) (Fig. 4 F-H). MHCII staining failed to reach significance in the brainstem ($p = 0.0740$) due to large standard deviation of the untreated SD cohort (Fig. 4 I). Notably, 16 weeks after AAV gene therapy MHCII was normalized in all areas of the brain analyzed ($p > 0.05$) (Fig. 4 C-I). These results demonstrate that AAV-mediated gene therapy when delivered prior to symptom acquisition is capable of precluding the detrimental neuroinflammatory response seen in untreated SD cats. All treated cats had levels of therapeutic Hex enzyme restored to above normal levels throughout the brain (data not shown) and had largely ameliorated clinical signs of disease at the time of necropsy, with some cats demonstrating slight tremors and mild hind limb weakness.

One of the most advantageous properties of adeno-associated viruses is their ability to transduce non-dividing cells, such as neurons, and thus present a long-lasting source of enzyme production. Immunofluorescence with an antibody to the feline β -subunit of Hex demonstrated that vesiculated, intracytoplasmic inclusions within neurons near the thalamic injection site contained high levels of the therapeutic protein (Fig. 5 A). Transmission electron microscopy with immunogold labeling using the same β -subunit antibody confirmed the presence of the protein within the inclusions (Fig. 5 C). As we have previously shown (133), routine H&E staining revealed a population of highly eosinophilic neurons corresponding to the supranormal levels of Hex expression near the injection site (not shown). Although AAVrh8 is not known to transduce microglia, some expression of Hex was also noted in microglial cells (Fig. 5 A, white arrows), the majority of which were located in or near vessels (Fig. 5 B). To determine if the amount of Hex in the lymphatic system was elevated, an enzyme assay was conducted on the

brain draining lymph node (BDLN). Sixteen weeks after treatment, HexA levels in the BDLN were only 3.7% of normal, not substantially greater than levels found in untreated SD cats (2.2% of normal) (Supp. Table 1).

MIP-1 α functions in recruitment of microglial precursor cells from the blood and thus plays a role in expansion of the microglia population seen in the brain. We therefore measured MIP-1 alpha expression in the brain of SD, normal, and AAV treated SD cats by quantitative reverse transcription PCR and normalized expression to a ribosomal protein housekeeping gene, RPL-17. As anticipated, a significant upregulation of MIP-1 α was seen in the brain of SD cats ($p = 0.0019$, $n = 8$) at humane endpoint when compared to normal age-matched cats (Fig. 6). Furthermore, 16 weeks after treatment with AAV gene therapy, levels of MIP-1 alpha were completely normalized ($p = 0.5872$, $n=3$).

Discussion

HexB knockout mice have served as a valuable animal model of Sandhoff disease, closely resembling disease pathology and neurologic phenotype (23). In human patients (129) and HexB $^{-/-}$ mice (26), neuroinflammation contributes substantively to the process of neurodegeneration, with the expansion and activation of microglia arising as the most prominent contributor. Established over 30 years ago (38), the feline model of SD has played an important scientific role in phenotypic and biochemical disease characterization. However, to date the influence of the inflammatory response on CNS pathology had not been explored in this model. In this study we have demonstrated that activation of microglia is prominent, widespread throughout the CNS, and is associated with neuropathology in this large animal model. In contrast to normal, age-matched control cats, nearly the entire microglia population in the SD

brain consisted of activated microglia, characterized by amoeboid morphology and MHCII expression. MHCII was significantly elevated in all brain areas analyzed except for the brainstem, in which staining was unusually variable. As previously shown in SD mice (37), brain regions rich in white matter were most severely affected. Furthermore, microglia activation was greatest in the cerebellum, which contributes substantially to the clinical phenotype associated with SD.

Microglia respond to dying cells laden with ganglioside storage and remove the cellular debris by phagocytosis; however, microglia are also deficient in the hydrolytic enzyme necessary to degrade the glycolipid, and thus are unable to perform this function. In response, peripheral microglia precursors are recruited to the CNS, furthering the expansion of activated microglia and exacerbating neurodegeneration (26). The notion of recruited microglia from the periphery has been corroborated by pervasive and early elevation of MIP-1 α , a leukocyte chemokine, in the brain of HEXB $^{-/-}$ mice (37, 130, 131). Double knockout of MIP-1alpha and CCR2, a chemokine receptor involved in PBMC infiltration, showed improved survival in SD mice (130, 132), suggesting that targeted inhibition of MIP-1 α or CCR2 could prevent microglia recruitment and harmful downstream effects, such as secretion of pro-inflammatory cytokines. More recent characterization of SD microglial cell lines has allowed for identification of potential signaling pathways involved in the upregulation of MIP-1 α , and ultimately provides some promising targets for inhibition (134). Our results demonstrate the elevation of MIP-1 α in a large animal model and further substantiate the expected function in human SD patients. As expected, 16 weeks after intracranial delivery of AAV, HexA levels in peripheral blood mononuclear cells (1.6% of normal) were comparable to untreated SD cats (data not shown). In order to entirely treat the disease, the role of Hex-deficient microglia and PBMCs cannot be overlooked.

Interruption of the neuroinflammation early in the pathway, such as direct targeting of MIP-1 α or its receptors, may be a critical secondary treatment to enzyme restoration.

Although survival was increased in HEXB^{-/-}, CCR2^{-/-} mice due to decreased neuroinflammation, ganglioside storage was not reduced and animals ultimately still died of neurodegeneration (132). When Hex was selectively restored in neurons but not microglia of HEXB^{-/-} mice, neuroinflammation was not attenuated. This was evidenced by upregulation of MHCII, marking activated resident microglia, and CD45, signifying infiltration of peripheral monocytes (135). This data suggests that Hex production limited to the neurons is not sufficient to cross-correct, cross-correction is an advantageous property of lysosomal enzymes (136), neighboring microglia. Our treatment strategy for SD cats was intracranial injections of AAVrh8 encoding feline Hex, which is known to transduce neurons, providing a long-lasting source of Hex. However, AAVrh8 is not known to transduce microglia, as has been demonstrated with AAV2 and AAV5 serotypes (137). Sixteen weeks after intracranial injection, Hex expression was apparent in neurons, visualized by immunofluorescence and electron microscopy. Interestingly, Hex was also noted in select microglia surrounding the transduced neurons. However, it is unclear whether the microglia were transduced by the vector or phagocytosed the proteinaceous material. The majority of microglia expressing Hex were located in or near vessels, which could be explained if microglia are participating in an inflammatory condition by endocytosing Hex or phagocytosing Hex-positive cells. However, this does not rule out microglial transduction, or the possibility that microglia activated in one part of the brain are traveling through vasculature to another region.

Sixteen weeks after intracranial injection of AAVrh8-fHEX, all SD cats had Hex levels above normal throughout the brain (data not shown). This therapeutic approach largely corrected

the disease phenotype, as all treated cats had ameliorated clinical signs of disease at the time of necropsy, with some cats demonstrating only slight tremors and mild hind limb weakness. Importantly, SD cats treated with AAV showed marked attenuation of microglia activation, as evidenced by a lack of MHCII staining. A single cat that was the oldest at the time of treatment, 7.1 weeks, did have an isolated, discrete population of MHCII positive cells restricted to the reticular thalamic nuclei. This finding reiterates the importance of the age at which therapeutic intervention occurs, as previously demonstrated in SD mice (37). When quantified, levels of MHCII were normalized in all areas of the brain analyzed, demonstrating widespread dissemination of therapy and attenuation of neuroinflammation. Furthermore, levels of MIP-1 α were also normalized, suggesting diminished recruitment of microglia precursors from the blood. The prevention of microglia activation (as seen by an absence of MHCII staining) likely prevented the recruitment of additional cells from the periphery. However, an increase in the number of resting microglia was apparent near the thalamus and DCN in some of the treated cats. Localization of micogliosis without activation near the injection sites could be a response to the surgery opposed to disease pathology.

In conclusion, the data shows that intracranial administration of monocistronic AAVrh8 vectors encoding feline HEX α and β subunits to SD cats led to the transduction of brain cells, widespread attenuation of neuroinflammation, and amelioration of clinical symptoms. Such unparalleled short-term therapeutic benefit in a large animal model of SD merited long-term studies of this approach, which are ongoing. In conjunction with success of AAV therapy in SD mice, this data should encourage completion of necessary studies to advance towards human clinical trials. Furthermore, this approach may provide benefit to other monogenetic neurodegenerative diseases beyond the scope of lysosomal storage disorders.

Materials and Methods

Animals and Surgery All animal procedures were approved by the Auburn University Institutional Animal Care and Use Committee. Bilateral injections of the thalamus and deep cerebellar nuclei (DCN) were performed according to a previously published protocol (133). Intracerebroventricular injection was performed under ultrasound guidance to confirm the correct placement of the injection needle. After visualization of the left lateral ventricle with an 8-5 MHz Philips HDI 5000 ultrasound probe (Philips Healthcare, Andover, MA), a single entry site was made through the skull with a 20G spinal needle. Vector was then delivered using a Hamilton syringe (Harvard Apparatus, Holliston, MA) fitted with a 25G non-coring needle (Harvard Apparatus). A total of 200 μ L was delivered in 10-15 μ L aliquots at a rate of 3-5 μ L/second with approximately 1 minute between aliquots.

At a humane and predetermined endpoint animals were euthanized by pentobarbital overdose (100 mg/kg) and transcardially perfused with cold, heparinized saline. The brain was divided into coronal blocks of approximately 0.6 cm from the frontal pole through the cerebellum. The right hemisphere of the brain was preserved in optimal cutting temperature (OCT) medium for determination of enzyme activity. The left hemisphere of the brain and all other tissues were formalin fixed and flash-frozen in liquid nitrogen and preserved at -80 °C.

AAV Vectors The feline HEXA cDNA was amplified and cloned as previously described (133). Feline HEX transgene expression is driven by the hybrid promoter including the CMV immediate-early enhancer fused to the CBA promoter (116) and the woodchuck hepatitis virus post-transcriptional regulatory element (WPRE) was included for enhancement of gene

expression. AAVrh8 vector stocks encoding feline Hex subunits were produced as previously described (117).

Immunohistochemistry Prior to immunostaining, 6 μ m paraffin sections were deparaffinized, endogenous peroxidase activity was quenched with 0.3% hydrogen peroxide in methanol for 30 minutes, and antigen retrieval was performed by heat treatment in Tris-EDTA buffer (10 mmol/l Tris, 1 mmol/l EDTA, 0.05% Tween 20, pH 9.0) for 20 minutes. Subsequently sections were blocked with 5% normal horse serum in PBS (pH 7.5)+0.5% BSA for 1 hour followed by incubation with rabbit anti-human/rat mouse Iba1 (1:100; Biocare, Concord, CA) or mouse anti-feline MHCII (1:4, AbD Serotec, Oxford, UK) for 1 hour. Sections were then rinsed with PBS + 0.1%BSA and stained with horse anti-rabbit/mouse IgG labeled with HRP (pre-diluted; Vector Laboratories, Burlingame, CA) for 1 hour. Sections were again rinsed and incubated with Vectastain RTU ABC reagent (Vector Laboratories) for 30 minutes and stained cells were visualized with DAB peroxidase substrate (Vector Laboratories).

For immunofluorescence, sections were alternatively blocked with 5% normal donkey serum in PBS+0.05% Tween 20 for 1 hour followed by incubation with rabbit anti-human/rat mouse Iba1 (1:100; Biocare), mouse anti-feline MHCII (1:4, Serotec), or mouse anti-feline Hex β -subunit (39) (1:1000) for 1 hour. Sections were then rinsed with PBS+0.05% Tween 20 and stained with DyLight 488-conjugated donkey anti-mouse or 594-conjugated donkey anti-rabbit IgG (1:100; Jackson ImmunoResearch).

Cell quantification Stained brain sections were scanned on an Aperio ScanScope CS2 (Aperio, Vista, CA) and quantified using Visiopharm Quantitative Digital Pathology software (Visiopharm, Hoersholm, Denmark).

EM Biopsy of brain tissue was fixed in 2% paraformaldehyde + 0.1 % glutaraldehyde in Sorenson phosphate buffer (pH 7.2). The area of interest was defined under a dissection scope and the tissue was thinly sliced to facilitate dehydration and infiltration. Dehydration was accomplished in graded ethanol series; the sample was infiltrated with LR White resin (London Resin Company Limited, Berkshire, England) and thermally cured at 50 degrees Celsius (C). Thin sections were cut with Reichert ultra-tome at 95 nm and collected on nickel mesh grids. After aldehyde dehydration and blocking, tissue grids were incubated in mouse anti-feline Hex β -subunit (1:50) for an extended time at 4 degrees C. Following a series of buffer washes, grids were incubated in donkey anti-mouse, 6 nm gold conjugate (Aurion ImmunoGold Reagents, Wageningen, Netherlands). Images were recorded using a Philips 301 transmission electron microscope (Philips, Eindhoven, Netherlands) at 60kv acceleration.

Quantitative PCR Total RNA was isolated from OCT embedded brain tissue using the RNeasy mini kit (Qiagen, Limburg, Netherlands) according to the manufacturer's instruction. RNA was treated with DNase (Invitrogen, Carlsbad, CA) and complementary DNA synthesis was performed using the qScript cDNA synthesis kit (Quanta Biosciences, Gaithersburg, MD). Quantitative PCR was conducted using TaqMan Fast Universal PCR Master Mix (Applied Biosystems, Carlsbad, CA) and a C1000 Thermal Cycler (BioRad, Hercules, CA) with 300ng of complementary DNA. The MIP-1 α and RPL-17 primers were used at a concentration of 18 μ M

and probes at a concentration of 5 μ M in a reaction volume of 20 μ L. The thermal cycling parameters were as followed: 95° for 20 seconds; 95° for 3 seconds, repeated for 40 cycles; and 60° for 30 seconds. MIP-1 α mRNA expression was normalized to a ribosomal protein housekeeping gene, RPL-17.

Statistics Significance was determined by two-tailed t-test with SAS software (SAS, Cary, NC).

Figures and tables

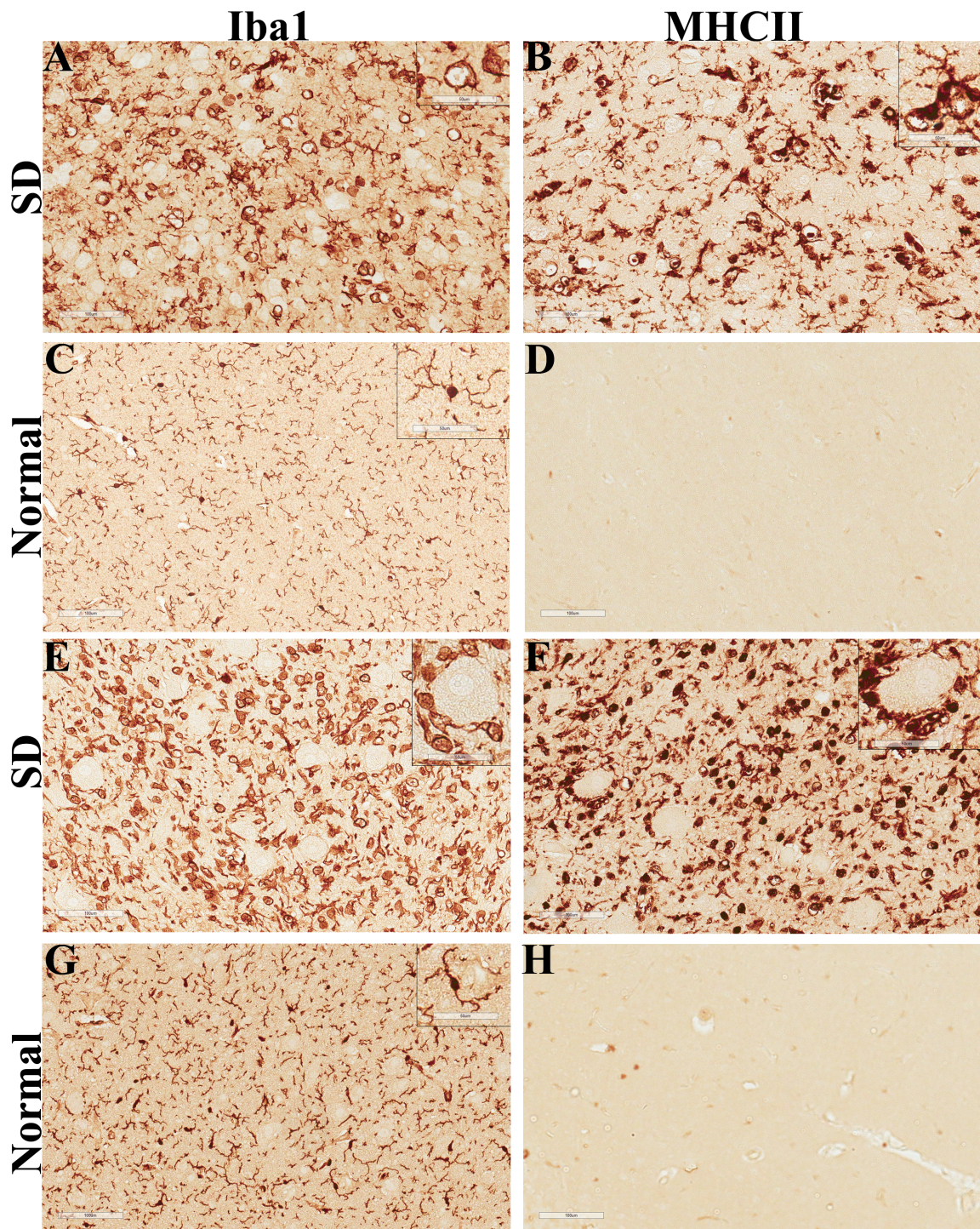


Figure 1. Activation of microglia in feline Sandhoff disease. Iba1 and MHCII expression in the thalamus were evaluated in SD cats at humane endpoint (n=5). A representative image of

staining with Iba1 shows activation of microglia characterized by an amoeboid morphology with a large cell body and shortened processes (A) and expression of MHCII (B). A representative image of Iba1 staining from a normal, age-matched control cat shows a resting microglia population characterized by a small cell body and long, branching processes (C) and a lack of MHCII staining (D). Microglia activation was also evaluated in the deep cerebellar nuclei (DCN) with consistent results in the SD (E-F) and normal (G-H) cats.

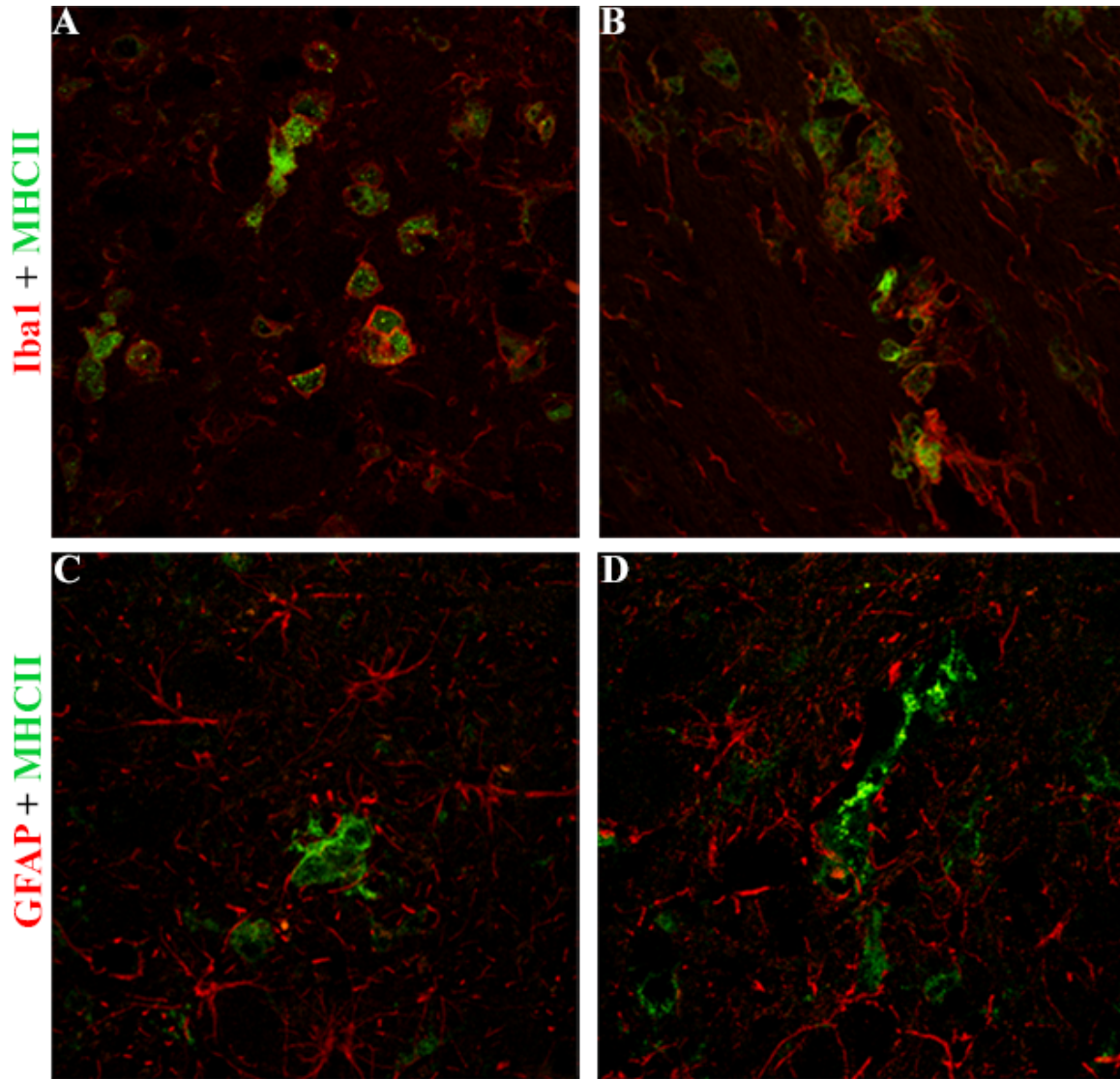


Figure 2. MHCII expression associated with microglia but not astrocytes. Colabeling of Iba1 (red) and MHCII (green) confirms that activated microglia express MHCII (A) and the majority of microglia are located in or near vessels (B). Colabeling of GFAP (red) and MHCII (green) verifies that astrocytes are not expressing MHCII (C, D).

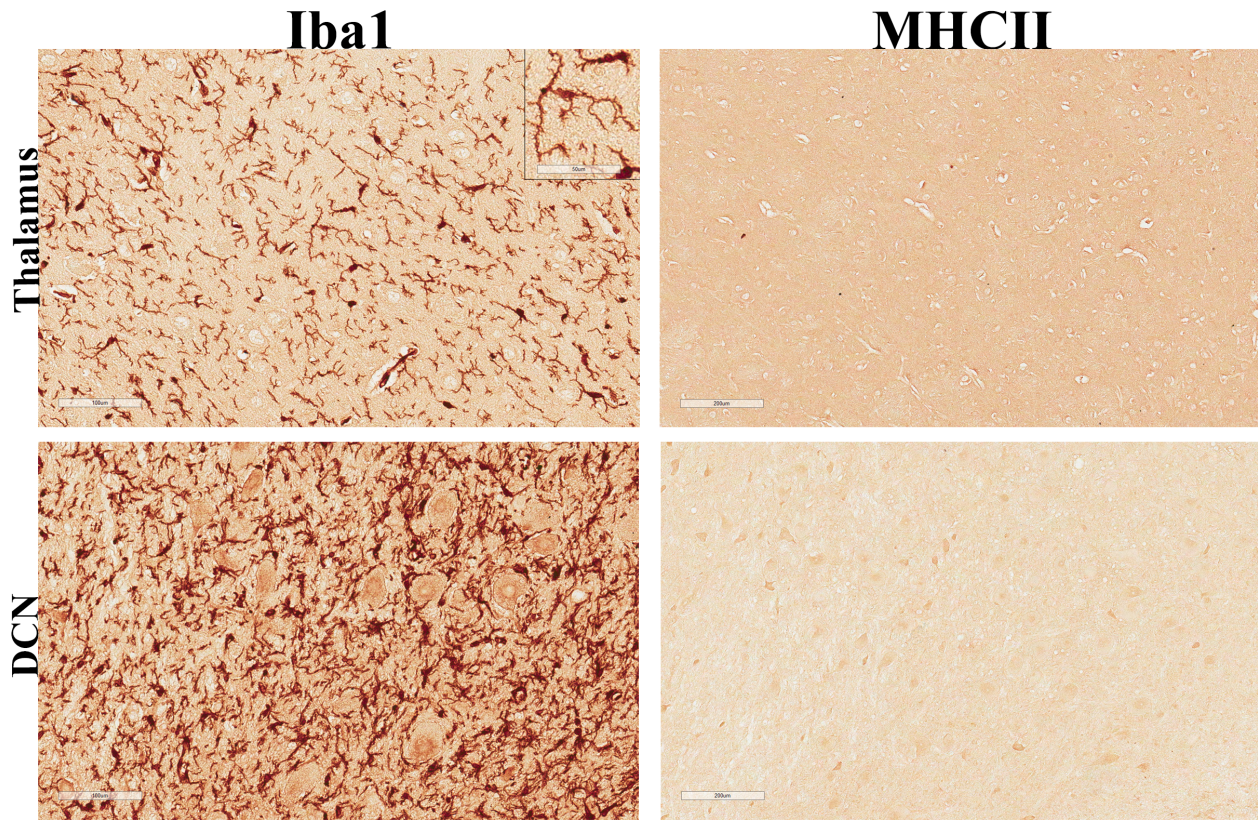


Figure 3. AAV therapy attenuates microglia activation. Iba1 and MHCII expression were evaluated in SD cats sixteen weeks after intracranial injection of monocistronic vectors encoding feline Hex A and B (n=3). A representative image of staining with Iba1 shows a population of resting, ramified microglia at both the thalamic and DCN injection sites. MHCII staining was negligible at both the thalamic and DCN injection sites.

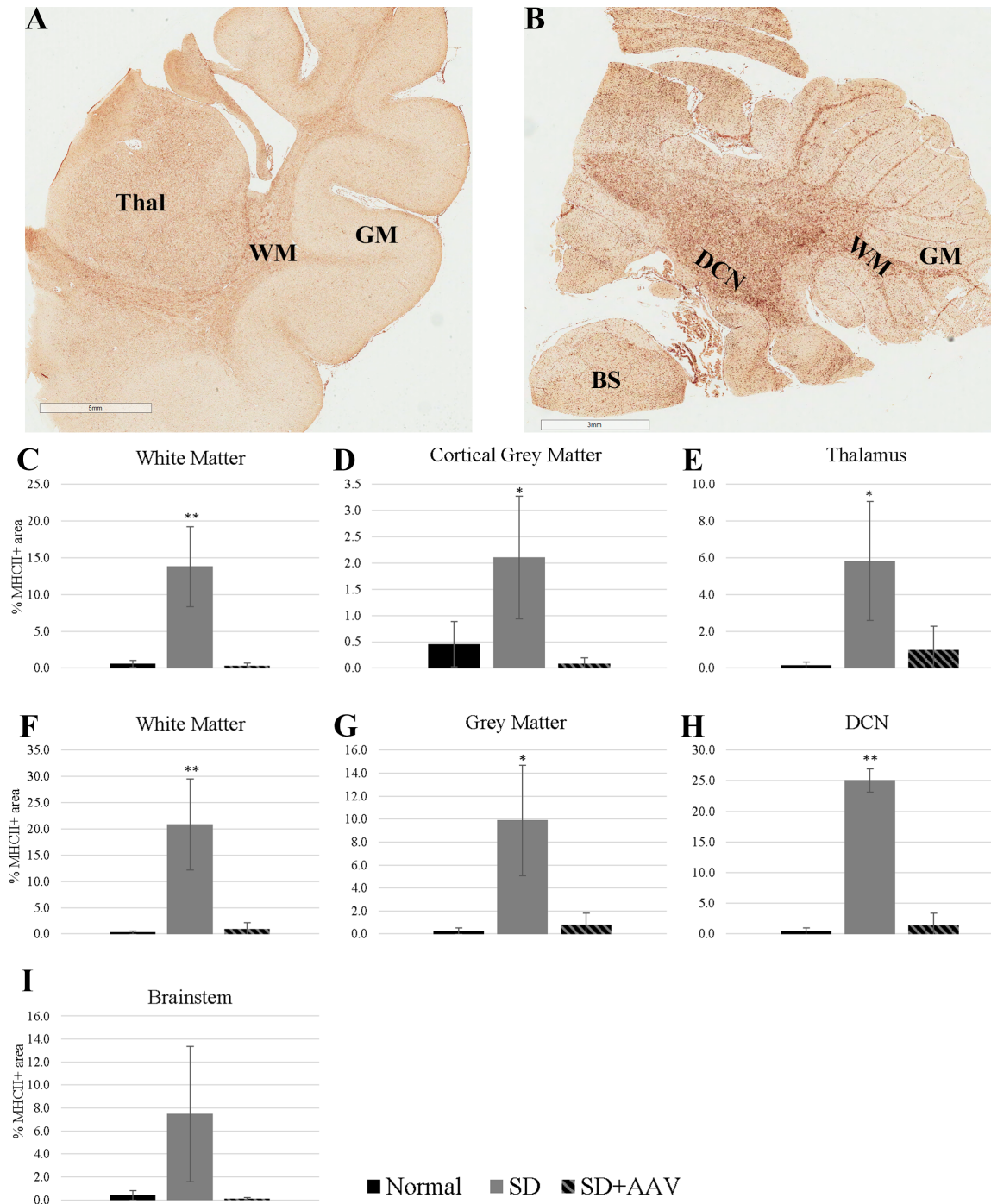


Figure 4. Upregulation of MHCII in untreated SD cat brains and normalization with AAV-mediated gene delivery. MHCII staining was quantified in white matter, gray matter, and thalamus at the level of the thalamic injection site (A) and white matter, grey matter, DCN, and brainstem at the level of the DCN injection site (B) of SD (n=5) and normal, age-matched cats

(n=6). The area of positive staining was significantly increased in SD cats in all areas of the brain analyzed (C-H) except for the brainstem (G). Sixteen weeks after AAV therapy (n=3), MHCII was normalized in all areas of the brain analyzed (C-G). * = $p < 0.05$; ** = $p < 0.01$; error bars represent standard deviation.

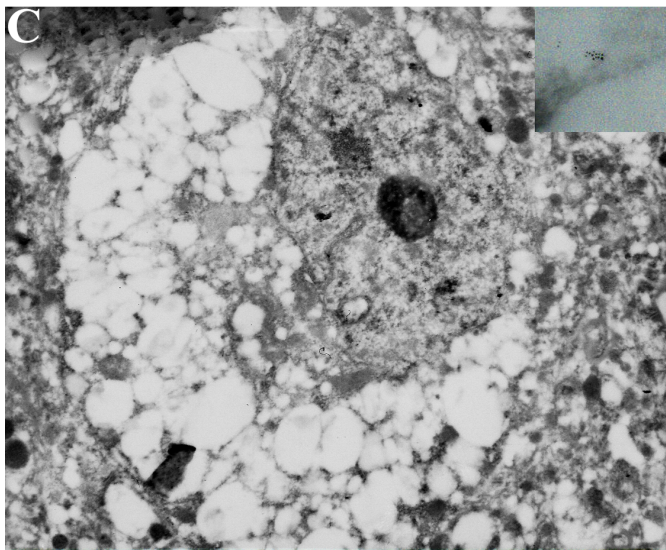
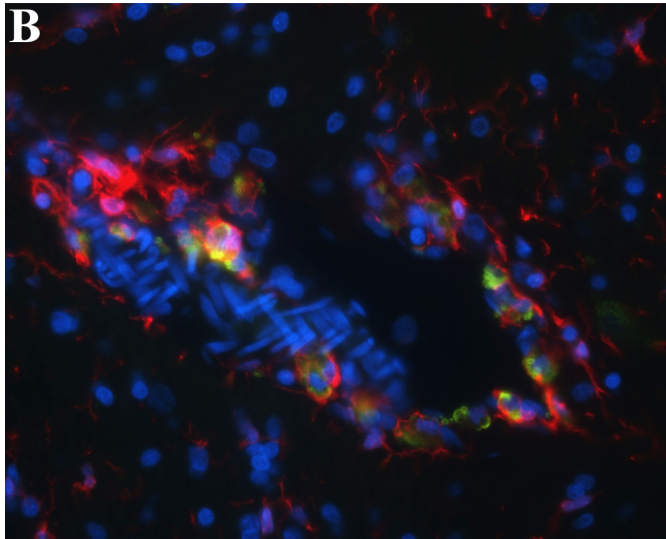
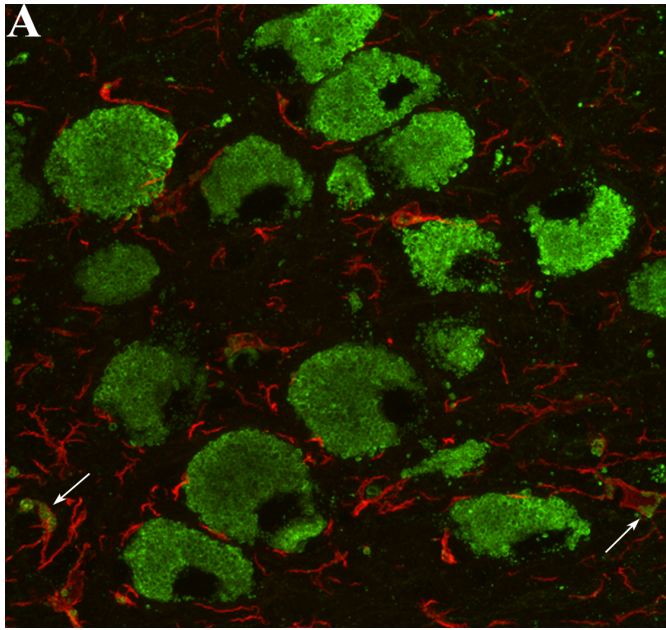


Figure 5. AAV-fHEX successfully transduces neurons. Immunofluorescence with an antibody to the feline Hex β -subunit (green) demonstrated high levels of the therapeutic protein within neurons near the thalamic injection site (A). Hex staining is also noted in select microglial cells (red), indicated by white arrow. The majority of Hex staining associated with microglia occurred in or near vessels (B). Secondary immunogold labeling of the anti-Hex antibody confirms presence of the therapeutic protein within cytoplasmic inclusions as visualized by electron microscopy. Inset demonstrates gold labeling (C).

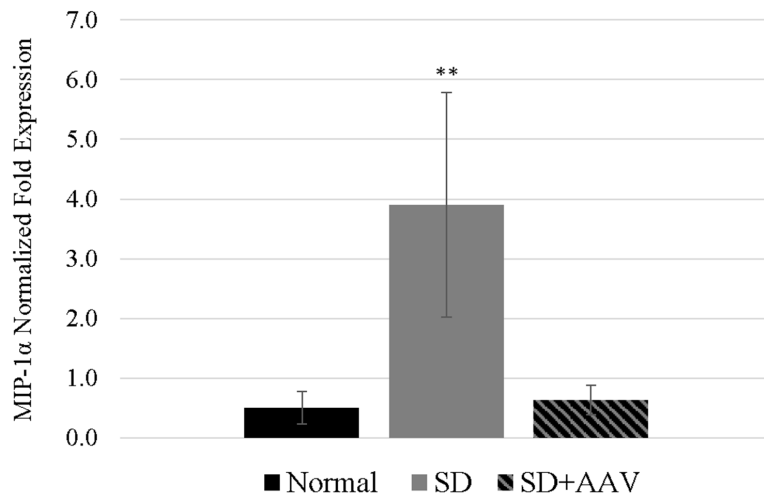
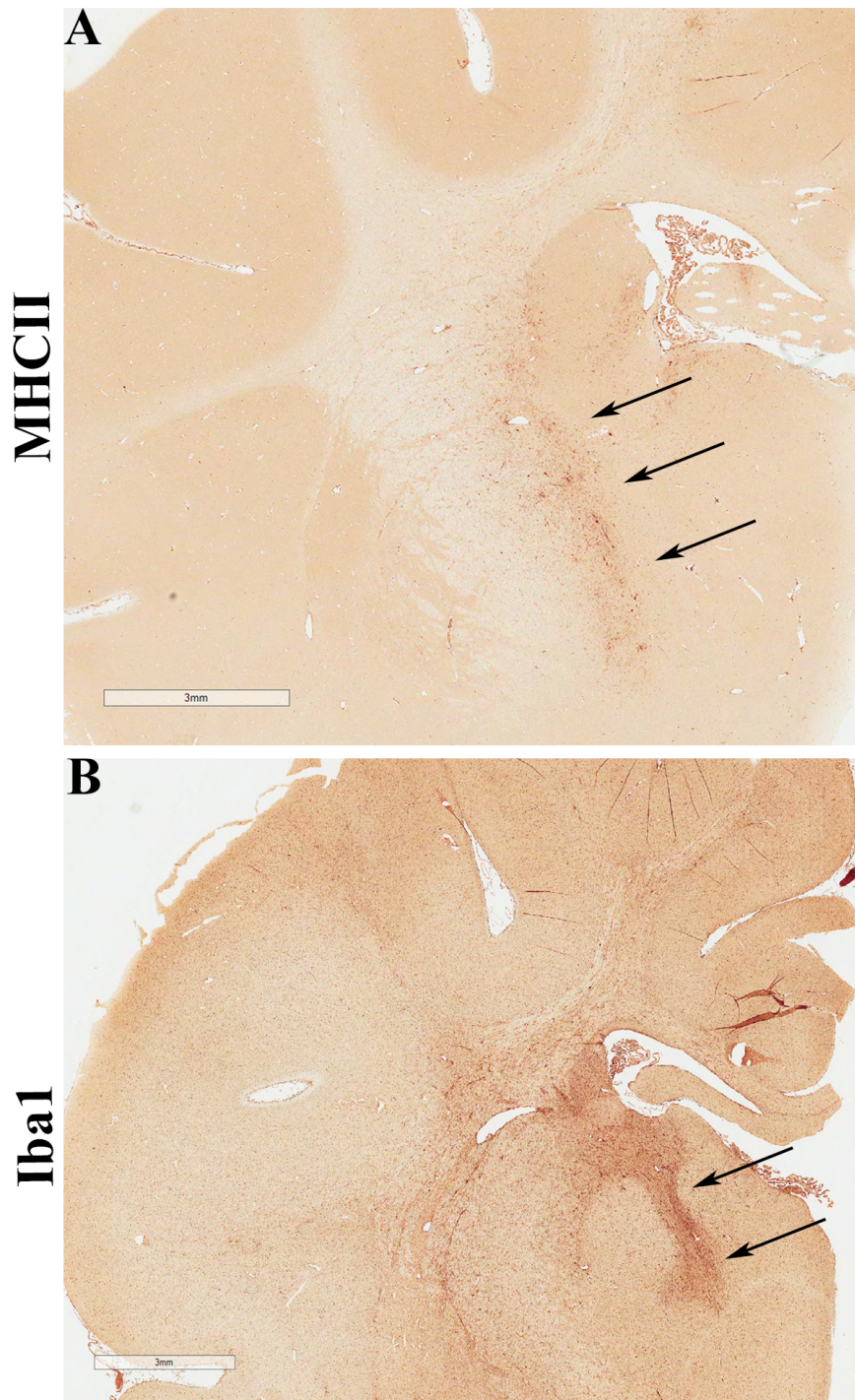


Figure 6. Upregulation of MIP-1 α expression in untreated SD cat brain and normalization with intracranial injection of AAV. MIP-1 α was measured by reverse transcription quantitative PCR. mRNA expression was significantly elevated in the brain of SD cats (n = 8; p = 0.0019) at humane endpoint when compared to a normal age-matched cats (n=5). Sixteen weeks after AAV gene therapy, MIP-1 alpha expression was not increased (n=3; p = 0.5872) compared to normal age-matched cats. ** = p < 0.01; error bars represent standard deviation.



Supplementary Figure 1. Isolated areas of microglia activation and expansion in AAV-treated SD cats. 16 weeks after AAV-therapy one treated cat showed isolated activation of microglia cells, indicated by MHCII staining, in the region of the reticular thalamic nuclei (A).

Another treated cat showed discrete expansion of microglia cells, indicated by Iba1 staining (B), despite an absence of MHCII staining in the region (shown in Figure 3). Scale bars represent 3 mm.

Table S1. Enzyme activity in medial retropharyngeal brain draining lymph node

	Hex A S.A. (St. Dev)	Hex total S.A. (St. Dev)	β-Gal S.A. (St. Dev)	Mann S.A. (St. Dev)
Normal	280.14 (24.38)	6871.05 (442.31)	348.55 (33.95)	707.51 (24.08)
SD	6.30 (1.36)	22.92 (4.94)	607.93 (50.10)	1692.51 (182.70)
SD+AAV	10.26 (1.97)	65.06 (17.71)	477.14 (49.87)	1355.59 (49.08)

Specific activities (S.A.) and standard deviation (St. Dev) were calculated for lysosomal enzymes: HexA (MUGS), total Hex (MUG), and β -galactosidase (β gal) and Mannosidase (Mann) 16 weeks after intracranial delivery of AAVrh8-fHEXA/B (n=3). Normal age-matched (n=2) and untreated SD (n=2) values are included for comparison.

CHAPTER 3

Systemic Effects after Intracranial Delivery of AAV in Feline Sandhoff Disease

Allison M Bradbury^{1,2}, Jamie L Shirley¹, Victoria J McCurdy^{1,2}, Heather Gray-Edwards¹, Ashley N Randle¹, Brandon L Brunson², Nancy R Cox^{1,3}, Henry J Baker¹, Miguel Sena-Esteves⁴, Douglas R Martin^{1,2}

¹Scott-Ritchey Research Center, College of Veterinary Medicine, Auburn University, Auburn, Alabama, USA; ²Department of Anatomy, Physiology & Pharmacology, College of Veterinary Medicine, Auburn University, Auburn, Alabama, USA; ³Department of Pathobiology; College of Veterinary Medicine, Auburn University, Auburn, Alabama, USA; ⁴Department of Neurology and Gene Therapy Center; University of Massachusetts, Worcester, MA, USA.

Abstract

In recent years recombinant adeno-associated viral gene therapy has shown unequivocal therapeutic success in small and large animal models of Sandhoff disease. Concerns surrounding use of AAV-mediated gene therapy in human clinical trials are largely based on potential deleterious immune response to the therapeutic agent. In this study, we analyze the humoral immune response in two intracranial delivery routes and at two different dosages of AAVrh8 encoding feline hexosaminidase in a cat model of SD. We have established that intracranial delivery of recombinant AAV vectors will result in a robust humoral immune response; however, high levels of circulating antibodies did not preclude sustained Hex expression, amelioration of clinical symptoms, or significant extension of lifespan. Furthermore, sera antibody titers did not correlate with life span and were not an indicator of survival. Lowering the dose of treatment lowered sera antibody titers; however, clinical symptoms were not as completely attenuated. Furthermore, directly targeting the ventricular system did not increase sera antibody titers when compared to injecting the brain parenchyma. AAV vector and therapeutic protein have previously been shown to reach peripheral tissues after intracranial injection, which could explain extraordinarily high levels of circulating titers after intracranial injection. Herein we elucidate a strong tissue tropism of AAVrh8 for the liver, sciatic nerve, and quadriceps after intracranial injection. Lastly, the immune response to intracranial delivery of AAVrh8 in healthy non-human primates is assessed as part of safety and toxicity studies.

Introduction

Sandhoff disease is a fatal lysosomal storage disorder caused by a deficiency in β -N-acetylhexosaminidase (Hex, EC 3.1.2.52), a lysosomal hydrolytic enzyme. A mutation in the

gene *HEXB* results in insufficient production of two isozymes, HexA, responsible for cleavage of the primary substrate GM2 ganglioside, and HexB, which facilitates cleavage of secondary neutral substrates. In the absence of Hex, GM2 ganglioside accumulates primarily within neurons leading to progressive and relentless damage to the central nervous system (CNS). Infantile SD has a mean age at onset of 4.4 ± 3.5 months and life span of 47 months. The most frequent initial symptoms reported are developmental arrest, abnormal startle response, and low muscle tone, which progress to seizures, blindness, and ultimately a vegetative state (2). Although discovered over a century ago, this disorder still remains incurable today. Both murine (23) and feline (38) models of SD have allowed detailed characterization of the disease and opportunities to explore therapeutic interventions. Recombinant adeno-associated viruses for gene delivery of Hex have emerged as the most promising therapy to date in both HexB^{-/-} mice (36, 37, 85) and SD cats (133). Use of recombinant AAV vectors has already been approved for human clinical trials in neurodegenerative diseases such as Parkinson's disease and Alzheimer's disease, and more recently in two lysosomal storage diseases, Batten's disease and Pompe disease. Despite ongoing approvals, clinical trials utilizing recombinant AAV vectors have not always proven efficacious. One of the first clinical trials employing a recombinant AAV2 vector encoding Factor IX to treat hemophilia found expression of the therapeutic protein was transient, lasting only 8 weeks, due to an immune response mounted against the AAV capsid (68). Prior to utilizing rAAV for clinical trials in SD patients, the role of immunity must be fully explored and understood in order to prevent major impediments as seen in the case of the hemophilia clinical trial.

We have previously shown that both SD and phenotypically normal cats mounted a robust humoral immune response to the vector when treated by direct thalamic injection of AAV

serotype 1 vector expressing human Hex (133). Serum antibody titers ranged from 1:16,384 – 1:196,608, and there was no significant difference in titers between SD and normal cats. However, when serum antibody titers to the therapeutic protein were measured, normal cats had a significantly higher immune reaction to the human Hex protein product (1:8,192–1:87,381) than SD cats (1:1,024–1:5,120) ($p = .011$). Due to the vigorous, and potentially detrimental immune response, viral vectors were reengineered to encode species-specific feline cDNA in an AAVrh8 backbone. In comparison to sera titers to AAV1-hHEX, the immune response to the AAVrh8 vector was drastically reduced in phenotypically normal cats treated with AAVrh8-fHEX (1:4096-1:32,768). SD cats treated with the same vector showed an even greater reduction in serum antibody titers (1:1,024-1:3,072), which was significantly lower than the cohort of normal cats treated with AAVrh8-fHEX ($p = 0.024$). Purified feline HexA was unavailable for comparable serum antibody titer studies; however, titers were undetectable when sera from AAVrh8-treated heterozygotes were tested against human HexA or a feline β -subunit-specific 14-mer peptide (fHEXB 240) and also when tested against supernatant from 293T cells transduced with the same viral vectors. These results suggest that the immune response to the therapeutic protein was dramatically decreased by use of a species-specific transgene. Furthermore, this study revealed a disparate immune response to human HexA protein and AAVrh8 vector between phenotypically normal and SD cats. This could be explained by immune deficiencies in feline SD, which could potentially have an advantageous effect on treatment response due to diminished immune reaction to the therapeutic agent. It is therefore necessary to evaluate the effect of AAV treatment on immune response through peripheral mechanisms.

AAV vector and therapeutic lysosomal enzymes have been detected in peripheral tissues after intracerebral treatment in animal models, demonstrating that AAV injected into the brain

may also have peripheral effects, which could be influencing the humoral immune response. Single-track administration of rAAV1, rAAV2, and rAAV5 to the putamen and internal capsule of non-human primates (NHPs) demonstrated distribution in the injected hemisphere, spinal cord, and cranial and peripheral nerves. Interestingly, AAV1, but not AAV2 or 5, vector sequences were found in the liver. All 3 serotypes were present transiently in the serum, while lymph nodes, PBMCs, and gonads, remained consistently negative (104). A mouse model of late infantile neuronal ceroid lipofuscinosis (LINCL) was treated with AAVrh10 encoding the deficient enzyme of tripeptidyl peptidase I (TPP-I), injected 8 locations in the brain parenchyma (bilaterally into the upper striatum, lower striatum, thalamus, and cerebellum). Enzyme activity was \geq wild-type levels in multiple peripheral organs, with the highest levels detected in liver > spleen > heart, kidney, lung, muscle, and serum. However, when measured by qPCR, only a small amount of vector was detectable in lung, spleen, and liver of some AAVrh.10-treated mice (105). A mouse model of neuronal ceroid lipofuscinosis (NCL) received AAVrh8 encoding the missing protease, cathepsin D, via ICV injection. Utilizing a cathepsin D-specific fluorescent probe, it was determined that treated mice had four-fold increase of fluorescent signal in the brain and 1.5 fold increase of signal in the liver, when compared to PBS-treated NCL mice. However, no significant increase in signal was seen in the heart, spleen, or kidneys. Self reported low sensitivity of the imaging system could have resulted in underestimation of AAVrh8 transduction of peripheral tissues (138). Direct measurements of enzyme activity and vector copies in our large animal model will provide more evidence regarding biodistribution of AAVrh8 after intracranial injection.

SD cats treated with feline-specific AAVrh8 vectors by bilateral injection of the thalamus lived to 10.4 ± 3.7 months of age ($n = 3$), or 2.3 times as long as untreated cats. Demise of the

animals was believed to be resultant from lack of enzyme distribution to the cerebellum after thalamic injection. In corroboration, a study in SD mice found that combined injection to the cerebrum (striatum or hippocampus) and cerebellum was necessary to reach maximal survival (36). We therefore hypothesized that targeting the cerebellum in conjunction with bilateral thalamic injections would improve enzyme distribution throughout the brain. We subsequently adapted our injection route in the feline model of SD to directly treat the cerebellum by injection to the deep cerebellar nuclei (DCN) or indirectly by intracerebroventricular (ICV) injection via the left lateral ventricle. This study addresses the short and long-term humoral immune response after two different intracranial injection routes of AAVrh8 vector encoding feline hexosaminidase. Also for the first time, the peripheral biodistribution of the therapeutic protein and vector are analyzed after intracranial injection of AAVrh8. Furthermore, the effect of vector dosage on production of serum antibody titers in both the feline model of SD and healthy NHPs is established.

Results

In order to determine if directly targeting the cerebellum would increase distribution of therapeutic protein, three SD cats were treated with bilateral thalamic and bilateral DCN injections of monocistronic AAVrh8 vectors encoding feline HEXA and HEXB cDNA at a total dose of 4.4×10^{12} genome equivalents (g.e.)/vector/kg. The treatment occurred between 4.3 and 5.6 weeks in age and the animals were euthanized sixteen weeks later for short-term analysis. Sera antibody titers to the vector were measured prior to surgery, 6 weeks post-treatment, and lastly at the time of necropsy. All cats had undetectable titers prior to surgery; however, 2 of the 3 cats mounted a robust immune response to the vector, reaching 1:65,536 16-weeks after

surgery (Figure 1). Despite the pronounced immune response, HexA levels were above normal throughout the brain, GM2 ganglioside levels were substantially reduced, and the disease phenotype was largely ameliorated (data not shown). Serum antibody titers were higher than expected based on results from cats injected solely in the thalamus. Increased titers could be attributed to the slightly higher dose resulting from two additional injection sites. Importantly, high levels of circulating antibodies did not preclude successful transduction of AAV and sustained Hex expression 16 weeks post-injection.

It was previously believed that injection in to the brain parenchyma would be retained in the ‘immune privileged’ CNS and prevent a systemic immune response. The high titers present in the sera 16-weeks after intracranial injection suggest that injectate from the parenchymal injection site reached peripheral sources. To test this hypothesis, we conducted enzyme assays on numerous peripheral tissues (Table 1). Most notably, HexA levels in the liver reached an average of 62.5% of normal activity. The adrenal gland and heart contained 26.0% and 22.6% of normal HexA activity, respectively, while bone marrow, spleen, quadriceps, skin, and gonad had on average < 6% of normal activity. For the most part, increased levels of HexA resulted in decreased levels of β -galactosidase (β -gal) and mannosidase (Mann), which are lysosomal enzymes upregulated in an undefined mechanism in the absence of HexA. Furthermore, the number of vector copies generally correlated with the amount of enzyme present in a given tissue (Table 2). Surprisingly, 16-weeks after intracranial injection the liver contained 2.0×10^4 vector copies per 50ng of DNA. As expected from enzyme data, the heart had the next largest presence of vector at 162.9 copies/50ng of DNA. All other tissues analyzed contained, on average, less than 25 vector copies. This data confirms our hypothesis that intracranial injection of AAV

inadvertently reached peripheral tissues, namely the liver, which likely contributed to the pronounced sera antibody titers seen 16 weeks after treatment.

Short-term (16-week) analysis of 3 SD cats treated by bilateral thalamic and DCN injections of AAVrh8 proved widespread expression of HexA in the CNS, reduction of GM2 ganglioside, and amelioration of clinical symptoms. Additionally, inadvertent expression of HexA in the periphery, with a strong tissue tropism towards the liver, and a pronounced presence of sera antibody titers were established. The success of these experiments warranted long-term studies to determine efficacy of the therapy and lasting effects of the immune response on the treatment. Short-term results led us to believe that sera antibody titers are not as injurious as previously thought; however, we were unable to conclude if the response was transient or would perhaps continue to increase beyond 16 weeks. Nine SD cats were treated between 4.0 and 5.9 weeks of age with the same AAVrh8-fHEX monocistronic vectors at a total dosage of $4.2 - 4.7 \times 10^{12}$ g.e./vector/kg. Life span of treated SD cats was significantly increased compared to untreated controls ($p < 0.0001$); however, survival proved to be highly variable, ranging from 9.8 – 35.7 months of age (Figure 2). Serum antibody titers were measured to determine if an immune response mounted against the vector played a role in the variability of survival and could possibly even serve as a predictive measure of therapeutic outcome (Figure 3). The single cat to live less than 1 year had serum antibody titers of 1:49,152 approximately 1 month after intracranial injection. Interestingly, titers decreased with time and were 1:12,288 and 1:4,779 at 4 and 8.8 months post-treatment, respectively. In order to determine if these high but transient sera antibody titers contributed to premature death, a cat that lived beyond 1 year of age was analyzed for comparison. Surprisingly, approximately 1 month post-treatment antibody titer in the sera for this animal reached 1:109,227 and continued to increase until 5.5 months post-injection, when

titers reached a maximum of 1:218,453. Titers gradually decreased, yet still remained 1:65,536 at the time of necropsy, 13.3 months after intracranial injection. These results demonstrate that a robust humoral immune response occurs subsequent to intracranial injection of AAVrh8-fHEX; however, the levels of titers are not likely to be detrimental to the therapy and are not a good indicator of survivability.

Peripheral tissues were then analyzed for the long-term presence of HexA enzyme (Table 3). As seen with the short-term cohort, AAVrh8 appears to have a strong tissue tropism for the liver, with HexA activity averaging 45.0% of normal. Levels of HexA activity in the quadriceps were highly variable, ranging from undetectable to 164.0% of normal activity. Interestingly, the 3 cats with the shortest life span all had undetectable levels of HexA while the 4 cats that survived the longest had the highest HexA values in the quadriceps. Remarkably, HexA levels in the sciatic nerve were > 100% of normal for all animals analyzed, with an average of 291.1% of normal activity. Levels of HexA in the gonad averaged < 3% for all animals analyzed (n=7) and vector copies were undetectable (n=7) (data not shown), ensuring the therapy is not transferred vertically. Vector copies in the liver remained at 4.0×10^3 (n=7) at the humane endpoint of the long-term cohort, demonstrating lasting presence of the vector peripherally.

Despite achieving a positive therapeutic effect in the presence of high antibody titers, it was still necessary to determine the lowest dosage of treatment at which maximum efficacy could be achieved. This is especially important with the long-term goal of translating this therapy to human patients. Six SD cats were treated with $1/10^{\text{th}}$ of the original dose (4.4×10^{11} g.e./vector/kg) utilizing the same AAVrh8-fHEX vector construct. All cats were treated between 4.0 - 5.0 weeks of age by bilateral injection of the thalamus and DCN and allowed to reach humane endpoint. Lifespan ranged from 7.5 - 16.9 months of age and resulted in a significant

increase in survival ($p = 0.0002$), which was not significantly different from the full dose treatment group ($p = 0.0811$) (Figure 4). Serum antibody titers were measured to see if a 10-fold reduction in AAV dosage resulted in a lower humoral immune response (Figure 5).

Approximately one month post-treatment serum antibody titers were variable, ranging from 1:32 – 1:8,192 (mean = 1:3,594.7, standard deviation = 3,319.8; $n=6$). Titers decreased with time post-treatment, measuring $1:1,659.2 \pm 1,989.7$ and $1:1,244.8 \pm 1,492.1$ (mean \pm standard deviation, $n=5$) approximately 8 and 12 months after intracranial injection, respectively. The single highest titer was seen approximately 4 months after treatment, 1: 16,384, and occurred in the animal (7-787) that lived to 15.3 months of age. This again supports our hypothesis that titers are not a good indication of clinical outcome. Overall the titers were substantially decreased in the $1/10^{\text{th}}$ dose cohort (range 0 – 1:16,384) when compared to the full-dose cohort (range 1:4,778.7 – 218,453.3). Titers were not analyzed for statistical differences due to inconsistencies in the ages at which serum was collected between the two cohorts.

Vector copies and enzyme levels of HexA were quantified in the liver to determine if reduction of the dose diminished the amount of available vector to reach the periphery. Liver HexA levels ranged from 8.0 – 37.3% of normal with a mean and standard deviation of $23.8\% \pm 11.5$ (Table 4) which is lower, albeit not significantly, from the full dose treatment group. The number of vector copies in the liver ranged from 0 – 649, with a mean and standard deviation of 242.3 ± 228.9 (Table 4), which was significantly lower than the vector copy number in the liver of the full dose treatment cohort ($p = 0.0034$). Interestingly, the two $1/10^{\text{th}}$ dose treated cats with the lowest maximum serum antibody titers seen to date (1:32), had no detectable copies of the vector in the liver. This data further suggests that unintentional leakage of vector to the periphery is responsible for the pronounced serum antibody titers seen in some treated animals. Thus the

variability seen within treatment groups can be explained by varying amounts of vector leakage from the injection site.

Although these unprecedented results extending life span of a large animal SD model more than 4 fold provided persuasive evidence to initiate a human clinical trial, injecting the DCN is technically challenging and increases surgical risks. Delivery of gene therapy vector through the cerebrospinal fluid by way of intracerebroventricular injection (ICV) in conjunction with bilateral thalamic injection could eliminate the need for direct injection of the cerebellum. Furthermore, since inadvertent leakage of vector into the CSF led to substantial amounts of HexA in select peripheral tissues, it was hypothesized that targeting the ventricular system directly could increase the peripheral stores of the therapeutic enzyme. To test the new therapeutic approach, 4 SD cats were treated by bilateral thalamic and ICV injection via the left lateral ventricle at a total dose of 1.1×10^{12} g.e./vector/kg. The cats were treated between 4.7 and 7.1 weeks of age and euthanized 16-weeks after treatment for short-term analysis. Quantification of HexA enzyme activity in the liver, quadriceps, and bone marrow (Table 5) revealed therapeutic enzyme levels that were comparable and not significantly different from the thalamus and DCN short-term cohort shown in Table 1.

While peripheral stores of HexA were not elevated, ICV injection was advantageous due to decreased surgical risks and proved capable of effectively disseminating vector to the cerebellum. In order to test long-term efficacy of this injection route, 6 SD cats were treated between 4.0 - 5.4 weeks of age with AAVrh8-fHEX at a dosage ranging from 1.1×10^{12} g.e./vector/kg. To date, life span ranges from 11.2 - 30.4 months of age, with an increased survival of $p = 0.0002$; however, this study is ongoing (Figure 6). At the present time, there is no significant difference in survival between the full dose thalamus and DCN and the thalamus and

ICV injection routes ($p = 0.5467$). As with the long-term thalamus and DCN treatment group, we compared serum antibody titers of a cat that lived less than a year to a cat that lived beyond one year of age to determine if an immune response mounted against the vector (Figure 7) played a role in the variability of survival. In agreement with our previous results, the cat that lived less than one year of age had lower serum antibody titers than the cat that lived beyond one year of age. The only cat to reach humane endpoint prior to one year of age had a maximum serum antibody titer of 1:6,144 at approximately 2 months post-treatment and a titer at humane endpoint of just 1:16. In contrast, the cat that lived to 25.9 months of age had a maximum titer of 1:16,384 3.6 months post-surgery. All time points could not be analyzed due to limiting quantities of vector stock; however, at approximately 20 months post-treatment sera titers had decreased to 1:1,024. This data strengthens our hypothesis that circulating antibodies are not detrimental to AAV-mediated gene therapy and are not an indicator of survival. Furthermore, targeting the CSF opposed to the brain parenchyma does not appear to intensify the humoral immune response.

The first 3 cats to reach humane endpoint after thalamic and ICV injection have been analyzed for long-term HexA expression in peripheral tissues (Table 6). As seen after thalamus and DCN injection, HexA activity was highest in the sciatic nerve, reaching 230.3% of normal activity. Also closely mimicking previous findings, HexA activity in the liver was 53.8% of normal, followed by quadriceps at 20.7%, heart at 16.9%, and small intestines at 4.3% of normal enzyme activity. Levels of HexA in the periphery after thalamic and ICV injection were not significantly different than levels after thalamus and DCN injection in any tissues analyzed. These findings negate the hypothesis that targeting the ventricular system directly could increase the peripheral stores of the therapeutic enzyme.

In order to progress towards human clinical trials, safety and toxicity studies are compulsory. Healthy non-human primates (NHP) were chosen as the subjects due to the similarity to humans in brain size and complexity. All procedures were conducted at the University of Massachusetts under the direction of Dr. Miguel Sena-Esteves. Juvenile cynomolgus macaques aged 2.5-3.5 years were treated with AAVrh8 vectors encoding NHP HEXA and HEXB cDNA by bilateral thalamic and ICV injection route. A dose reduction approach was utilized, establishing 3 different cohorts based on dosage: 1) full dose = 3.2×10^{12} vg (n=3); 2) $1/10^{\text{th}}$ dose = 3×10^{11} vg (n=2); 3) $1/30^{\text{th}}$ dose = 1×10^{11} vg (n=2). In addition, control groups included a PBS-injected control (n=1) and transgene-empty AAVrh8 vector at a dose identical to the full dose treatment group (3.2×10^{12} vg, n=2). All macaques were screened for the absence of AAVrh8 neutralizing antibodies prior to treatment. At the time of necropsy (20 - 28 days post-surgery), the full dose treatment group had serum antibody titers ranging from 1:1,024 – 1:3,072 (mean = 1:2,048, standard deviation = 836.1) (Table 7). Unexpectedly, the $1/10^{\text{th}}$ dose treatment group had higher sera titers than the full dose treatment group, with both animals measuring 1:49,152 at the time of necropsy (57 and 91 days post-injection), while the $1/30^{\text{th}}$ had lower titers than the full dose group at 1:128 and 1:384 at the time of necropsy (66 and >90 days post-surgery). As anticipated the NHP injected only with PBS (no vector) had no detectable titers at a sera dilution of 1:8 at the time of necropsy (90 days post-injection). The transgene empty cohort had disparate titers, with one NHP's titer measuring at 1:1,024 and comparable to the full dose treatment group, while the other NHP of this group reached 1:49,152 at the time of necropsy (>90 days post-surgery). Purified NHP HexA protein was not available; however, human HexA is 97.7% homologous and was consequently used to measure humoral immune

response to the expressed protein. Titers to purified human HexA protein were not detectable at a sera dilution of 1:8 in any treatment group.

Discussion

This study demonstrates a robust humoral immune response in SD cats after intracranial injection of AAVrh8-fHEX. Short-term analysis revealed serum antibody titers that reached 1:65,536 16-weeks after bilateral thalamic and DCN injection of the vector. Long-term analysis established that titers continue to increase up to 5.5 months post-treatment, after which they begin a steady and gradual decline. Decreasing the total injected dose of vector to 1/10th of the original dose substantially lowered serum antibody titers (range 0 – 1:16,384) when compared to the full-dose cohort (range 1:4,778.7 – 218,453.3). Although survival was not significantly different compared to full dose ($p = 0.0811$), disease phenotype presented differently between the two treatment cohorts. SD cats treated with the lower dose showed delayed onset of symptoms seen in untreated cats, such as tremors, that the full dose treatment fully attenuated. Since the immune response to the full dose was not disadvantageous, the loss of efficacy seen with the lower dose is not likely to justify its use. In addition to determining the optimal dose, the safest yet most effective injection route must also be solidified before planning human clinical trials. The risk of serious hemorrhage in the posterior fossa (cavity housing the cerebellum) is much greater than in the cerebrum (e.g., thalamus) and left alternative injection routes to be desired by pediatric neurosurgeons. In this study, 10 additional SD cats (4 short-term and 6 long-term) were treated by ICV injection in combination with bilateral thalamic injection in attempt to lessen surgical risks while still providing necessary distribution to the cerebellum. Targeting the ventricular system instead of the brain parenchyma (DCN) did not increase antibody titers

present in the sera. In all 3 long-term treatment groups analyzed (full dose thalamus and DCN injection, 1/10th dose thalamus and DCN injection, and full dose thalamus and ICV injection) sera antibody titers failed to correlate with survival. Therefore, humoral immune response cannot explain the variability among or between treatment groups and cannot serve as a predictor of clinical outcome. Importantly, this also demonstrates that an immune response does not nullify therapeutic benefit from gene-mediated treatment for SD, as also reported in the mouse SD model (personal communication, MB Cachon-Gonzalez and TM Cox).

AAV vector and therapeutic lysosomal enzymes have been detected in peripheral tissues after intracerebral treatment in animal models (104, 105, 138) and AAVrh8 specifically has shown to have a strong tissue tropism for the liver (138, 139). In this study we demonstrate unexpectedly high levels of the therapeutic protein and vector copies in the liver after intracranial therapy. Full dose short and long-term treatment groups, regardless of injection route, had comparable Hex activity in the liver, reaching near or above 50% of normal activity. AAVrh8 vector copies were retained in periphery long term, as all cats from the long term thalamus and DCN group that were analyzed (n=7) had liver vector copies on the order of 10³, which was reduced from 10⁴ seen in the short-term group 16-weeks after therapy. Reducing vector dosage to 1/10th of the original dose decreased activity to 23.8% of normal and vector copies to < 300/50ng of DNA. HexA levels in the sciatic nerve were also surprisingly high with average of 291.1% of normal activity after thalamus and DCN injection (n=9) and 230.3% of normal activity after thalamus and ICV injection (n=3). The high levels are likely due to pooling of vector in lumbar spinal cord, which then disseminates down peripheral nerves. HexA levels in the quadriceps strongly correlated with survival in the long-term thalamus and DCN group, with the first 3 cats to reach humane endpoint having undetectable enzyme levels and the 4 longest

surviving cats having the highest levels. The first 3 cats to reach humane endpoint in the thalamic and ICV group had only 20.7 % of normal activity in the quadriceps, which is ~ 50% of the average activity seen in the thalamus and DCN group. As more cats in that group reach humane endpoint it will be important to see if this correlation holds true. If so, measuring Hex activity by muscle biopsy could function as an indicator of clinical outcome.

Healthy non-human primates were used to conduct safety and toxicity studies of intracranial delivery of AAVrh8 to a brain comparable in size and complexity to a human infant. We have previously shown sera antibody titers in normal cats treated bilaterally in the thalamus and DCN at a dose of 4.2×10^{12} to be substantial, ranging from 1:4,096 - 1:32,768 (133), and therefore expected a pronounced immune response in the healthy NHPs. Unexpectedly, NHPs treated by bilateral thalamic and ICV injection at a comparable dose of 3.2×10^{12} had modest serum antibody titers ranging from 1:1,024 – 1:3,072. The cynomolgus macaques were treated at a juvenile age, 2.5-3.5 years, compared to the normal cats treated between 1-2 months of age, which could explain disparities in immune response between the species. Based on results seen in SD cats, we anticipated reduction of dosage of the vector would lessen the humoral immune response. Therefore, 2 additional NHPs were treated at $1/10^{\text{th}}$ of the original dose and surprisingly had higher sera antibody titers measuring 1:49,152. It was then hypothesized that induction of tolerance at the full dose reduced the titers of that treatment group, while $1/10^{\text{th}}$ dose failed to induce tolerance. Two additional NHPs were then treated at $1/30^{\text{th}}$ of the original dose and unexpectedly had lower titers than the full dose group at 1:128 and 1:384, negating the induction of tolerance postulate. Variability in titers between treatment groups may also be a result of differences in survival. The $1/30^{\text{th}}$ dose treatment group had the longest survival; therefore, the lowest titers seen in that group could be due to the greatest duration in time after

injection. With such low animal numbers (n= 2 or 3 per treatment group) it is difficult to draw any conclusions from this study and more animals are currently being analyzed. Despite inconclusive evidence regarding immune response to the vector, the clear lack of an immune response to the therapeutic protein is important evidence to move forward towards clinical trials.

Overall this study demonstrates that intracranial delivery of recombinant AAV vectors will result in a robust humoral immune response. However, high levels of circulating antibodies did not preclude sustained Hex expression, amelioration of clinical symptoms, or significant extension of lifespan. Furthermore, sera antibody titers in no way correlated with life span and were not an indicator of survival. Lowering the dose of treatment does appear to lower sera antibody titers; however, in light of data herein loss of therapeutic efficacy solely for an attenuated humoral immune response is not warranted. This study also elucidates a strong tissue tropism of AAVrh8 for the liver after intracranial injection, restoring HexA levels to nearly 50% of normal in all full dose treatment groups. Individuals with a mutation resulting in residual HexA activity as low as 10% of normal have remained asymptomatic (15); and therefore, partial restoration of enzyme could be highly beneficial. This study is the largest of its kind, compiling data from 28 SD cats among 5 treatment groups. The long-term cohorts show greater extension of lifespan than any other therapy attempted in a large animal model of a neurologic lysosomal storage disease. We hope that these results encourage the progression towards the use of AAV-mediated gene delivery in human clinical trials for SD and other neurodegenerative disorders.

Materials and Methods

Animals and Surgery All animal procedures were approved by the Auburn University Institutional Animal Care and Use Committee. Bilateral injection of the thalamus and deep

cerebellar nuclei (DCN) were performed according to a previously published protocol (133). Intracerebroventricular injection was performed under ultrasound guidance to confirm the correct placement of the injection needle. After visualization of the left lateral ventricle with an 8-5 MHz Philips HDI 5000 ultrasound probe (Philips Healthcare, Andover, MA), a single entry site was made through the skull with a 20G spinal needle. Vector was then delivered using a Hamilton syringe (Harvard Apparatus, Holliston, MA) fitted with a 25G non-coring needle (Harvard Apparatus). A total of 200uL was delivered in 10-15 uL aliquots at a rate of 3-5 uL/second with approximately 1 minute between aliquots.

At humane or a predetermined endpoint animals were euthanized by pentobarbital overdose (100 mg/kg) and transcardially perfused with cold, heparinized saline. The brain was divided into coronal blocks of approximately 0.5 cm from the frontal pole through the cerebellum. The right hemisphere of the brain was preserved in optimal cutting temperature (OCT) medium for determination of enzyme activity. The left hemisphere of the brain and all other tissues were formalin fixed and flash-frozen in liquid nitrogen and preserved at -80 °C.

Safety and toxicity studies of intracranial delivery of AAVrh8 vector were conducted in juvenile cynomolgus macaques. Animal housing, surgeries, and necropsies were conducted at the University of Massachusetts and all animal procedures were approved by the University of Massachusetts Institutional Animal Care and Use Committee. Juvenile cynomolgus macaques (2.5-3.5 years old male and female) were screened for the absence of AAVrh8 neutralizing antibodies prior to bilateral thalamic + ICV delivery of two monocistronic vectors in a 1:1 formulation of AAVrh8-HexA and AAVrh8-HexB vectors (n=7). PBS-injected (n=1) and transgene-empty AAVrh8 vector (n=2) controls were included. Convection-enhanced delivery of the vector was performed using SmartFlow™ neuroventricular cannulas (MRI Interventions)

and PHD 2000 Harvard Pump set at 2 μ l/min and infused volumes equaled 150 μ l /thalamus and 300 μ l lateral ventricle.

AAV Vectors The feline HEXA cDNA was amplified and cloned as previously described (133). Feline HEX transgene expression is driven by the hybrid promoter including the CMV immediate-early enhancer fused to the CBA promoter (116) and the woodchuck hepatitis virus post-transcriptional regulatory element (WPRE) was included for enhancement of gene expression. AAVrh8 vector stocks encoding feline Hex subunits were produced as previously described (117).

Serum antibody titers For serum antibody titers, 100 ng of AAV1 vectors or purified human HexA (Sigma, St Louis, MO) were coated onto ELISA plates (Nunc, Rochester, NY) and incubated overnight at 4 °C. AAVrh8 vectors had undetectable levels of protein and thus titration experiments were conducted and vectors were coated at a dilution of 1:167. Plates were washed and then blocked with 5% non-fat powdered milk in phosphate-buffered saline for 90 minutes at room temperature; 100 μ l of twofold serial dilutions of feline or NHP serum samples were added. Goat anti-feline IgG:HRP (Jackson ImmunoResearch; 1:20,000) or mouse anti-rhesus IgG:HRP (NIH Nonhuman Primate Reagent Resource; 1:10,000) was used for color development with tetramethylbenzidine (Pierce, Rockford, IL). After the subtraction of background, a titer of 0.15 was considered positive.

Enzyme Assay Lysosomal enzyme activity of peripheral tissues was determined according to a previously published protocol (40) with the appropriate 4-methylumbelliferyl (4-MU) substrates:

β -gal, 0.5 mmol/l 4-MU- β -D- galactoside, pH 3.8; HexA, 1 mmol/l MUGS, pH 4.2; and total Hex, 1 mmol/l 4-MU-N-acetyl- β -D-glucosaminide (MUG), pH 4.3. Fluorescence of the samples was measured on a BioTek Synergy HT plate reader (BioTek, Winooski, VT) with excitation at 360 nm and emission at 450 nm. Protein concentrations were measured by the method of Lowry, and specific activity was expressed as nmol 4-MU cleaved/mg protein/hour.

Quantitative PCR Total genomic DNA was extracted from frozen peripheral tissues with the Qiagen DNeasy Blood and Tissue kit (QIAGEN Sciences, MA). AAV vector copy number was measured by SYBR Green quantitative PCR using primers specific for the woodchuck hepatitis virus post-transcriptional regulatory element (WPRE) in the AAV vector (coding strand primer, 5'-AGTTGTGGCCCGTTGTCA-3'; noncoding strand primer 5'-GAGGGGGAAAGCGAAAGT-3'). Amplification reactions were run in triplicate on a Bio-Rad CFX96 Real-Time System, and contained Applied Biosystems (Warrington, UK) SYBR®Green PCR Core Reagents (1X SYBR buffer, 3.0 mM MgCl₂, 0.2 mM dNTPs, 0.25 U uracil-N-glycosylase and 0.625 U Taq Gold), 20 ng DNA template and 0.4 μ M of each coding and noncoding primer. Samples were incubated for 2 minutes at 50°C, 10 minutes at 95°C, and then amplified for 40 cycles. Cycling conditions were: 95°C for 30 seconds, 62°C for 30 seconds, and 72°C for 45 seconds. A standard curve was generated by amplification of serial dilutions of plasmid DNA containing the WPRE sequence (1×10^8 - 1×10^0 copies per reaction).

Statistics Significance of serum antibody titers, enzyme activity, and vector copies was determined by two-tailed t-test and survival data was created using the LIFETEST procedure and log-rank Test with SAS software (SAS, Cary, NC).

Figures and tables

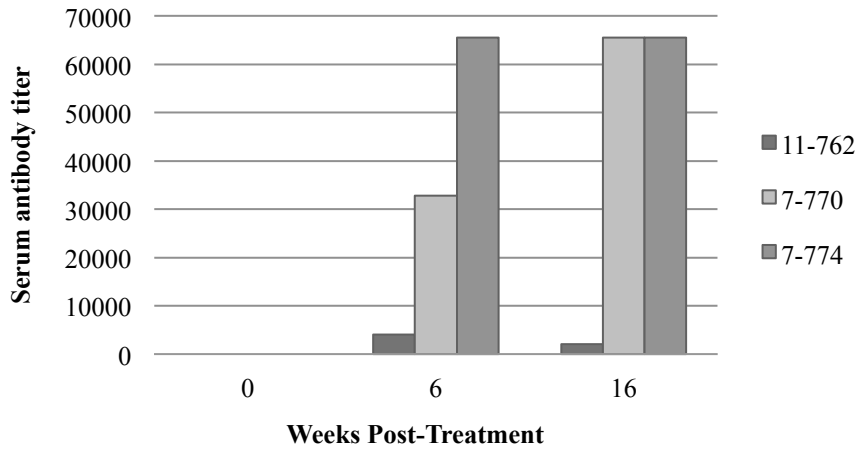


Figure 1. Serum antibody titers to AAVrh8-fHEX in treated SD cats. Three Sandhoff disease (SD) cats treated by bilateral thalamic and DCN injection of AAV vectors expressing feline Hex (4.4×10^{12} g.e./vector/kg) were assayed prior to, 6 weeks after, and at the predetermined endpoint of 16 weeks post-treatment for serum antibodies to the vector. Cats 7-770 and 7-774 had a maximum serum antibody titer of 1:65,536 16 weeks post-treatment while cat 11-762 had a maximum serum antibody titer of 1:4096 6 weeks post-treatment.

Table 1. Enzyme activity in peripheral tissues 16 weeks post Thal+ DCN AAV treatment

Tissue	HexA% Normal (S.A. \pm standard deviation)	HexT % Normal (S.A. \pm standard deviation)	β -Gal % Normal (S.A. \pm standard deviation)	Mann % Normal (S.A. \pm standard deviation)
Liver	62.5 (131.0 \pm 20.1)	47.9 (1202.7 \pm 256.8)	115.2 (142.5 \pm 5.0)	138.0 (1206.1 \pm 280.9)
Adrenal	26.0 (41.3 \pm 5.5)	29.1 (386.1 \pm 49.8)	138.3 (233.9 \pm 67.9)	311.3 (785.0 \pm 165.4)
Heart	22.6 (6.2 \pm 4.2)	7.8 (109.1 \pm 67.8)	125.7 (12.7 \pm 2.0)	162.7 (116.3 \pm 16.5)
Quadriceps	5.7 (0.9 \pm 0.8)	2.7 (9.6 \pm 7.9)	192.9 (18.0 \pm 4.1)	338.0 (260.6 \pm 83.9)
Bone Marrow	5.0 (8.8 \pm 0.7)	2.0 (48.8 \pm 2.4)	122.0 (158.7 \pm 13.6)	106.1 (1145.4 \pm 127.3)
Gonad	3.9 (8.8 \pm 3.2)	1.9 (47.5 \pm 5.4)	124.9 (148.4 \pm 34.4)	170.0 (588.1 \pm 73.5)
Spleen	2.7 (2.5 \pm 0.6)	0.9 (13.6 \pm 7.2)	101.3 (85.8 \pm 20.8)	250.1 (485.5 \pm 164.3)
Skin	2.7 (2.4 \pm 0.7)	0.7 (15.0 \pm 6.4)	108.8 (64.6 \pm 7.9)	228.7 (826.8 \pm 98.4)

Specific activities were calculated for lysosomal enzymes HexA (MUGS), total Hex (MUG), β -galactosidase (β -gal), and Mannosidase (Mann) in various peripheral tissues 16 weeks after AAV gene delivery (4.4×10^{12} g.e./vector/kg; n=3). Values are presented as % of normal with specific activity (S.A.; nmol 4-MU cleaved/mg protein/hour) and standard deviation shown in parenthesis.

Table 2. Vector copies in peripheral tissues 16 weeks post Thal+DCN AAV treatment

Tissue	Liver	Heart	Bone Marrow	Quadriceps	Gonad	Spleen
Vector Copies / 50ng DNA (± standard deviation)	2.0x10 ⁴ (± 6.6x10 ³)	162.9 (± 184.9)	22.5 (± 3.4)	19.3 (± 16.7)	4.8 (± 5.0)	0.8 (± 0.9)

Vector copies were quantified in peripheral tissues by quantitative PCR with primers designed to amplify the woodchuck hepatitis virus post-transcriptional regulatory element (WPRE) of the AAV vector. Values are presented as vector copies per 50ng of genomic DNA (n=3).

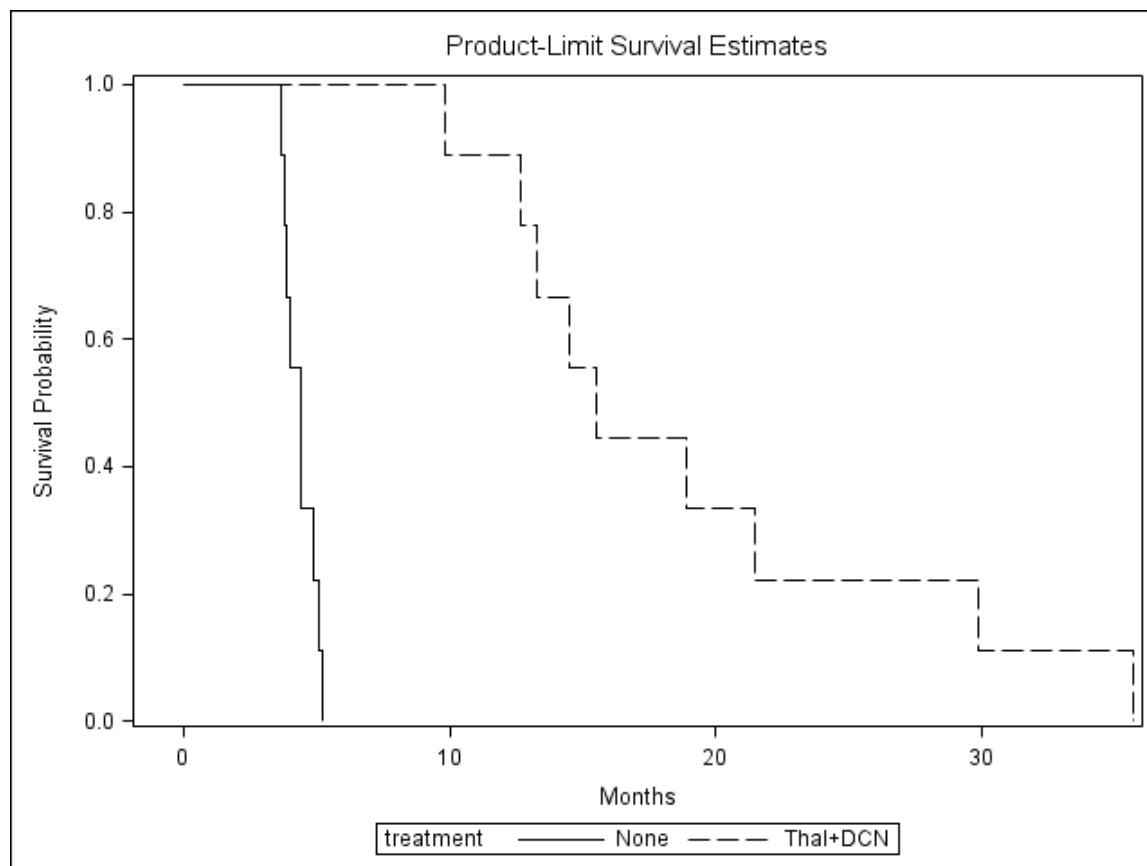


Figure 2. Survival in SD cats after bilateral Thal+DCN injections of AAVrh8-fHEX. Mean survival of AAV-treated SD cats was 19.1 months (n=9); a statistically significant increase compared to untreated SD cats (n=9; $p < 0.0001$; log-rank test). Survival for individual cats: 7-857: 9.8 months; 7-826: 12.7 months; 7-821: 13.3 months; 7-714: 14.5 months; 7-816: 15.5 months; 7-748: 18.9 months; 7-746: 21.5 months; 7-732: 29.9 months; 7-763: 35.7 months.

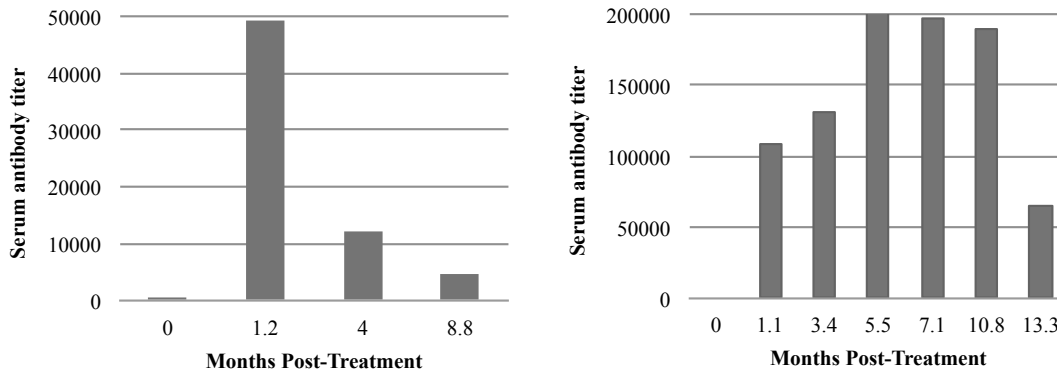


Figure 3. Serum antibody titers to AAVrh8-fHEX in long-term Thal+DCN treated SD cats.

A representative two Sandhoff disease (SD) cats treated by bilateral thalamic and DCN injection of AAV vectors expressing feline Hex were assayed prior to and at multiple time points post-treatment for serum antibodies to the vector. The single cat of this treatment cohort that failed to reach one year of age had a maximum serum antibody titer of 1:49,152 1.2 months post-treatment. In contrast, a representative cat that lived beyond 1 year of age had a higher maximum serum antibody titer of 1:218,453, which occurred later at 5.5 months post-treatment.

Table 3. Enzyme activity in peripheral tissues after long-term Thal+DCN AAV treatment

Tissue	HexA % Normal (S.A. \pm standard deviation)	HexT % Normal (S.A. \pm standard deviation)	β-Gal % Normal (S.A. \pm standard deviation)	Mann % Normal (S.A. \pm standard deviation)
Sciatic Nerve	384.2 (173.9 \pm 133.4)	291.1 (1942.5 \pm 1631.7)	142.6 (20.8 \pm 4.1)	310.5 (184.2 \pm 59.5)
Liver	45.0 (63.5 \pm 45.4)	37.3 (671.5 \pm 619.6)	144.1 (111.3 \pm 51.6)	167.0 (1087.5 \pm 648.9)
Quadriceps	42.9 (2.7 \pm 3.3)	32.7 (53.6 \pm 88.5)	491.9 (8.2 \pm 3.7)	615.3 (108.4 \pm 45.7)
Heart	25.1 (11.7 \pm 13.2)	8.6 (219.3 \pm 241.7)	376.1 (27.4 \pm 19.4)	388.5 (374.1 \pm 292.8)
Small Intestine	3.3 (5.5 \pm 2.9)	0.6 (24.5 \pm 8.8)	194.4 (326.8 \pm 149.2)	373.6 (3191.5 \pm 721.5)

Specific activities were calculated for lysosomal enzymes HexA (MUGS), total Hex (MUG), β -galactosidase (β -gal), and Mannosidase (Mann) in various peripheral tissues of SD cats after long-term treatment with AAVrh8-fHEXA/B (n=9, except heart n=8). Values are presented as % of normal with specific activity (S.A.; nmol 4-MU cleaved/mg protein/hour) and standard deviation shown in parenthesis.

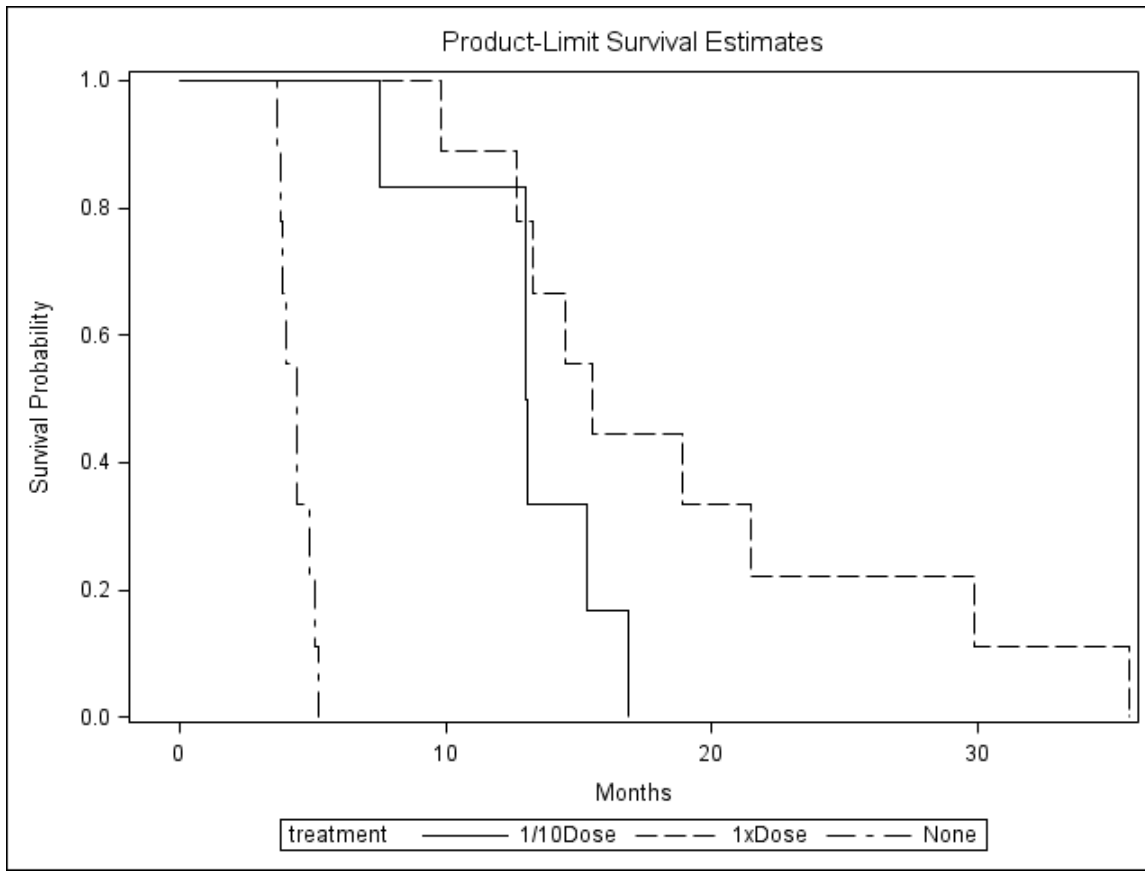


Figure 4. Survival in SD cats after 1/10th dose Thal+DCN injection of AAVrh8-fHEX.

Mean survival of AAV-treated SD cats was 13.1 months (n=6); a statistically significant increase compared to untreated SD cats (n=9; p = 0.0002; log-rank test), but is not significantly different from 1x Dose treated cats (n=9; p = 0.0811; log-rank test). Survival of individual cats: 11-777: 7.5 months; 11-778: 13.0 months; 7-789: 13.0 months; 11-793: 13.1 months; 7-787: 15.3 months; 7-773: 16.9 months.

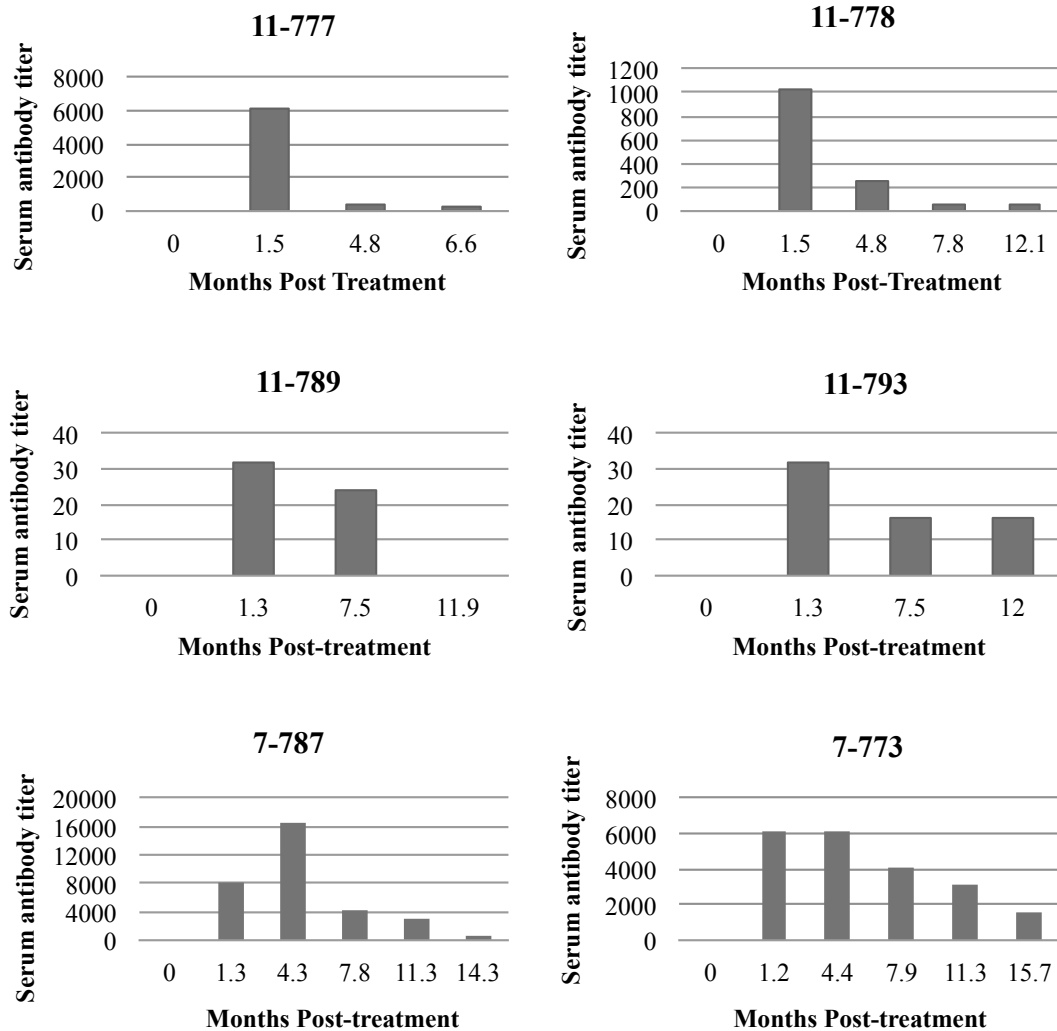


Figure 5. Serum antibody titers to AAVrh8-fHEX in 1/10th dose Thal+DCN treated SD

cats. Six Sandhoff disease (SD) cats treated with 1/10th of the original dose by bilateral thalamic and DCN injection of AAV vectors expressing feline Hex were assayed prior to and at multiple time points post-treatment for serum antibodies to the vector. The maximum serum antibody titer in this cohort, 1:16,384, occurred 4.3 months post-treatment in cat 7-787, which was the second longest living of the treatment group. Of note, two cats that lived beyond 1 year of age had a maximum serum antibody titer of only 1:32.

Table 4. Enzyme activity and vector copies in liver after 1/10th dose Thal+DCN AAV treatment

Cat #	Post-Tx (Months)	HexA % Normal (SA)	HexT % Normal (SA)	Vector Copy#/50ng DNA
7-773	15.7	29.4 (58.8)	36.2 (846.0)	209
7-787	14.3	37.3 (74.5)	41.0 (957.0)	188
11-793	12.0	8 (15.9)	5.7 (133.3)	0
11-789	11.9	8.3 (16.6)	9.6 (224.9)	0
11-778	12.1	26.3 (52.4)	23.2 (542.0)	649
11-777	6.6	33.2 (66.3)	34.9 (814.0)	408

Specific activities were calculated for lysosomal enzymes HexA (MUGS) and total Hex (MUG) in the liver. Values are presented as % of normal with specific activity (S.A.; nmol 4-MU cleaved/mg protein/hour) shown in parenthesis. Vector copies were quantified in the liver by quantitative PCR with primers designed to amplify the woodchuck hepatitis virus post-transcriptional regulatory element (WPRE) of the AAV vector. Values are presented as vector copies per 50ng of genomic DNA.

Table 5. Enzyme activity in peripheral tissues 16 weeks post Thal+ICV AAV treatment

Tissue	HexA % Normal (S.A. \pm standard deviation)	HexT % Normal (S.A. \pm standard deviation)	β-Gal % Normal (S.A. \pm standard deviation)	Mann % Normal (S.A. \pm standard deviation)
Liver	45.3 (95.0 \pm 54.8)	52.7 (1322.6 \pm 882.3)	77.5 (95.9 \pm 48.9)	192.4 (1680.9 \pm 1626.0)
Quadriceps	7.1 (1.1 \pm 0.4)	3.2 (11.4 \pm 4.1)	110.9 (10.3 \pm 1.2)	224.6 (173.2 \pm 30.4)
Bone Marrow	5.1 (9.1 \pm 4.1)	2.6 (64.0 \pm 39.4)	81.2 (105.6 \pm 17.6)	67.7 (730.9 \pm 326.4)

Specific activities were calculated for lysosomal enzymes HexA (MUGS), total Hex (MUG), β -galactosidase (β -gal), and Mannosidase (Mann) in liver, quadriceps, and bone marrow 16 weeks after Thal+ICV delivery of AAVrh8fHEXA/B (1.1×10^{12} g.e./vector/kg; n=4). Values are presented as % of normal with specific activity (S.A.; nmol 4-MU cleaved/mg protein/hour) and standard deviation shown in parenthesis.

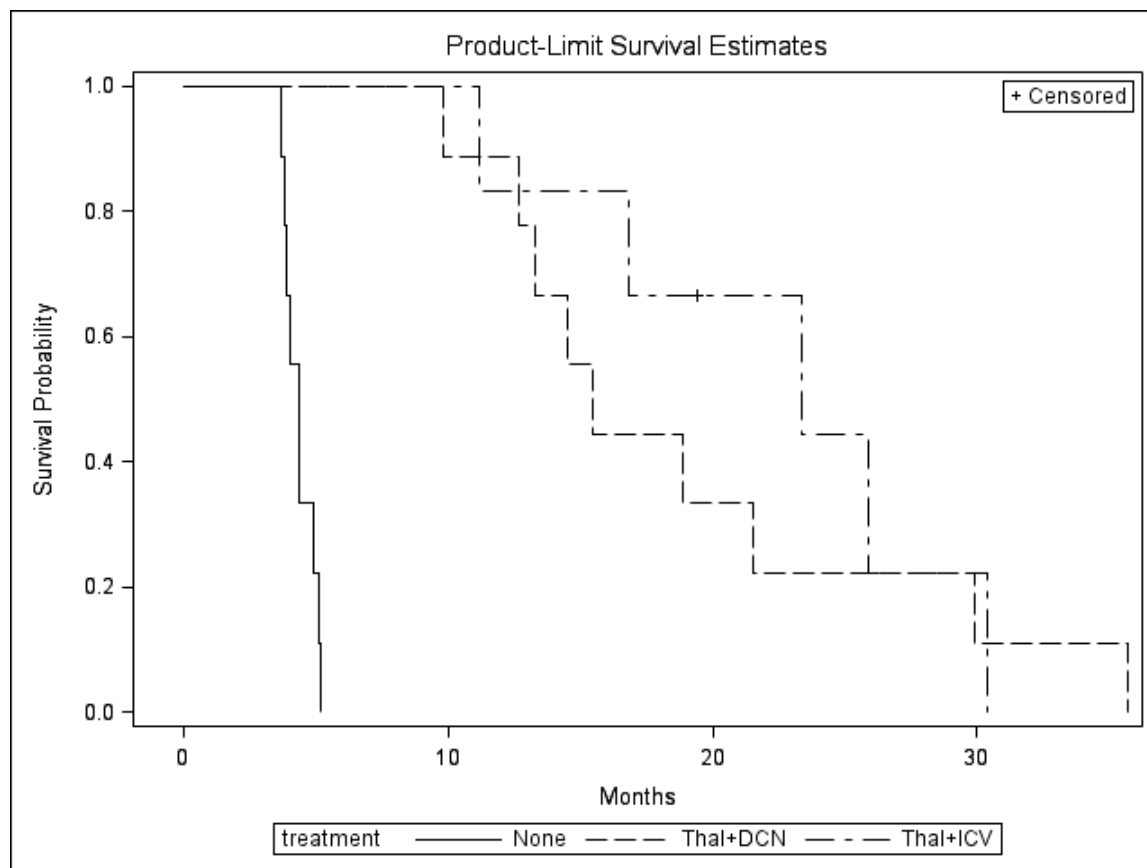


Figure 6. Survival in SD cats after bilateral thalamic and ICV injections of AAVrh8-fHEX.

Mean survival of AAV-treated SD cats to date is 21.2 months (n=6, with one animal ongoing indicated by + on survival plot); a statistically significant increase compared to untreated SD cats (n=9; $p = 0.0002$; log-rank test), but not significantly different from Thal+DCN injected cats (n=9; $p = 0.5467$; log-rank test). Survival of individual cats: 11-907: 11.2 months; 7-945: 16.8 months; 7-943 23.4 months; 7-760: 25.9 months; 11-900: 30.4 months.

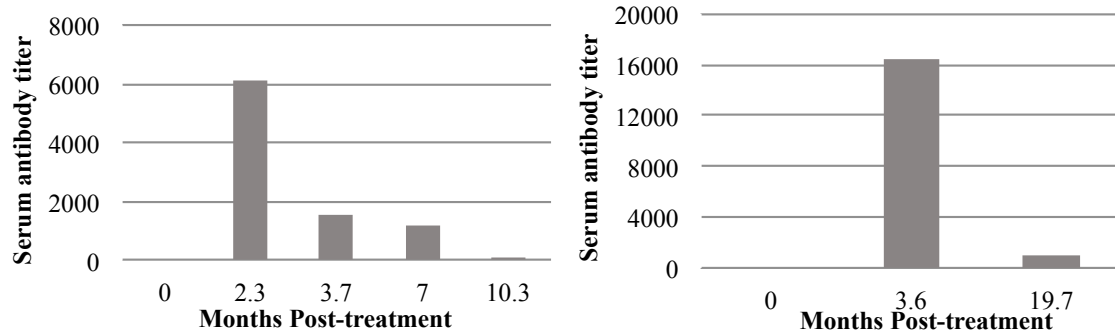


Figure 7. Serum antibody titers to AAVrh8-fHEX in Thal+ICV treated SD cats.

Representative two Sandhoff disease (SD) cats treated by bilateral thalamic and ICV injection of AAV vectors expressing feline Hex were assayed prior to and at multiple time points post-treatment for serum antibodies to the vector. The only cat to reach humane endpoint prior to one year of age had a maximum serum antibody titer of 1:6,144 at approximately 2 months post-treatment. In contrast, a representative cat that lived beyond one year of age had a maximum titer of 1:16,384 3.6 months post-surgery.

Table 6. Enzyme activity in peripheral tissues after Thla+ICV injections of AAVrh8-fHEX

Tissue	HexA % Normal (S.A. \pm standard deviation)	HexT % Normal (S.A. \pm standard deviation)	β -Gal % Normal (S.A. \pm standard deviation)	Mann % Normal (S.A. \pm standard deviation)
Sciatic Nerve	230.3 (104.6 \pm 39.9)	171.6 (1149.2 \pm 430.5)	217.0 (29.7 \pm 15.4)	358.1 (196.3 \pm 105.6)
Liver	53.8 (81.2 \pm 26.3)	60.5 (1105.2 \pm 296.4)	103.5 (79.1 \pm 32.2)	120.5 (794.4 \pm 374.7)
Muscle	20.7 (1.4 \pm 0.1)	13.3 (21.1 \pm 14.9)	762.7 (11.7 \pm 7.6)	641.2 (148.5 \pm 56.3)
Heart	16.9 (8.3 \pm 8.72)	5.5 (140.4 \pm 134.4)	133.9 (10.0 \pm 2.3)	112.6 (98.3 \pm 17.1)
Small Intestine	4.3 (5.9 \pm 2.0)	0.9 (41.1 \pm 29.6)	148.8 (264.4 \pm 88.4)	222.0 (2642.3 \pm 1144.6)

Specific activities were calculated for HexA (MUGS), total Hex (MUG), β -galactosidase (β -gal), and Mannosidase (Mann) in various peripheral tissues after long-term treatment with AAVrh8-fHEXA/B (n=3). Values are presented as % of normal and specific activity (S.A.; nmol 4-MU cleaved/mg protein/hour) and standard deviation are also shown in parenthesis.

Table 7. Serum antibody titers to AAVrh8-nhpHEX in treated healthy non-human primates

NHP	Treatment	Antibody Titer to AAVrh8	Average (\pm Standard Deviation)
0908087	1x	1:2,048	
0909589	1x	1:1,024	1:2,048
0908068	1x	1:3,072	(\pm 836.1)
8963934563	PBS	ND 1:8	ND
09087133	1/10	1:49,152	1:49,152
8722431552	1/10	1:49,152	(\pm 0)
0908997	1/30	1:384	1:256
0909587	1/30	1:128	(\pm 128)
7667353701	Transgene Empty	1:1,024	1:25,088
5347096796	Transgene Empty	1:49,152	(\pm 24,064)

Healthy NHPs treated by bilateral thalamic and ICV injection of AAV vectors expressing nhp Hex at 3 different doses: full dose = 3.2×10^{12} vg (n=3); 1/10th dose = 3×10^{11} vg (n=2); 1/30th dose = 1×10^{11} vg (n=2) as well as PBS only (n=1) and transgene-empty AAVrh8 vector (n=2) controls were assayed for serum antibody titers to vector. ND = Not Detectable.

CHAPTER 4

Biomarkers for disease progression and AAV therapeutic efficacy in feline Sandhoff

Disease

Allison M Bradbury^{1,2*}, Heather Gray-Edwards^{1*}, Victoria J McCurdy^{1,2}, Jamie L Shirley¹, Alexandria N Colaco³, Ashley N Randle¹, Peter W Christopherson⁴, Allison C Bird⁴, Nicholas L De Pompa⁵, Donald Sorjonen⁵, Brandon L Brunson², Mylvaganam Jeyakumar³, Frances M Platt³, Nancy R Cox^{1,4}, Henry J Baker¹, Miguel Sena-Esteves⁶, Douglas R Martin^{1,2}

¹Scott-Ritchey Research Center, College of Veterinary Medicine, Auburn University, Auburn, Alabama, USA; ²Department of Anatomy, Physiology & Pharmacology, College of Veterinary Medicine, Auburn University, Auburn, Alabama, USA; ³Department of Pharmacology, University of Oxford, Oxford, UK; ⁴Department of Pathobiology, College of Veterinary Medicine, Auburn University, Auburn, Alabama, USA; ⁵Department of Clinical Sciences, College of Veterinary Medicine, Auburn University, Auburn, Alabama USA; ⁶Department of Neurology and Gene Therapy Center, University of Massachusetts Medical School, Worcester, Massachusetts, USA.

*Authors contributed equally to this work

Abstract

The GM2 gangliosidoses, Tay-Sachs disease (TSD) and Sandhoff disease (SD), are fatal neurodegenerative disorders of children that are caused by a mutation in the enzyme β -N-acetylhexosaminidase (Hex). Due to the recent emergence of novel experimental treatments, biomarker development has become particularly relevant in GM2 gangliosidosis as an objective means to measure therapeutic efficacy. Here we describe blood, cerebrospinal fluid (CSF), magnetic resonance imaging (MRI) and electro-diagnostic methods for evaluating disease progression in the feline SD model and application of these approaches for the assessment of AAV-mediated gene therapy. SD cats were treated by intracranial injections bilaterally in the thalami and the left lateral ventricle or thalamus and deep cerebellar nuclei with AAVrh8 vectors encoding feline HEX. Blood and CSF based biomarkers were significantly altered in SD cats, and were normalized after AAV gene therapy. Lysosomal expansion in peripheral blood mononuclear cells and compensatory lysosomal enzymatic activities in SD cats were quantified and reduction correlated with therapeutic success after AAV gene therapy. MRI changes characteristic to the gangliosidoses were documented in SD cats and normalized after AAV gene therapy. Here we describe minimally invasive biomarkers for GM2 gangliosidosis and application to evaluate AAV gene therapy.

Introduction

GM2 gangliosidoses are lysosomal storage diseases caused by inherited deficiency in a hydrolytic enzyme, β -N-acetylhexosaminidase (Hex; EC 3.2.1.52), and clinically characterized by progressive neurological impairment resulting in premature death. The enzymatic deficiency leads to accumulation of several enzymatic substrates throughout the body, Degeneration of

neurons initially affects fine motor skills, but rapidly progresses to loss of all body faculties, a vegetative state, and death by the age of five in children. The GM2 gangliosidoses include both Tay-Sachs disease (TSD) and Sandhoff disease (SD), which are almost clinically indistinguishable. Hex functions in the ganglioside degradation pathway by cleaving the terminal N-acetylgalactosamine (GalNAc) residue from GM2 ganglioside. Structurally, Hex is comprised of two subunits, α and β , which dimerize to form distinct isozymes. A mutation in *HEXA*, encoding the α subunit, leads to a deficiency of HexA (α/β) and results in Tay-Sachs disease. A mutation in *HEXB*, encoding the β subunit, leads to a deficiency in both HexA (α/β) and HexB (β/β) and results in SD.

Although mouse models are invaluable in biomedical research, with a brain size >1000 times smaller than an infant (24, 140, 141), their anatomy and physiology are not always true to human disease. Their reduced lifespan precludes long-term studies, and, in diseases where severity is determined by residual enzyme activity, data generated by “knockout” mouse models must be interpreted carefully. Feline models are a logical intermediate step between mice and humans because of similarities in neuropathology (142-145), immunology (146-148) and biodistribution (149). With a brain size 75x larger and more complex than mice, cats are also an improved model for therapeutic evaluation (142-149). A feline model of SD first identified in the 1970s (38) has been extremely well-characterized (39, 40) and presents an unparalleled opportunity to test therapeutic options for translation to human clinical trials. Feline SD results from a 25-base-pair inversion in the terminal exon of *HEXB*, resulting in enzyme activity levels < 3% of normal, allowing for therapeutic assessment of a severe disease phenotype in the presence of, albeit minimal, residual enzymatic activity (39).

The use of adeno-associated virus (AAV) gene therapy has shown great promise in both murine and feline models of SD. SD mice treated with bilateral injections of the striatum and deep cerebellar nuclei (DCN) with monocistronic vectors encoding human *HEX* α - and β -subunits survived to 2 years without significant neurologic disease, which is the maximum age permitted by institutional animal welfare mandates (36, 85). SD cats treated with the same vectors with bilateral injection to the thalamus lived to 7.0 and 8.2 months of age, compared with an untreated life span of 4.5 ± 0.5 months ($n = 11$). Due to a marked humoral immune response to both the AAV vectors and human Hex, SD cats were subsequently treated with feline-specific vectors and lived to 10.4 ± 3.7 months of age ($n = 3$), or 2.3 times as long as untreated cats (133). While injection to the thalamus significantly increased lifespan, this injection route failed to treat the cerebellum. Additional routes of delivery, including direct injection to the deep cerebellar nuclei (DCN) and intracerebroventricular (ICV) injection via the left lateral ventricle, are currently being explored in SD cats (150-152). The success of both murine and feline studies support the therapeutic potential of AAV vectors for SD and underscore the potential for translational research.

To translate large animal models to human clinical trials it would be exceptionally beneficial to have a minimally invasive, highly sensitive, and reproducible method of tracking disease progression and effectiveness of treatment. An ideal biomarker should be reflective of the disease as a whole (including central nervous system and peripheral disease) and should correlate with results of routine neurological exams and clinical evaluations (including MRI, radiographs, ultrasound, and CT). To date, few prospective biomarkers have been identified in murine models and human SD patients, but as they are technically difficult and time consuming they have not been adopted into clinical practice (153). Neurodegeneration is a common feature

of many lysosomal storage diseases making it likely that biomarkers developed and validated in one disease may also be useful for many others in this group of diseases. Elevations of aspartate aminotransferase (AST), and lactate dehydrogenase (LDH) have been noted in serum and CSF of patients with Tay-Sachs disease (20, 154, 155) and canine GM1 gangliosidosis (156). After validation in a mouse model of Niemann-Pick C (NPC) disease (157), LysoTracker, a fluorescent, acidotropic probe, has recently been validated as biomarker in more than 100 NPC patients (158). Increased fluorescence signifies expansion of acidic compartments, indicative of lysosomal storage, and correlated with age and disease progression. Furthermore, in response to substrate reduction therapy, LysoTracker levels were substantially reduced. Lastly, a neonatal screening program demonstrated elevation of lysosome associated membrane protein (LAMP-1) in plasma of approximately 70% of LSD patients and is being developed as a newborn screening assay (159).

To date, limited research has been conducted on biomarkers of SD and no results have been reported in a large animal model. In this study we evaluate biomarkers of disease progression in a feline SD model and utilize these biomarkers to measure the efficacy of intracranial AAV gene therapy. To our knowledge this is the first effort to investigate the validity of a number of minimally invasive measures to track disease progression and therapeutic response of AAV gene therapy in a large animal model of SD. Our results support their inclusion in future of AAV gene therapy clinical trials in GM2 gangliosidosis patients as investigational endpoints.

Results

Blood chemistry and complete blood count

We examined routine blood chemistry profiles of SD and normal control cats from birth to 23 weeks of age, the approximate humane endpoint for SD cats. Seven additional SD cats were treated with a 1:1 formulation of monocistronic AAVrh8 vectors encoding feline Hex α and β subunits (AAVrh8-fHEXA/B). SD cats were divided into two treatment cohorts based on injection route: bilateral thalamic and DCN injection (Thal+DCN, n=3) or bilataeral thalamic and ICV injection (Thal+ICV, n=4). For all AAV-treated cats analyzed, the initial time point was prior to intracranial surgery which is conducted at 4-5 weeks of age. The analysis of 18 routine blood chemistry analytes revealed several values that were significantly altered in untreated SD cats. Aspartate aminotransferase (AST) activity steadily rose in SD cats and was significantly different from normal control cats at 16-23 weeks of age ($p < 0.01$). After treatment with AAVrh8-fHEXA/B, SD cats showed complete normalization of AST by 8-12 weeks of age, which remained normalized at 16-23 weeks regardless of injection route (Fig. 1 A). Mild but significant reductions were seen in albumin concentration by 8-12 weeks of age in SD cats, compared to normal controls ($p < 0.01$) and by 16-23 weeks of age, both AAV treatment groups showed normal albumin levels (Fig. 1 B). Similarly, calcium was significantly decreased by 8-12 weeks of age in SD cats when compared to normal controls ($p < 0.05$), but was normalized by 16-23 weeks subsequent to treatment (Fig. 1 C). The earliest onset and most significant difference was a reduction in serum cholesterol levels, which reached a significance of $p < 0.01$ in SD cats prior to 6 weeks of age, compared to normal controls, and continually decreased with disease progression. In the Thal+DCN treatment group there was no improvement in cholesterol levels at any time point, while there was partial normalization by 8-12 weeks of age in the Thal+ICV treatment group (Fig. 1 D). SD cats exhibited mild to moderate anemia with significant reduction in red blood cell count (RBC) by humane endpoint ($p < 0.01$; Fig 1E),

without significant changes in the hemoglobin content (MCHC, MCH) or red blood cell size (RDW; data not shown). RBC was restored to normal in the Thal+DCN treatment group and trended to significance in the Thal+ICV group. Blood Urea Nitrogen (BUN) concentration was elevated in the SD cat at humane endpoint ($p < 0.01$) and was not normalized after Thal+DCN injection but largely corrected after Thal+ICV treatment. Mean platelet volume was increased in SD cats at 16-23 weeks and returned to normal levels in the Thal+DCN treatment group ($p < 0.05$) but not the Thal+ICV treatment group (data not shown).

Cerebrospinal fluid analysis

Unlike blood-based biomarkers, cerebrospinal fluid (CSF) analysis is more likely to provide information regarding alterations specific to the central nervous system (CNS). In agreement with serum chemistry findings, routine CSF analysis revealed significant elevation of AST activity in SD cats. Elevated AST activity in CSF was detected as early as 4-8 weeks of age compared to normal controls ($p < 0.01$) and continued to increase with disease progression. Complete normalization of CSF AST levels was documented in the Thal+DCN treatment group by 16-23 weeks. In the Thal+ICV treatment group there was a large decrease in CSF AST levels ($p < 0.01$ compared to untreated) without complete normalization ($p < 0.05$ compared to normal) (Fig. 2A). The increase in CSF lactate dehydrogenase (LDH) activity in SD cats became statistically significant at 8-12 weeks of age ($p < 0.01$). LDH levels in CSF were normal in both AAV-treatment groups at 16-23 weeks of age (Fig 2B). CSF creatine kinase activity, total protein and total calcium were also evaluated in SD and normal cats, but differences were not noted. Normal AST and LDH levels were established using cats of all ages, and levels remain constant across all age ranges.

LysoTracker analysis of PBMCs

To determine whether expansion of the lysosomal system itself could serve as a marker of disease progression, we measured relative lysosomal volume in peripheral blood mononuclear cells (PBMCs) beginning at 8 weeks of age and successively in four week intervals until SD cats reached the humane endpoint. LysoTracker is a fluorescent, acidotropic probe used to selectively label acidic organelles in live cells to examine the biosynthesis or pathogenesis of lysosomes. After staining isolated PBMCs with LysoTracker, the cells were analyzed by flow cytometry and positive cells were sorted for further identification. Sorting determined the vast majority (> 65%) of the LysoTracker positive cell population to be granulocytes (Fig. 3 C). At 8 weeks of age the average percent of LysoTracker positive granulocytes in SD cats was 25.6% and this value progressively increased to 47.9% at humane endpoint (n=5, 20.6 ± 1.3 weeks) (Fig. 3 A), indicating expansion of the lysosomal compartment due to increased storage. In contrast, normal control littermates maintained between 6.5% and 10.3% of LysoTracker positive granulocytes throughout the duration of the experiment. There was no difference in the percentage of granulocytes comprising the entire white blood cell population between normal (2.87%) and SD cats (2.68%). In the Thal+ICV treatment group there was partial normalization of the lysosomal compartment, averaging 37.5% LysoTracker positive granulocytes (n=3, 22.3 ± 1.0 weeks) at sixteen weeks post-injection (Fig. 3 B). However, this value was significantly higher than normal control cats (n=5, $p < 0.05$).

Complete blood count data showed a slight increase in neutrophils in untreated SD cats by 5 weeks of age compared to normal cats of the same age ($p < 0.05$) (Fig. 3 D). Neutrophil counts continued to increase with disease progression, reaching a greater significance ($p < 0.01$) by 8-12 weeks of age, and remained unchanged until the humane endpoint. Neutrophil counts were normal in both AAV treatment groups at 8-12 weeks of age regardless of injection route. At

the last data point analyzed (16-23 weeks of age) neutrophil counts remained normal in the Thal+ICV treatment group, but were significantly higher than normal in the Thal+DCN treatment group ($p < 0.05$).

Echinocytosis

Analysis of blood smears of SD cats revealed an abnormally large population of echinocytes, or spiculated red blood cells. In SD cats < 2 months of age, the percent of echinocytes comprising all red blood cells was 25.3% (Fig. 4 A). After 2 months of age the percentage of echinocytes increased to $> 50\%$ of all red blood cells and this was maintained until SD cats reached the humane endpoint. In contrast, echinocytes comprised $\leq 1\%$ of the red blood cell population in normal control cats. At humane endpoint, the percentage of echinocytes in SD cats (Fig. 4 C) was significantly greater ($p < 0.01$, $n=4$) than normal control cats (Fig. 4 D). Bilateral thalamic and DCN injection of AAV failed to attenuate echinocyte formation, while bilateral thalamic and ICV injection route showed partial normalization (Fig. 4 B, E, F). Statistics were not conducted on the treatment group due to few data points available ($n=2$ for each group).

Lysosomal enzyme activity

In the absence of β -N-acetylhexosaminidase, other lysosomal enzymes are upregulated by an unknown mechanism. Specifically, increased activity of β -galactosidase (β gal) and α -mannosidase (Mann) has been seen in numerous tissues of SD cats. Enzyme activity measured in PBMCs isolated from whole blood of SD cats showed a 2-fold increase in β gal and a 2.5-fold increase in Mann when compared to normal controls. Sixteen weeks after AAV-mediated gene therapy, activities of both enzymes were decreased, but to varying degrees. Four Thal+ICV AAV-treated cats were sacrificed 16-weeks after treatment for short term analysis. Post-mortem

analysis of enzyme activity in the brain and liver showed a direct correlation between Hex restoration and reduction of β gal and Mann in PBMCs (Fig. 5 A). Specifically, cat 7-972 attained the highest Hex activity at the thalamic injection site, reaching 92-fold normal, and also had complete normalization of Hex activity in the liver. Consequently, β gal activity in PBMCs was completely normalized and Mann was reduced more than 50% compared to untreated SD cats. In contrast, Hex activity at the thalamic injection site of cat 7-957 reached 50-fold normal and the liver achieved only 57% of normal Hex activity. In this cat the β gal and Mann levels in PBMCs were above those of untreated SD cats.

As evident by routine H&E staining in SD cats, approximately 95% of hepatocytes contained large, discrete, intracytoplasmic vacuoles which displaced the nucleus of the affected cell peripherally. Additionally the stroma of the portal triads was mildly edematous and rare Kupffer cells located adjacent to the sinusoids were swollen and contained fine, clear cytoplasmic vacuoles (Fig. 5 B). In contrast, normal cat hepatocytes and Kupffer cells lacked vacuolization, had centrally located nuclei, and portal edema was absent (Fig. 5 C). Hepatocytes from AAV treated SD cats had sporadically contained 1-3 small, discrete clear vacuoles and Kupffer cells lacked vacuolization. The change was noted to be minimal, and did not affect a specific region of the hepatic lobule, however, an area with the most severe changes was chosen for visualization (Fig. 5 D).

MRI

Alterations in brain architecture were evaluated non-invasively using MRI. SD cats imaged at humane endpoint (4.5 ± 0.5 months) on T2 weighted (T2w) MRI exhibited profound brain atrophy as well as indistinguishable or inverted gray matter (GM) and white matter (WM) intensities (Fig. 6 B). Changes of signal intensity (SI; $p < 0.05$) were noted within the olfactory

bulb, precuneate gray matter, caudate nucleus (Fig. 6 E), suprasplenic gyrus GM and WM, temporal lobe WM (Fig. 6 G), caudal colliculus, occipital cortex WM (Fig. 6 F), DCN and ventral brainstem (Fig. 6 H). Sixteen weeks after AAV-mediated gene therapy brain architecture was normalized as measured by preservation of gray and white matter intensities and prevention of cortical atrophy. Signal intensities were restored to normal in the Thal+DCN group in all aforementioned areas, with partial normalization in the DCN. One Thal+ ICV cat is included in the analysis, but statistics were not performed (Fig. 6 C-D).

BAER and ERG

To characterize auditory pathway abnormalities in feline SD, brainstem auditory evoked response (BAER) was performed at 8-12 weeks and 16-23 weeks (humane endpoint). Increased latencies were observed in waves II, III and V in SD cats at 8-12 and 16-23 weeks and correlated with neurologic disease progression (Fig. 7 A). Interwave latencies of I - III were significantly increased in SD cats at 16-23 weeks and interwave latencies for III-V and I-V were increased at both 8-12 and 16-23 weeks of age (Fig. 7 B).

Scotopic ERG (ERG) analysis revealed no significant difference between the amplitude or implicit times of the A or B waves in SD cats. The implicit time of the A wave was 17.1 ± 2.5 ms, 16.5 ± 1.9 ms and 15.25 ± 0.5 ms for SD cats at 8-12 weeks, SD cats at 16-23 weeks and normal kittens of similar age, respectively. The implicit times for the B waves were 58.0 ± 7.8 ms, 58.6 ± 3.7 and 26.1 ± 3.3 ms for three month old SD cats at 8-12 weeks, SD cats at 16-23 weeks and normal kittens of similar age, respectively. The amplitude for the B waves were 159.2 ± 47.1 μ V, 119.83 ± 39.2 μ V and 145.2 ± 56.6 μ V for 3 month SD cats, SD cats at humane endpoint and normal cats, respectively.

Discussion

In lysosomal storage diseases, disease progression has historically been restricted to the identification of disease etiology and severity. With the development of new therapeutics, like enzyme replacement, chaperone therapy, substrate reduction and gene therapy, biomarker discovery is increasingly important as the means to assess therapeutic effects objectively. This is particularly relevant to Tay-Sachs and Sandhoff disease, where only small cohorts of patients are available to participate in clinical trials. In these cases, effective biomarkers could be used to compensate for limited patient numbers by providing physicians with validated methods for evaluation. Here we described multimodal biomarkers in a large animal model of Sandhoff disease and applied these biomarkers in a therapeutic setting.

The natural history of neurologic disease progression in SD cats consists of a profound whole body tremor, spasticity and progressive neurologic decline (38). Sixteen weeks after pre-symptomatic gene therapy SD cats do not exhibit these profound neurologic deficits and are almost indistinguishable from normal controls. AAV-treated cats developed mild hind limb weakness, but subsequently disease progression in treated cats was stabilized. At the study endpoint, subtle tremors of the head and tail were present in all AAV-treated cats; however, none developed overt whole body tremors, which are evident in untreated SD cats at an early age. Although these clinical findings are outside the scope of this article, biomarkers described herein reflect changes in the neurologic state of untreated SD cats as well as amelioration of disease after AAV gene therapy.

CSF and blood based biomarkers

Clinicopathologic parameters measured here are already regularly used in medicine. AST (EC 2.6.1.1) is a ubiquitously expressed enzyme that catalyzes the interconversion of

aspartate and α -ketoglutarate to oxaloacetate and glutamate and, in the CNS, functions to manage levels of excitatory neurotransmitters. Elevations of AST in the CNS have previously been reported in human GM2 gangliosidosis, Alzheimer's disease, canine GM1 gangliosidosis, brain insult and stroke and are thought to be due to leakage from neurons and other CNS cells (154-156, 160, 161). Similarly, lactate dehydrogenase (LDH: EC 1.1.1.27 & EC1.1.1.28), which catalyzes the interconversion of pyruvate and lactate, is ubiquitously released from all cells after damage to the plasma membrane. LDH is thought to be a biochemical index of neuronal cytotoxicity (162) with elevations in a wide array of neurological disorders including meningitis (163), prion disease (164), leukemia (165), trauma (166), infantile spasms (167), stroke (160), canine GM1 gangliosidosis (156) and can be used to distinguish various neurological disorders (166, 168). In our feline SD model, levels of AST and LDH in CSF correlate with disease progression and therapeutic impact after gene therapy. Plasma AST levels also reflect the neurologic status in the SD cat, but the source of AST release remains unknown.

Albumin, the main component of plasma, is reduced in human GM2 gangliosidosis (155), and in SD cats by 8-12 weeks of age. Intracranial delivery of AAV-gene therapy resulted in restoration of plasma albumin levels. Calcium levels trended similarly, with reduced levels in the SD cat and restoration after AAV-gene therapy, but its changes are likely a direct consequence of reduced albumin-calcium binding in circulation. Unfortunately, ionized calcium was not assessed. Altered calcium homeostasis is a common feature of lysosomal storage diseases (169, 170), and elevated cytosolic calcium has been shown in SD mice and attributed to endoplasmic reticulum defect (171). Hepatic disease, as suggested in Figure 5, is present in both human (172) and feline (144) Sandhoff disease, and is a potential etiology of albumin reduction. The role of albumin remains unknown, but interestingly human serum albumin has been

suggested to promote neuronal survival through production of glutamate (173), prevent formation of amyloid β self-association in Alzheimer's disease (174) and improve outcomes in models of focal cerebral ischemia (175-177).

Circulating cholesterol was decreased in the SD cat at 8-12 weeks and reduction continued with advancement of neurologic signs. Cholesterol levels were not restored after AAV therapy by either injection route. Cholesterol that is destined for neuronal metabolism is thought to be primarily synthesized by astrocytes (178, 179), making reduced plasma cholesterol more likely a finding specific to the effects of SD in peripheral tissues. Anemia is also a prominent finding in several lysosomal storage disorders including Gaucher disease (180) and is used as a powerful biomarker to score severity and need for enzyme replacement therapy (181). Our findings here within suggest that this may also be an applicable clinical test in SD.

Echinocytosis is a morphologic change of the erythrocyte that is hypothesized to be part of erythrocyte apoptosis (182) and may provide a potential etiology for anemia present in the SD cat. The red cell membrane of the TSD patient contains many alterations, including lipids, glycoproteins and proteins (183-187) and altered red cell membrane composition has been reported to increase susceptibility to oxidative stress and echinocytosis (188, 189). Gene therapy partially decreased echinocyte formation in the SD cat after Thal+ICV injection, which suggests erythrocyte morphology as a potential indicator of therapeutic efficacy.

Blood Urea Nitrogen (BUN) was also elevated in SD cats, but creatinine levels remained unchanged, suggesting an extra-renal source. Potential sources include gastrointestinal hemorrhage and dehydration; but reduced albumin and normal serum protein levels make dehydration less likely. While platelet number remains within the normal range, platelet size is increased in SD cats, suggesting that increased platelet size may not be secondary to

thrombocytopenia. Platelets are an emerging biomarker for ischemic stroke, multiple sclerosis, Alzheimer's Disease and glioblastoma through absorption of microvesicles (for a review see (190)). Platelets have been shown to contain RNA released from tumor cell microvesicles, and these tumor specific RNAs isolated from platelets may potentially be used to screen glioma and prostate cancer (191). Although the role of platelet size was not investigated in these studies, platelet alterations may be indicative of neurologic change.

Marked expansion of the lysosomal compartment to nearly fivefold normal was demonstrated in granulocytes of SD cats. Sixteen weeks after AAV-gene therapy, LysoTracker staining of the cells was only marginally reduced indicating failure to reduce storage in this cell population or its bone marrow precursor. This finding was in agreement with sub-therapeutic levels of Hex in PBMCs after AAV therapy, 1.69% of normal (n=3), which is comparable to untreated controls (1.84% of normal, n=5). Despite not being the intended population of PBMC isolation, neutrophils were found to be the primary cell population with amplification of the lysosomal compartment in SD cats. In circulation, neutrophils are expected to comprise nearly 70% of all white blood cells; however, after the isolation procedure neutrophils accounted for only ~3% of total white cells. A protocol specific for neutrophil isolation may provide a more accurate representation of alterations in the lysosomal compartment of neutrophils. However, common protocols of neutrophil isolation utilize large volumes of blood, which is greater than what we are able to safely remove from cats \leq 5 months of age. Furthermore, after validation in a mouse model of Niemann-Pick C (NPC) disease, the use of LysoTracker as a biomarker has recently been validated in more than 100 NPC patients. As seen in our SD cats, NPC mice and patients demonstrated significant elevation of the acidic compartment, which correlated with age and disease progression. In response to substrate reduction therapy with miglustat, LysoTracker

levels were substantially reduced. In this study CD19+ B cells were isolated from mononuclear cells prior to staining with LysoTracker, which offers another alternative to our approach (158).

In agreement, complete blood counts revealed nearly a threefold increase of neutrophils in the blood of SD cats at humane endpoint. Neutrophilia is also observed in the Gaucher mouse, with a hypothesized etiology of antigen presenting cell intracellular storage and release of granulocyte colony stimulating factors (GCSF) to mobilize hematopoietic progenitor cells. Additionally, neutrophil recruiting chemokines CXCL-1 and 2 were also detected in sera from Gaucher mice (192). Levels of CXCL and GCSF have not been measured in SD cats but could further elucidate the cause of neutrophilia.

Partial correction of the periphery after intracranial delivery of gene therapy has been described in mucopolysaccharidosis (MPS) IIIA mice (193), late infantile neuronal ceroid lipofuscinosis (LINCL) mouse (105) and distribution of AAV in peripheral tissues has been described in nonhuman primates after intraparenchymal brain injection (104). The importance of this finding is twofold; the application of peripheral tissue correction as a marker for CNS improvement, as well as a therapeutic strategy for neuronopathic diseases with secondary peripheral involvement. As previously stated, hepatic disease is a common feature in feline and human SD. In the SD cat there is an increased activity of other lysosomal enzymes, β -galactosidase and α -mannosidase, which are thought to be up-regulated in a compensatory manner. AAV-gene therapy and subsequent Hex enzymatic restoration normalizes the activities of other lysosomal enzymes and these findings correlate with histological changes. Reductions in vacuolation and stromal edema in AAV treated animals is clearly apparent, which is suggestive of partial hepatocyte function restoration. Perhaps most importantly, is a potential correlation of restoration of Hex activity in the liver to that of the brain in individual animals. Liver biopsies

are much less invasive than brain biopsies and these data suggest that liver enzyme restoration may correlate to that of enzymatic restoration of the CNS, providing invaluable insight into therapeutic efficacy. Furthermore, reduction of other lysosomal enzymes in PBMCs correlated with brain and liver Hex levels, providing a minimally invasive peripheral tissue that could afford evidence towards the outcome of intracranial therapy.

Clinical biomarkers

Routine clinical examinations, like brainstem-evoked auditory responses (BAER) and MRI, can be used to assess therapeutic efficacy of AAV mediated gene therapy in GM2 gangliosidosis. On MRI, human and feline GM2 gangliosidosis follow characteristic patterns of neurodegeneration, which on T2w images show increased signal in the white matter, and decreased signal in gray matter (194-196). As glycosphingolipid storage increase in neuronal cell bodies of the gray matter and as the white matter undergoes demyelination, these two tissues become MR indistinguishable, or isointense. When glycosphingolipid accumulation in gray matter exceeds that within white matter an inversion of intensities is observed. AAV-gene therapy resulted in significant normalization of intensities in all brain areas regardless of injection route. These data suggest that MRI will continue to be a clinically valuable tool in evaluating success of novel therapeutics for GM2 gangliosidosis.

Most SD and TSD patients develop deafness and blindness (2, 197) and assessment of therapeutic efficacy is important in predicting quality of life after AAV-gene therapy. In this study BAER was used to localize neurodegeneration associated with the auditory pathway in the SD cat. In the cat, peak I is associated with latency of the cochlear nerve, peak II is correlated with the latency of the cochlear nucleus, peak III is associated with the region of the nucleus of the trapezoid body, and peak V with latencies recorded in the caudal colliculus (198, 199).

BAER tracings from SD cats at 8-12 weeks suggest abnormalities in the cochlear nucleus, the nucleus of the trapezoid body and the caudal colliculus but normal function of the cochlear nerve. Mean latencies at these areas increased at 16-23 weeks, but did not reach significance (Figure 6). These data correlate with findings in human patients (200), suggesting the cat is an appropriate model to study electrophysiology. Unfortunately BAER was not used to evaluate the AAV treated cats, but represents a potential technique to evaluate cortical electrophysiology after gene therapy. Electroretinograms were used in an effort to determine the source of reduced vision in SD cats and were noted to be within normal limits. Normal ERGs have been reported in human patients with GM2 gangliosidosis (200), further validating the cat as a translatable model. The ERG findings point to a non-photoreceptor etiology for decreased vision, and visually evoked potentials would likely be more appropriate for visual assessment after therapy.

Summary

Minimally invasive biomarkers are particularly relevant for orphan class diseases, like GM2 gangliosidosis, with reduced numbers of patients. Regulatory procedures designed for more common diseases pose difficulty in small cohorts because of the time required to reach sufficient power. Therefore, development of novel therapeutics for rare diseases will benefit from more rigorous scrutiny using sensitive, validated biomarkers to monitor therapeutic response(201). Here we describe clinically translatable biomarkers of feline GM2 gangliosidosis and describe their use in assessment of SD cats after AAV gene therapy, which, at the time of testing had substantial amelioration of the disease phenotype. It is our hope that the biomarkers described herein will provide insight into the effects of AAV gene therapy in neurodegeneration and assist clinicians in assessment of therapeutic efficacy.

Materials and Methods

Animals and Surgery All animal procedures were approved by the Auburn University Institutional Animal Care and Use Committee. Bilateral injection of the thalamus and deep cerebellar nuclei (DCN) were performed according to a previously published protocol (133). Intracerebroventricular injection was performed under ultrasound guidance to confirm the correct placement of the injection needle. After visualization of the left lateral ventricle with an 8-5 MHz Philips HDI 5000 ultrasound probe (Philips Healthcare, Andover, MA), a single entry site was made through the skull with a 20G spinal needle. Vector was then delivered using a Hamilton syringe (Harvard Apparatus, Holliston, MA) fitted with a 25G non-coring needle (Harvard Apparatus). A total of 200uL was delivered in 10-15 uL aliquots at a rate of 3-5 uL/second with approximately 1 minute between aliquots.

At humane or a predetermined endpoint animals were euthanized by pentobarbital overdose (100 mg/kg) and transcardially perfused with cold, heparinized saline. The brain was divided into coronal blocks of approximately 0.5 cm from the frontal pole through the cerebellum. The right hemisphere of the brain was preserved in optimal cutting temperature (OCT) medium for determination of enzyme activity. The left hemisphere of the brain and all other tissues were formalin fixed and flash-frozen in liquid nitrogen and preserved at -80 °C.

AAV Vectors The feline HEXA cDNA was amplified and cloned as previously described (133). Feline HEX transgene expression is driven by the hybrid CBA promoter including the CMV immediate-early enhancer fused to the CBA promoter (116) and the woodchuck hepatitis virus post-transcriptional regulatory element (WPRE) was included for enhancement of gene expression. AAVrh8 vector stocks encoding Hex were produced as previously described (117).

Blood and cerebrospinal fluid analysis Blood was collected from the jugular vein at predetermined time points after tranquilization with dexmedetomidine (0.4mg/kg IM). Blood for complete blood count was put into EDTA tubes and analyzed using ADVIA 120 Hematology System (Seimens Medical Solutions, Malvern, PA). Blood for serology was placed in heparinized tubes and analyzed using a Cobas C311 chemistry analyzer (Roche Diagnostics, Indianapolis, IN). For quantification of echinocytes, Diff-Quick stained blood smears were scanned on an Aperio ScanScope CS2 (Vista, CA) and three 40x magnification fields were counted.

Cerebrospinal fluid (CSF) collection was performed while under general anesthesia. Cats were anesthetized using dexmedetomidine (0.4mcg/kg IM) and ketamine (10mg/kg IM), underwent tracheal intubation and anesthesia was maintained using isoflurane (0.5-2%). CSF was collected from the cerebromedullary cistern as previously described (202). CSF samples were collected and aliquots were analyzed for cytology and total protein. Samples were then immediately centrifuged at 100x g for 5 minutes to remove any blood contamination. Samples then underwent one freeze thaw cycle at -80°C and were analyzed using Cobas C311 chemistry analyzer (Roche Diagnostics, Indianapolis, IN).

LysoTracker® staining and quantification of PBMCs Peripheral blood mononuclear cells (PBMCs) were isolated from whole blood with Ficoll-Paque PLUS (GE Healthcare, Buckinghamshire, United Kingdom) according the manufacturer's instructions. Isolated PBMCs were incubated with 200 nM of LysoTracker® Green (Molecular Probes, Grand Island, NY) for 20 minutes in the dark, centrifuged for 5 minutes at 200 x g in an IEC HN-SII centrifuge

(Damon/IEC, Needham Heights, MA), and resuspended in 250 uL of MACS buffer. Samples were analyzed on an Accuri C6 flow cytometer (BD Biosciences, San Jose, California) and data collected using CFlow software. Further sorting of select samples was conducted using MoFlow XDP cell sorter (Beckman Coulter, Brea, CA) and differential cell counts were performed on prepared cytopins.

Enzyme Assay The activity of lysosomal enzymes was determined using a previously published protocol (40). The fluorescence of 4-methylumbelliferyl (4-MU) substrates (β -gal, 0.5 mmol/l 4-MU- β -D-galactoside, pH 3.8; HexA, 1 mmol/l MUGS, pH 4.2; and total Hex, 1 mmol/l 4-MU-N-acetyl- β -D-glucosaminide (MUG), pH 4.3.) was measured at an excitation/emission of 360 nm/ 450 nm on a BioTek Synergy HT plate reader (BioTek, Winooski, VT). Specific activity was expressed as nmol 4-MU cleaved/mg protein/hour.

1.5T MRI Quantification MRIs were performed in SD cats at humane endpoint and in AAV-treated cats at 16 weeks post treatment. Cats were anesthetized with dexmedetomidine (0.4mcg/kg) and ketamine (10mg/kg), and maintained on 0.5-2% Isoflorane after tracheal intubation. All MRI scans were performed on an Infinion 1.5 Tesla MRI scanner (Phillips Healthcare, Andover, MA) using a lower extremity quadrature coil (Phillips Healthcare, Andover, MA). Scan parameters are as follows: 2D transverse T2 weighted turbo spin echo (TSE) images with 5mm³ resolution, TR/TE of 4072/141.7 ms, echo train length of 16, BW of 20.8 KHz/pix, and 3 averages.

MRI based cortical and cerebellar changes were quantified using pixel intensity measurement. Pixel intensities were measured in quadruplicate at the individual area of interest.

The average pixel values were then normalized to the intensity of CSF, also measured in quadruplicate, on that particular slice. All measurements were performed using the probe tool included in EFilm 3.2 software (Merge Healthcare, Chicago, IL, USA).

Brainstem Auditory Evoked Responses (BAER) BAER assessments were performed in SD cats at 8-12 weeks and at humane endpoint (16-23 weeks). Cats were sedated with 0.4 ug/kg dexmedetomidine and BAER was performed using a Nicolet VikingQuest electrodiagnostic instrument (CareFusion, San Diego, CA). BAER was performed using earplug and hollow tubing auditory transmission apparatus, a click stimulus of 11.4 Hz at 75dB, contralateral noise at 40dB. Electrode placement was as previously described (203) and is as follows: mastoid reference (negative electrode), vertex reference (positive electrode) and ground placed on midline at the level of the occipital condyles. Response to click stimulus was acquired over 1.5 ms sweep with an amplitude of 0.2 μ V and 1000 averages. Measurements were repeated 3 times per side per time point. Peak identification was performed as previously described (199, 204).

Electroretinogram (ERG) ERG was performed at 3 months and humane endpoint in SD cats. Ophthalmologic examination was performed and eyes were dilated using 1-2 drops tropicamide (1% solution). Cats were then sedated using dexmedetomidine (0.4mcg/kg) intramuscularly. Cats were dark adapted for 15 minutes prior to the procedure. Scotopic ERGs were recorded using a BPM-100 instrument (Retiongraphics, Norwalk, CT) with an active corneal contact lens electrode (Bausch & Lomb, Rochester, NY). The reference and ground electrodes were placed subcutaneously at the lateral canthus and skull vertex.

Figures and tables

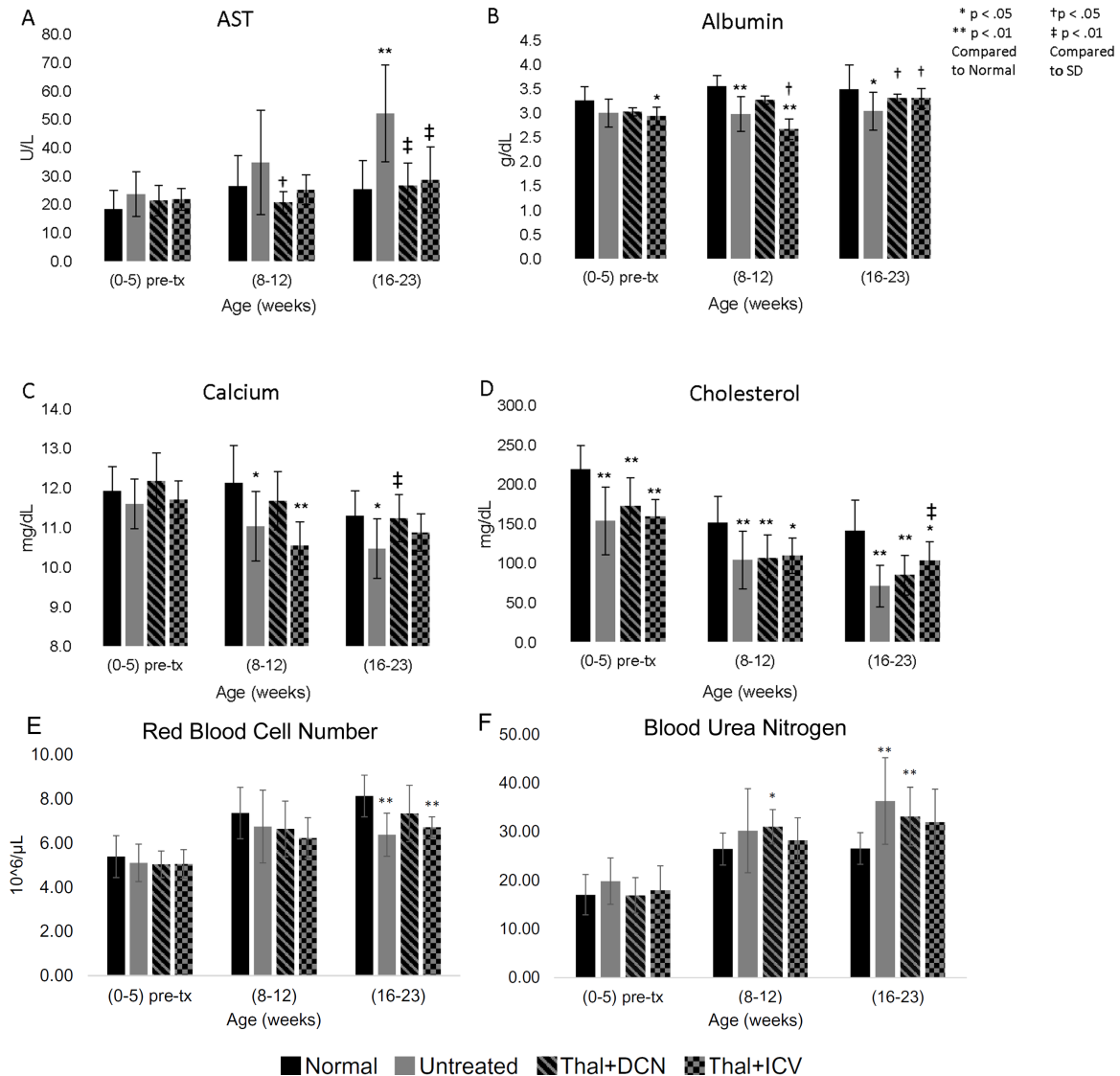


Figure 1. Blood Chemistry Findings in normal, untreated SD, and SD cats 16 weeks after AAV gene therapy. A) Aspartate aminotransferase (AST) levels increase over time in SD cats and are normalized after AAV gene therapy in both groups by 16-23 weeks. B) Albumin levels decrease with time in the SD cats and are restored to normal by 16-23 weeks. C) Calcium levels also decrease over time, with normalization in the Thal+DCN group. D) Blood Cholesterol levels also decrease over time, but are only partially normalized in the Thal+ICV cohort at 16-23

weeks. E) Red blood cell number is decreased in SD cats and is normalized in the Thal+DCN but not the Thal+ICV treatment group. F) Blood urea nitrogen is significantly elevated in SD cats at endpoint. Thal+ICV injection route, but not Thal+DCN, normalize levels. Normal cats: 0-5 weeks n=10; 8-12 weeks n=9; 16-23 weeks n=8; SD cats: 0-5 weeks n=9, 8-12 weeks n=11, 16-23 weeks n=17 (except BUN n=14); Thal+DCN: 0-5 weeks n=13; 8-12 weeks n=9; 16-23 weeks n=10; Thal+ICV: 0-5 weeks n=6; 8-12 weeks n=6; 16-23 weeks n=8 (except AST n=7). (*denotes $p < 0.05$ from normal, **denotes $p < 0.01$ from normal, † denotes $p < 0.05$ from SD, ‡ denotes $p < 0.01$ from SD; error bars represent standard deviation).

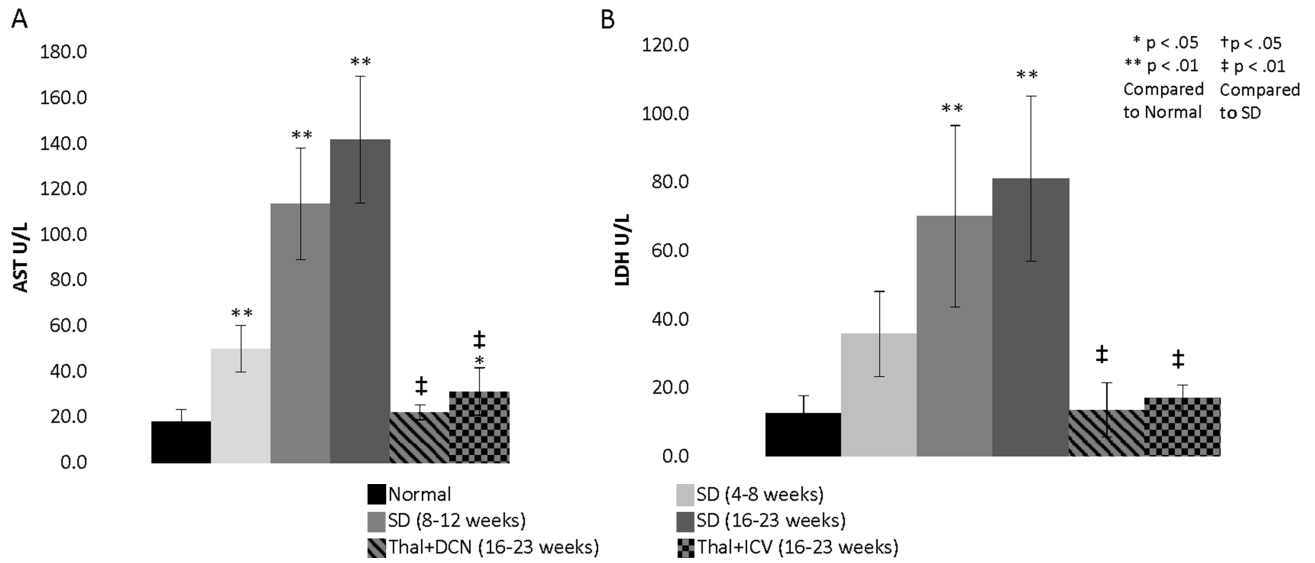


Figure 2. CSF based biomarkers in normal, untreated SD, and SD cats 16 weeks after AAV gene therapy. A) Aspartate aminotransferase (AST) and B) Lactate Dehydrogenase (LDH) in CSF of normal, Sandhoff (SD), and Sandhoff cats 16 weeks after AAV gene therapy by Thal+DCN and Thal+ICV injection routes. Levels of AST and LDH significantly increase over time in the SD cat. AST and LDH are restored to normal levels after AAV gene therapy by Thal+DCN and Thal+ICV injection routes (*denotes $p < 0.05$ from normal, **denotes $p < 0.01$ from normal, † $p < 0.05$ denotes from SD, ‡ denotes $p < 0.01$ from SD).

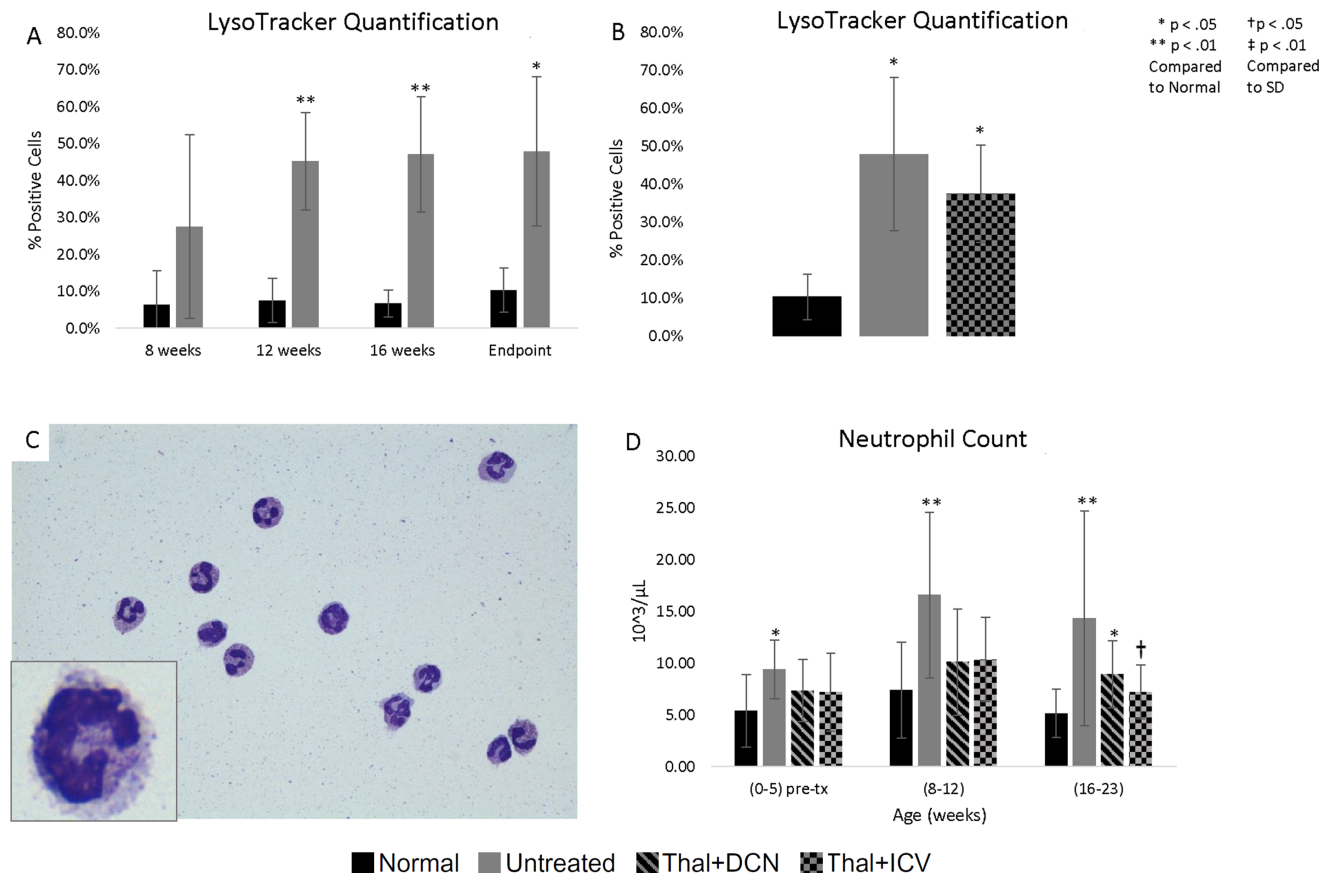


Figure 3. LysoTracker quantification in peripheral blood mononuclear cells. Percent of positive cells increased in SD cats and were significantly higher than normal control cats by 12 weeks of age (A). Gene therapy decreased the percentage of LysoTracker positive cells, yet values remained significantly higher ($p < 0.05$) than normal cats (B). Cytopsin from sorted LysoTracker positive cells were comprised primarily of neutrophils, many of which were noted to have intracytoplasmic granules (C). Neutrophils were significantly increased, as compared to normal controls, at all time points measured by CBC. Treatment with AAV by Thal+ICV, but not Thal+DCN, returned the neutrophil count to normal levels. Normal cats: 0-5 weeks $n=10$; 8-12 weeks $n=9$; 16-23 weeks $n=8$; SD cats: 0-5 weeks $n=9$, 8-12 weeks $n=11$, 16-23 weeks $n=14$; Thal+DCN: 0-5 weeks $n=13$; 8-12 weeks $n=9$; 16-23 weeks $n=10$; Thal+ICV: 0-5 weeks $n=6$; 8-

12 weeks n=6; 16-23 weeks n=8. (*denotes $p < 0.05$ from normal, **denotes $p < 0.01$ from normal, ‡ $p < 0.05$ denotes from SD, † denotes $p < 0.01$ from SD; error bars represent standard deviation).

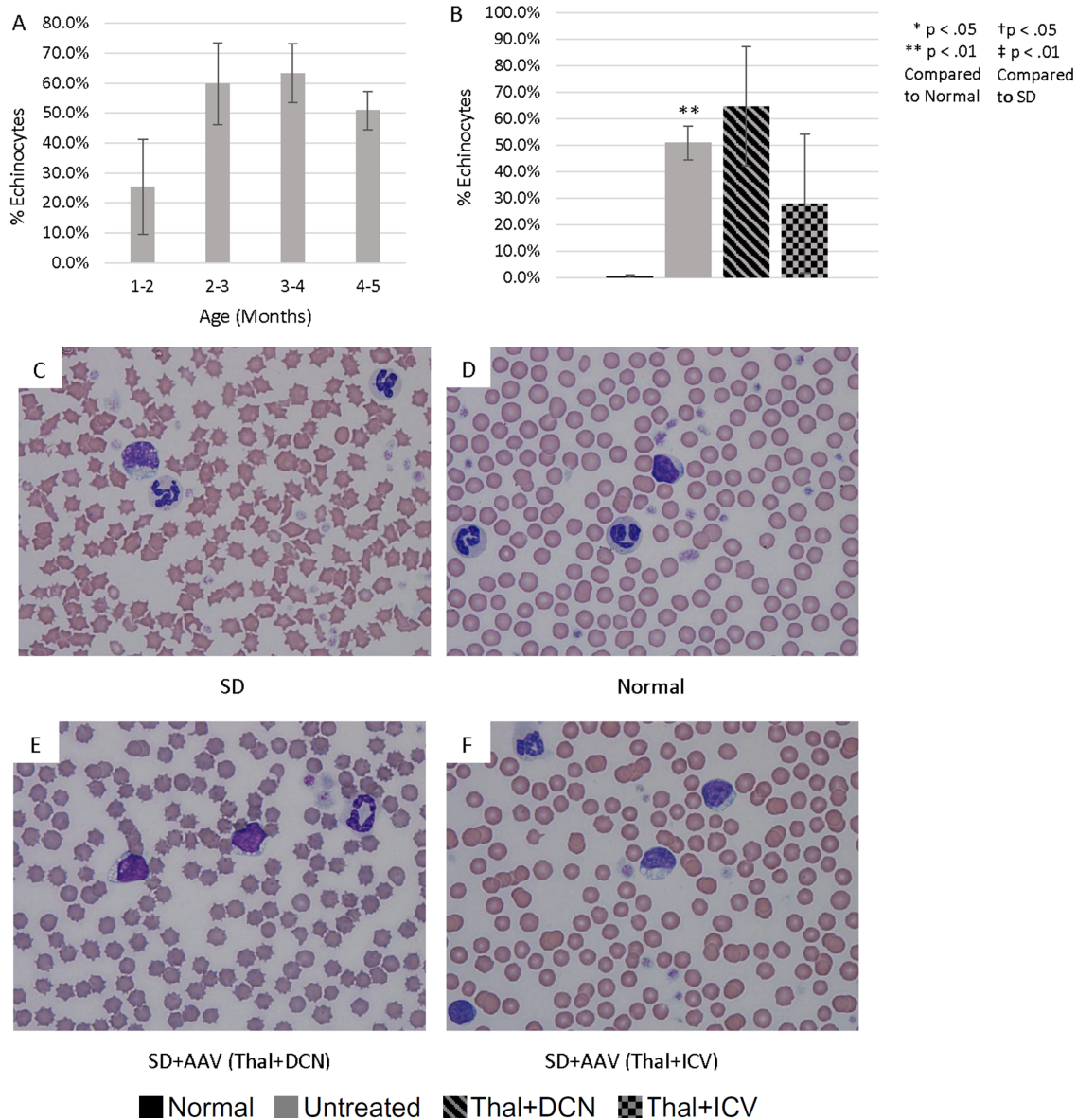


Figure 4. Echinocyte formation in normal, untreated SD cats, and AAV-treated SD cats.

In SD cats echinocyte formation increases by 2-3 months of age (n=4) (A) and remains elevated after AAV therapy (normal: n=4; SD: n=4; Thal+DCN: n=2; Thal+ICV: n=2) (B).

Representative photomicrographs show increased echinocytosis in the SD cat (C) as compared to normal (D). Echinocyte levels appear intermediate in the Thal+DCN (E) and Thal+ICV (F) groups. (*denotes $p < 0.05$ from normal, **denotes $p < 0.01$ from normal, † $p < 0.05$ denotes from SD, ‡ denotes $p < 0.01$ from SD; error bars represent standard deviation).

A	Brain	Liver	PBMC	
	Hex A	Hex A	Bgal	Mann
SD+AAV (7-957)	2547.4	122.0	218.8	854.8
SD+AAV (7-960)	4492.2	201.7	89.3	455.1
SD+AAV (7-972)	4643.4	214.1	84.0	441.6
Normal	50.6	214.5	97.8	341.8
SD	0	3.4	193.3	839.3

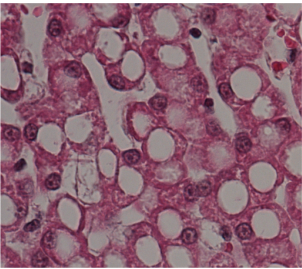
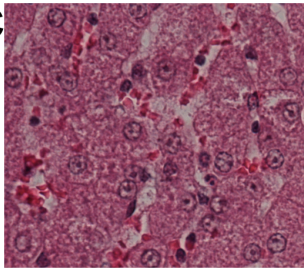
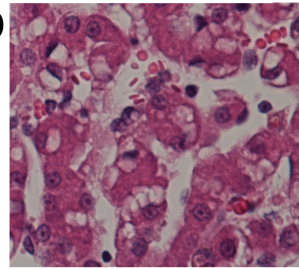
B		C		D	
	SD		Normal		SD+AAV (7-957)

Figure 5. Brain and peripheral tissue enzyme activity in normal, untreated SD, and AAV-treated SD cats. Following Thal+ICV injection, levels of Hex A in the brain of cats reach >50-fold normal at the injection site and correspond directly to levels of Hex A achieved in the liver. Hex A in the brain and liver also directly correlate with normalization of β gal and Mann in PBMCs. Normal (n=4) and SD (n=5) values are provided for reference. Values are reported as specific activity (A). H&E stains of the liver show notable vacuolization of hepatocytes in SD cat at humane endpoint (B) compared to a normal age-matched control cat (C). Sixteen weeks after intracranial AAV therapy, cat 7-972 had normal levels of Hex activity in the liver and architecture was partially normalized, with areas of hepatocytes containing multiple, small intracytoplasmic vacuoles.

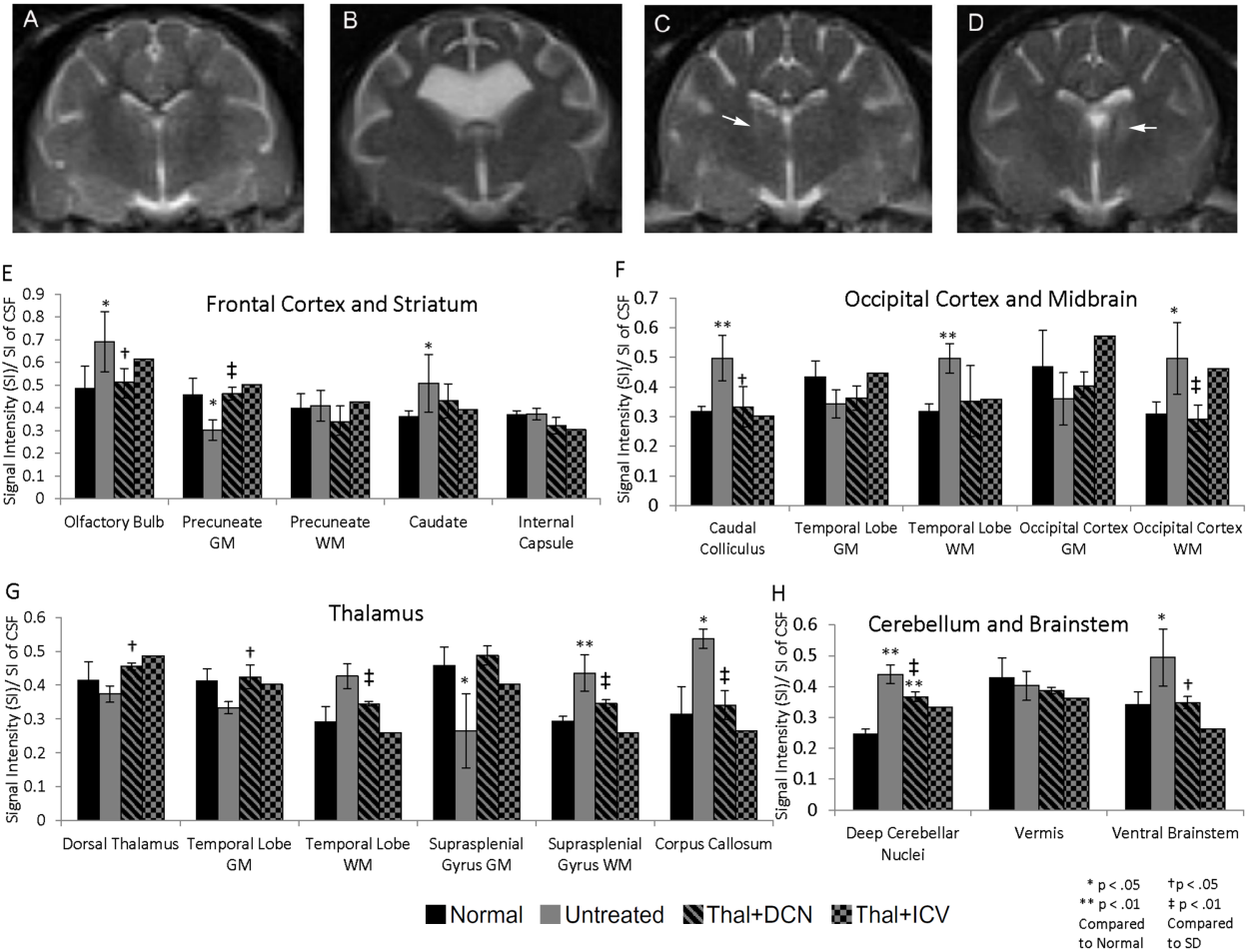


Figure 6. MRI signal intensity in normal, untreated SD, and AAV-treated SD cats. Changes in in normal (n=3), SD (n=6), and SD cats after AAV gene therapy by Thal+DCN (n=3) and Thal+ICV (n=1) injection routes. Loss of definition, or isointensity, of gray and white matter and cortical atrophy are noted in the untreated SD cat (B) compared to normal (A). AAV gene therapy by Thal+DCN (C) and Thal+ICV (D) restored gray and white matter intensities. Aberrant thalamic intensities (arrow) are noted in the dorsal thalamus in both Thal+DCN and Thal+ICV groups at approximately the level of the surgical injection site. MRI changes are quantified in the frontal cortex and striatum (E), thalamus (G), occipital cortex and midbrain (F) and cerebellum and brainstem (H). All significantly altered parameters were normalized in the Thal+DCN group except intensities of the deep cerebellar nuclei (*denotes $p < 0.05$ from normal,

**denotes $p < 0.01$ from normal, $t < 0.05$ denotes from SD † denotes $p < 0.01$ from SD; error bars represent standard deviation).

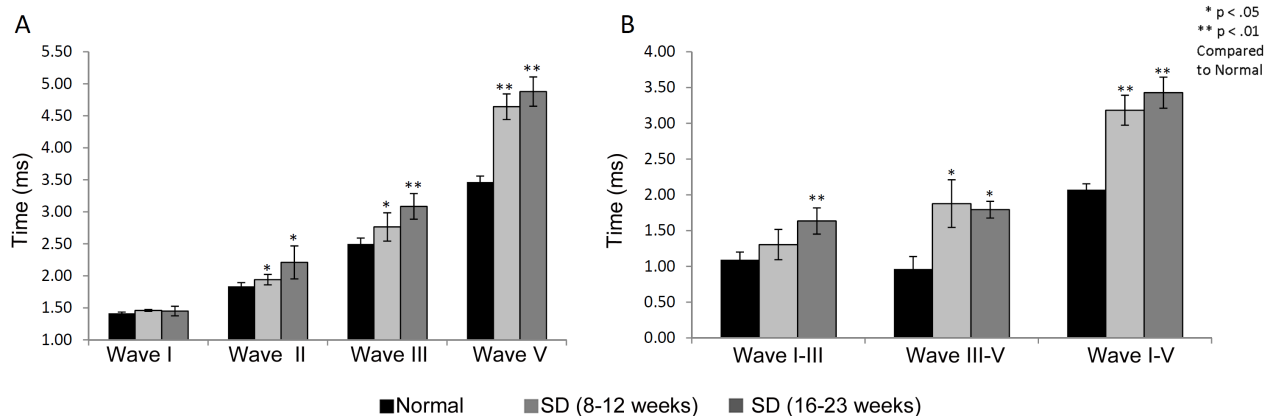


Figure 7. Brainstem Auditory Evoked Responses in SD cats. A) Significant increases in latencies were noted in waves II, III and V at both 8-12 and 16-23 week SD cats. Mean latencies in the 8-12 week group were higher but did not reach significance. B) Interwave latencies were present between waves I and III, III and V and I and V at 16-23 weeks, whereas prolonged interwave latencies were detectable between waves III and V and I and V (*denotes $p < 0.05$ from normal, **denotes $p < 0.01$ from normal).

CHAPTER 5

Summary

Despite being characterized over 100 years ago, the GM2 gangliosidoses remain incurable today. Valiant efforts to find a cure have been made by researchers and physicians alike. Therapeutic strategies including bone marrow transplantation, stem cell transplantation, enzyme replacement therapy, and substrate reduction therapy have been thoroughly researched in animal models (25-31) but have not successfully translated to clinical use (2, 20-22). The main limitations of therapeutic attempts have been globally correcting the brain and spinal cord in spite of isolation by the blood-brain barrier. SD presents additional challenges of concomitantly treating the periphery, as visceral involvement has also proven life threatening (36). Delivery of naïve cells, proteins, synthetic compounds, or vectors must also elude the immune system, which has the ability to negate even the most valiant therapeutic efforts.

The idea of gene therapy for the treatment of human genetic diseases arose in the early 1970's (205). After nearly 20 years of development, gene therapy eventually made its way in to human clinical trials for the treatment of two patients with severe combined immunodeficiency (SCID). The therapy was proven both safe and effective, although results were only temporary (206). In 1999, the tragic death of 18 year old Jesse Gelsinger after administration of gene therapy for ornithine transcarbamylase deficiency led to suspension of many clinical trials and a major setback for the field (207). Furthermore, in 2003 a patient developed T cell leukemia as a direct result of gene transfer with a retroviral vector and the clinical trial was placed on hold (208).

After occurrence of these adverse events, substantial efforts were made in the research community to improve the safety of gene therapy. Technological advances in vector engineering allowed for enhanced safety of retroviral vectors by decreasing the incidence of vector integration. Furthermore, non-integrating adenoviral vectors and adeno-associated viral vectors were developed which preclude many safety concerns associated with retroviral vectors. By 2006 gene therapy use in clinical trials had finally regained the momentum and the number of trials approved equated that seen in 1999. As of June 2012, 1843 gene therapy clinical trials had been approved in 31 countries, with the US undertaking the vast majority of trials at 63.7%. As far as diseases targeted by gene therapy, 64.4% of trials addressed cancer, followed distantly by monogenic diseases at 8.7%. The most common vectors used in clinical trials are adenoviral vectors (23.3%) and retroviral vectors (19.7%) (209).

In light of success in the clinic, gene therapy experiments using the latest and safest adeno-associated associated vectors were initiated in mouse models of SD disease (85). Initial studies of single striatal injections proved the therapy could extend lifespan, but revealed limited distribution throughout the CNS (35). Subsequent experiments proved that injections targeting the striatum or hippocampus in addition to the cerebellum were necessary to reach maximum survival. Achieving widespread distribution of the vector and therapeutic enzyme allowed the survival of SD mice in to the second year of life (36). All initial gene therapy experiments were conducted in 1 month old SD mice, which is prior to symptom onset. Pre-symptomatic treatment is not an achievable target for human patients, as the vast majority are not diagnosed until major developmental milestones are missed and many neurologic symptoms are present. Further experiments in SD mice revealed that treatment at 4, 8, or 10 weeks of age significantly extended lifespan; however, delaying therapy to 12 weeks of age did not allow for increased survival (37).

This decade of research in SD mice provided imperative groundwork in establishing effective gene therapy protocols. These studies also addressed fundamental challenges of gene therapy, including achieving widespread distribution and the ability of therapy to reverse neurological symptoms.

Success of gene therapy in the mouse model of SD garnered a lot of enthusiasm and warranted exploration in a larger animal model that more closely resembles human patients both anatomically and biochemically. The same viral vectors successfully utilized in mice experiments, AAV serotype 1 encoding human hexosaminidase (AAV1-hHEX), were adapted for use in our feline model of SD disease. As described in Chapter 1, our initial experiments included bilateral injections to the thalamus, which most closely recapitulates the striatal injections initially conducted in SD mice. Surprisingly, we demonstrated a robust immune response to both the AAV vector and the therapeutic transgene. The degree of immune response was greatly reduced by formulating new AAVrh8 vectors encoding a species-specific transgene and a significant extension of lifespan ($p < 0.0064$) was achieved. These results provided novel evidence to the importance of species-specific cDNAs for use in translational research as well as the first report of therapeutic benefit in a large animal model of SD. In the >35 year history of the feline SD colony, this was unquestionably the most successful therapeutic attempt to date.

The main limitation to our first therapeutic attempt in feline SD was achieving widespread distribution of the vector and therapeutic protein. In light of findings in SD mice after striatal injections, this was not surprising. We subsequently followed suit of the murine experiments and in addition to the thalamic injection site added direct targeting of the cerebellum via injection to the deep cerebellar nuclei (DCN). Remarkably, with two additional injections widespread distribution of vector and enzyme were achieved and lifespan was extended to an

average of 19.1 months of age (a significance of $p < 0.0001$) in nine SD cats. After intracerebral injection of AAVrh8-fHEX, serum antibody titers to the vector were astoundingly high, reaching $> 1:200,000$. It was then hypothesized that vector injectate was inadvertently leaking out the injection site, entering circulation, reaching peripheral organs and accounting for unexpected humoral immune response. Indeed, high levels of hexosaminidase and vector copies of AAV were detectable in the liver, sciatic nerve, and quadriceps. These results provide unequivocal evidence of therapeutic benefit of AAV mediated gene delivery in a large animal model. These data also challenges previously held beliefs that circulating serum antibodies have a detrimental effect on long-term transgene expression and clinical outcome. In contrast, in our experiments the antibody titers in no way correlated with survival and transgene expression was maintained in spite of the staggeringly high titers. Furthermore, this is the first account of the peripheral tropism of AAV serotype rh8 after intraparenchymal injection and in a large animal model.

In attempt to attenuate the immune response, six SD cats were treated with $1/10^{\text{th}}$ of the original dose, or 4.4×10^{11} g.e./vector/kg. While the goal of mitigating the immune response was achieved, amelioration of the disease phenotype was not as complete and lifespan was reduced to an average of 13.1 months of age. As anticipated with lower serum antibody titers, peripheral presence of Hex and AAV was also substantially diminished. Since the immune response to the full dose was not disadvantageous, the loss of efficacy seen with the lower dose is likely not justified. This study provides the first dose-response study of recombinant AAVrh8 in any animal model. As seen with the critical timeframe of treatment in SD mice, there is likely also a critical vector dose threshold below which little therapeutic benefit can be achieved. This study will help inform the dosage at which clinical trials in children will be conducted.

With achievement of a 4-fold increase in lifespan in cats, advancements towards human clinical trials were finally being realized. Of major concern to the pediatric neurosurgeons was the DCN injection route to target the cerebellum. Due to differences in brain anatomy, this injection route would lead to greater surgical risk in human patients than was appreciated in the feline model. Six SD cats were treated by bilateral thalamic and intracerebroventricular injection of AAVrh8-fHEX in attempt to circumvent directly injecting the cerebellum. Although experiments are still ongoing, to date survival has increased to an average of 21.2 months of age at a significance of $p < 0.0002$, which is not significantly different from the thalamus and DCN injection cohort. It was thought that directly targeting the ventricular system might increase peripheral biodistribution of the therapeutic enzyme and vector copies, and consequently increase serum antibody titers. However, visceral stores of Hex and AAV copies were not elevated when compared to cats treated by intraparenchymal injection. Furthermore, the humoral immune response was not exacerbated; instead numerous cats appear to decreased titers despite this injection route allowing a slightly higher vector dose. Due to equivalent (if not improved) efficacy, comparable (if not decreased) immunogenicity, and decreased surgical risks, thalamus and ICV injection appears to be the superior route. These experiments are the first comparison of intraparenchymal and intraventricular injections of AAV in a large animal model. These results will largely inform the injection route chosen for human clinical trials. Safety and toxicity studies are now underway using this thalamus and ICV injection route in non-human primates.

After the primary underlying disease was proven largely corrected, it was important to determine if secondary disease processes were also attenuated by gene therapy. Neuroinflammation is known to cause major pathogenesis in SD mice (26) and human patients (129), but had never been analyzed in our feline SD model. Similar to SD mice, untreated cats

displayed pronounced activation and infiltration of microglia cells, indicated by increased MHCII and Iba1 expression. Also similar to SD mice, MIP-1 alpha was upregulated in the brain of untreated SD cats indicating recruitment of peripheral mononuclear cells to the CNS. Remarkably, AAV therapy largely attenuated neuroinflammation, indicated by decreased MHCII and normalized levels of MIP-1 alpha. This proves complete correction of not only the neurodegenerative disease, but also the detrimental neuroinflammation process, which is known to exacerbate neuron loss and create cytotoxicity. These experiments detail neuroinflammation in a large animal model of SD for the first time and evaluate the ability of intracranial delivery of AAV to preclude this pathogenic process.

As the primary goal of these AAV experiments is translation in to human clinical trials, it is important to be able to measure therapeutic success. We therefore developed non-invasive biomarkers of disease progression in untreated SD cats and then applied the parameters as a way to measure therapeutic outcome in treated cats. Biomarkers ranged from simple and routine blood and CSF analytes, to clinical imaging and electro-diagnostic approaches. We found numerous parameters that significantly and gradually increased with disease progression, some of which were normalized with therapy. These experiments provide the first biomarkers of SD in a large animal model. The most reliable and minimally invasive measures demonstrated in the SD cat could be adapted for use in human clinical trial.

Overall the experiments described herein demonstrate clear therapeutic benefit in a large animal model of SD for the first time. Subsequent to completion of safety and toxicity studies in healthy non-human primates, it is our hope that the gene therapy protocols that we have established effective in feline SD will be translated to human clinical trial. The success of gene therapy has garnered great enthusiasm and resulted in humbling support from the lysosomal

storage disease community. Furthermore, it is likely that this therapeutic approach may be applied to other monogenic and neurodegenerative diseases for which there is currently no effective treatment.

References

1. P. J. Meikle, J. J. Hopwood, A. E. Clague, W. F. Carey, Prevalence of lysosomal storage disorders. *JAMA* **281**, 249 (Jan, 1999).
2. A. E. Bley *et al.*, Natural history of infantile G(M2) gangliosidosis. *Pediatrics* **128**, e1233 (Nov, 2011).
3. R. Marrocos de Aragao, Ramos, RMG, Pereira, FBA, Bezerra, AFR, Fernandes, DN, "Cherry red spot" in a patient with Tay-Sachs disease: case report *Arquivos brasileiros de oftalmologia* **72**, 537 (2009).
4. M. Ponce-Camacho, Melo-de la Garza, A, Barboza-, A. Quintana, Barboza-Quintana, O, Áncer-Rodríguez, J, Ramírez-, E. Bon, Garza-Alatorre, A, Rodríguez-Gutiérrez, NA., A Fatal Case of Generalized Lysosomal Storage Disease in an Infant. *Medicina Universitaria* **12**, 59 (2010).
5. E. Klenk, Die Fettstoffe des Gehirns bei Amaurotischer Idiotie und Niemann-Pick'scher Krankheit. *Ber Ges Physiol* **96**, 659 (1937).
6. K. Sandhoff, Metabolic and cellular bases of sphingolipidoses. *Biochemical Society transactions* **41**, 1562 (Dec, 2013).
7. K. Sandhoff, My journey into the world of sphingolipids and sphingolipidoses. *Proceedings of the Japan Academy. Series B, Physical and biological sciences* **88**, 554 (2012).
8. H. J. Kytzia, K. Sandhoff, Evidence for two different active sites on human beta-hexosaminidase A. Interaction of GM2 activator protein with beta-hexosaminidase A. *The Journal of biological chemistry* **260**, 7568 (Jun, 1985).
9. E. Conzelmann, K. Sandhoff, Purification and characterization of an activator protein for the degradation of glycolipids GM2 and GA2 by hexosaminidase A. *Hoppe-Seyler's Zeitschrift fur physiologische Chemie* **360**, 1837 (Dec, 1979).
10. E. Conzelmann, J. Burg, G. Stephan, K. Sandhoff, Complexing of glycolipids and their transfer between membranes by the activator protein for degradation of lysosomal ganglioside GM2. *European journal of biochemistry / FEBS* **123**, 455 (Apr, 1982).
11. M. Wendeler *et al.*, Photoaffinity labelling of the human GM2-activator protein. Mechanistic insight into ganglioside GM2 degradation. *European journal of biochemistry / FEBS* **271**, 614 (Feb, 2004).
12. M. Wendeler *et al.*, The enzyme-binding region of human GM2-activator protein. *The FEBS journal* **273**, 982 (Mar, 2006).

13. K. M. Gravel R, Proia RL, Sandhoff K, Suzuki K, Suzuki K, *The GM2 gangliosidoses*. . B. A. Scriver CR, Sly WS, Valle D, Ed., *The metabolic and molecular bases of inherited diseases* (McGraw-Hill, New York ed. 8, 2001).
14. P. Venugopalan, S. N. Joshi, Cardiac involvement in infantile Sandhoff disease. *Journal of paediatrics and child health* **38**, 98 (Feb, 2002).
15. B. Dlott, A. d'Azzo, D. V. Quon, E. F. Neufeld, Two mutations produce intron insertion in mRNA and elongated beta-subunit of human beta-hexosaminidase. *The Journal of biological chemistry* **265**, 17921 (Oct, 1990).
16. F. M. Platt *et al.*, Prevention of lysosomal storage in Tay-Sachs mice treated with N-butyldeoxynojirimycin. *Science (New York, N.Y.)* **276**, 428 (Apr, 1997).
17. T. M. Cox *et al.*, The role of the iminosugar N-butyldeoxynojirimycin (miglustat) in the management of type I (non-neuronopathic) Gaucher disease: a position statement. *Journal of inherited metabolic disease* **26**, 513 (2003).
18. J. L. Capablo *et al.*, Neurologic improvement in a type 3 Gaucher disease patient treated with imiglucerase/miglustat combination. *Epilepsia* **48**, 1406 (Jul, 2007).
19. M. C. Patterson, D. Vecchio, H. Prady, L. Abel, J. E. Wraith, Miglustat for treatment of Niemann-Pick C disease: a randomised controlled study. *Lancet neurology* **6**, 765 (Sep, 2007).
20. B. Bembi *et al.*, Substrate reduction therapy in the infantile form of Tay-Sachs disease. *Neurology* **66**, 278 (Jan, 2006).
21. C. M. Tallaksen, J. E. Berg, Miglustat therapy in juvenile Sandhoff disease. *Journal of inherited metabolic disease* **32 Suppl 1**, S289 (Dec, 2009).
22. S. B. Wortmann *et al.*, Substrate deprivation therapy in juvenile Sandhoff disease. *Journal of inherited metabolic disease* **32 Suppl 1**, S307 (Dec, 2009).
23. K. Sango *et al.*, Mouse models of Tay-Sachs and Sandhoff diseases differ in neurologic phenotype and ganglioside metabolism. *Nature genetics* **11**, 170 (Oct, 1995).
24. D. Phaneuf *et al.*, Dramatically different phenotypes in mouse models of human Tay-Sachs and Sandhoff diseases. *Human molecular genetics* **5**, 1 (Jan, 1996).
25. F. Norflus *et al.*, Bone marrow transplantation prolongs life span and ameliorates neurologic manifestations in Sandhoff disease mice. *The Journal of clinical investigation* **101**, 1881 (May, 1998).

26. R. Wada, C. J. Tiff, R. L. Proia, Microglial activation precedes acute neurodegeneration in Sandhoff disease and is suppressed by bone marrow transplantation. *Proceedings of the National Academy of Sciences of the United States of America* **97**, 10954 (Sep, 2000).
27. J. P. Lee *et al.*, Stem cells act through multiple mechanisms to benefit mice with neurodegenerative metabolic disease. *Nature medicine* **13**, 439 (Apr, 2007).
28. K. Matsuoka *et al.*, Therapeutic potential of intracerebroventricular replacement of modified human beta-hexosaminidase B for GM2 gangliosidosis. *Molecular therapy : the journal of the American Society of Gene Therapy* **19**, 1017 (Jun, 2011).
29. D. Tsuji *et al.*, Highly phosphomannosylated enzyme replacement therapy for GM2 gangliosidosis. *Annals of neurology* **69**, 691 (Apr, 2011).
30. U. Andersson *et al.*, Improved outcome of N-butyldeoxygalactonojirimycin-mediated substrate reduction therapy in a mouse model of Sandhoff disease. *Neurobiology of disease* **16**, 506 (Aug, 2004).
31. M. Jeyakumar *et al.*, NSAIDs increase survival in the Sandhoff disease mouse: synergy with N-butyldeoxynojirimycin. *Annals of neurology* **56**, 642 (Nov, 2004).
32. S. Kyrkanides, J. H. Miller, S. M. Brouxon, J. A. Olschowka, H. J. Federoff, beta-hexosaminidase lentiviral vectors: transfer into the CNS via systemic administration. *Brain research. Molecular brain research* **133**, 286 (Feb, 2005).
33. S. Kyrkanides *et al.*, Intraperitoneal inoculation of Sandhoff mouse neonates with an HIV-1 based lentiviral vector exacerbates the attendant neuroinflammation and disease phenotype. *Journal of neuroimmunology* **188**, 39 (Aug, 2007).
34. C. Bourgoin *et al.*, Widespread distribution of beta-hexosaminidase activity in the brain of a Sandhoff mouse model after coinjection of adenoviral vector and mannitol. *Gene therapy* **10**, 1841 (Oct, 2003).
35. T. J. Sargeant *et al.*, Adeno-associated virus-mediated expression of beta-hexosaminidase prevents neuronal loss in the Sandhoff mouse brain. *Human molecular genetics* **20**, 4371 (Nov, 2011).
36. M. B. Cachon-Gonzalez *et al.*, Gene transfer corrects acute GM2 gangliosidosis--potential therapeutic contribution of perivascular enzyme flow. *Molecular therapy : the journal of the American Society of Gene Therapy* **20**, 1489 (Aug, 2012).
37. M. B. Cachon-Gonzalez, S. Z. Wang, R. Ziegler, S. H. Cheng, T. M. Cox, Reversibility of neuropathology in Tay-Sachs-related diseases. *Human molecular genetics*, (Oct, 2013).

38. L. C. Cork *et al.*, GM2 ganglioside lysosomal storage disease in cats with beta-hexosaminidase deficiency. *Science (New York, N.Y.)* **196**, 1014 (May, 1977).
39. D. R. Martin *et al.*, An inversion of 25 base pairs causes feline GM2 gangliosidosis variant. *Experimental neurology* **187**, 30 (May, 2004).
40. A. M. Bradbury *et al.*, Neurodegenerative lysosomal storage disease in European Burmese cats with hexosaminidase beta-subunit deficiency. *Molecular genetics and metabolism* **97**, 53 (May, 2009).
41. L. L. Muldoon, E. A. Neuwelt, M. A. Pagel, D. L. Weiss, Characterization of the molecular defect in a feline model for type II GM2-gangliosidosis (Sandhoff disease). *The American journal of pathology* **144**, 1109 (May, 1994).
42. Y. Kanae *et al.*, Nonsense mutation of feline beta-hexosaminidase beta-subunit (HEXB) gene causing Sandhoff disease in a family of Japanese domestic cats. *Research in veterinary science* **82**, 54 (Feb, 2007).
43. P. A. Torres *et al.*, Tay-Sachs disease in Jacob sheep. *Molecular genetics and metabolism* **101**, 357 (Dec, 2010).
44. B. F. Porter *et al.*, Pathology of GM2 gangliosidosis in Jacob sheep. *Veterinary pathology* **48**, 807 (Jul, 2011).
45. E. Kohlbrenner *et al.*, Successful production of pseudotyped rAAV vectors using a modified baculovirus expression system. *Molecular therapy : the journal of the American Society of Gene Therapy* **12**, 1217 (Dec, 2005).
46. Z. Wu, A. Asokan, R. J. Samulski, Adeno-associated virus serotypes: vector toolkit for human gene therapy. *Molecular therapy : the journal of the American Society of Gene Therapy* **14**, 316 (Sep, 2006).
47. Q. Xie *et al.*, The atomic structure of adeno-associated virus (AAV-2), a vector for human gene therapy. *Proceedings of the National Academy of Sciences of the United States of America* **99**, 10405 (Aug, 2002).
48. M. A. Goncalves, Adeno-associated virus: from defective virus to effective vector. *Virology journal* **2**, 43 (2005).
49. D. M. McCarty, S. M. Young, Jr., R. J. Samulski, Integration of adeno-associated virus (AAV) and recombinant AAV vectors. *Annual review of genetics* **38**, 819 (2004).
50. R. T. Surosky *et al.*, Adeno-associated virus Rep proteins target DNA sequences to a unique locus in the human genome. *Journal of virology* **71**, 7951 (Oct, 1997).

51. L. H. Vandenberghe, J. M. Wilson, AAV as an immunogen. *Current gene therapy* **7**, 325 (Oct, 2007).
52. C. Li *et al.*, Adeno-associated virus type 2 (AAV2) capsid-specific cytotoxic T lymphocytes eliminate only vector-transduced cells coexpressing the AAV2 capsid in vivo. *Journal of virology* **81**, 7540 (Jul, 2007).
53. V. Zhang, Miao, Y., Vaillancourt, P., Exceptionally Safe AAV Helper-Free Gene Delivery and Expression System. *Strategies* **14**, 46 (2008).
54. T. J. Kindt, *Immunology* Kuby, Ed., (W.H. Freeman, New York ed. 6, 2007).
55. A. Sarukhan *et al.*, Successful interference with cellular immune responses to immunogenic proteins encoded by recombinant viral vectors. *Journal of virology* **75**, 269 (Jan, 2001).
56. M. K. Matyszak, V. H. Perry, The potential role of dendritic cells in immune-mediated inflammatory diseases in the central nervous system. *Neuroscience* **74**, 599 (Sep, 1996).
57. T. Cartmell *et al.*, Interleukin-1 mediates a rapid inflammatory response after injection of adenoviral vectors into the brain. *The Journal of neuroscience : the official journal of the Society for Neuroscience* **19**, 1517 (Feb, 1999).
58. P. R. Lowenstein, Immunology of viral-vector-mediated gene transfer into the brain: an evolutionary and developmental perspective. *Trends in immunology* **23**, 23 (Jan, 2002).
59. P. R. Lowenstein, M. G. Castro, Progress and challenges in viral vector-mediated gene transfer to the brain. *Current opinion in molecular therapeutics* **4**, 359 (Aug, 2002).
60. A. K. Zaiss, D. A. Muruve, Immunity to adeno-associated virus vectors in animals and humans: a continued challenge. *Gene therapy* **15**, 808 (Jun, 2008).
61. G. L. Rogers *et al.*, Innate Immune Responses to AAV Vectors. *Frontiers in microbiology* **2**, 194 (2011).
62. J. Zhu, X. Huang, Y. Yang, The TLR9-MyD88 pathway is critical for adaptive immune responses to adeno-associated virus gene therapy vectors in mice. *The Journal of clinical investigation* **119**, 2388 (Aug, 2009).
63. R. J. Mandel *et al.*, Characterization of intrastriatal recombinant adeno-associated virus-mediated gene transfer of human tyrosine hydroxylase and human GTP-cyclohydrolase I in a rat model of Parkinson's disease. *The Journal of neuroscience : the official journal of the Society for Neuroscience* **18**, 4271 (Jun, 1998).

64. M. Y. Mastakov *et al.*, Immunological aspects of recombinant adeno-associated virus delivery to the mammalian brain. *Journal of virology* **76**, 8446 (Aug, 2002).
65. W. D. Lo *et al.*, Adeno-associated virus-mediated gene transfer to the brain: duration and modulation of expression. *Human gene therapy* **10**, 201 (Jan, 1999).
66. S. Reimsnider, F. P. Manfredsson, N. Muzyczka, R. J. Mandel, Time course of transgene expression after intrastriatal pseudotyped rAAV2/1, rAAV2/2, rAAV2/5, and rAAV2/8 transduction in the rat. *Molecular therapy : the journal of the American Society of Gene Therapy* **15**, 1504 (Aug, 2007).
67. J. D. Mount *et al.*, Sustained phenotypic correction of hemophilia B dogs with a factor IX null mutation by liver-directed gene therapy. *Blood* **99**, 2670 (Apr, 2002).
68. C. S. Manno *et al.*, Successful transduction of liver in hemophilia by AAV-Factor IX and limitations imposed by the host immune response. *Nature medicine* **12**, 342 (Mar, 2006).
69. F. Mingozzi *et al.*, CD8(+) T-cell responses to adeno-associated virus capsid in humans. *Nature medicine* **13**, 419 (Apr, 2007).
70. H. Jiang, Patarroyo-White, S., Liu, T., Yang, B., Nagy, D., He, L., Scallan, C., Sommer, J., Zhou, S., Couto, L., High, K., Pierce, G. , in *ASH Annual Meeting*, vol. 106, pp. 5532 (2005).
71. R. Calcedo, L. H. Vandenberghe, G. Gao, J. Lin, J. M. Wilson, Worldwide epidemiology of neutralizing antibodies to adeno-associated viruses. *The Journal of infectious diseases* **199**, 381 (Feb, 2009).
72. L. M. Sanftner *et al.*, Striatal delivery of rAAV-hAADC to rats with preexisting immunity to AAV. *Molecular therapy : the journal of the American Society of Gene Therapy* **9**, 403 (Mar, 2004).
73. C. S. Peden, C. Burger, N. Muzyczka, R. J. Mandel, Circulating anti-wild-type adeno-associated virus type 2 (AAV2) antibodies inhibit recombinant AAV2 (rAAV2)-mediated, but not rAAV5-mediated, gene transfer in the brain. *Journal of virology* **78**, 6344 (Jun, 2004).
74. K. Haddley, Alipogene tiparvovec for the treatment of lipoprotein lipase deficiency. *Drugs of today (Barcelona, Spain : 1998)* **49**, 161 (Mar, 2013).
75. V. Ferreira *et al.*, Immune responses to intramuscular administration of alipogene tiparvovec (AAV1-LPLS447X) in a phase II clinical trial of Lipoprotein Lipase deficiency (LPLD) gene therapy. *Human gene therapy*, (Dec, 2013).

76. C. W. Christine *et al.*, Safety and tolerability of putaminal AADC gene therapy for Parkinson disease. *Neurology* **73**, 1662 (Nov, 2009).
77. R. J. Mandel, CERE-110, an adeno-associated virus-based gene delivery vector expressing human nerve growth factor for the treatment of Alzheimer's disease. *Current opinion in molecular therapeutics* **12**, 240 (Apr, 2010).
78. S. Worgall *et al.*, Treatment of late infantile neuronal ceroid lipofuscinosis by CNS administration of a serotype 2 adeno-associated virus expressing CLN2 cDNA. *Human gene therapy* **19**, 463 (May, 2008).
79. R. A. Gravel *et al.*, in *The Metabolic and Molecular Bases of Inherited Disease*, C. R. Scriver, A. L. Beaudet, W. S. Sly, D. Valle, Eds. (McGraw-Hill, Inc., New York, 1995), vol. 2, pp. 2839-2879.
80. W. Tay, Symmetrical changes in the region of the yellow spot in each eye of an infant. *Trans.Ophthalmol.Soc.UK* **1**, 155 (1881).
81. A. Arfi *et al.*, Bicistronic lentiviral vector corrects beta-hexosaminidase deficiency in transduced and cross-corrected human Sandhoff fibroblasts. *Neurobiol Dis* **20**, 583 (Nov, 2005).
82. J. E. Guidotti *et al.*, Adenoviral gene therapy of the Tay-Sachs disease in hexosaminidase A-deficient knock-out mice. *Hum Mol Genet* **8**, 831 (May, 1999).
83. T. Itakura *et al.*, Inefficiency in GM2 ganglioside elimination by human lysosomal beta-hexosaminidase beta-subunit gene transfer to fibroblastic cell line derived from Sandhoff disease model mice. *Biol Pharm Bull* **29**, 1564 (Aug, 2006).
84. S. R. Schwarze, A. Ho, A. Vocero-Akbani, S. F. Dowdy, In vivo protein transduction: delivery of a biologically active protein into the mouse.[see comment]. *Science* **285**, 1569 (Sep, 1999).
85. M. B. Cachon-Gonzalez *et al.*, Effective gene therapy in an authentic model of Tay-Sachs-related diseases. *Proceedings of the National Academy of Sciences of the United States of America* **103**, 10373 (Jul, 2006).
86. M. B. Cachon-Gonzalez *et al.*, Gene Transfer Corrects Acute GM2 Gangliosidosis-Potential Therapeutic Contribution of Perivascular Enzyme Flow. *Mol Ther*, (Mar, 2012).
87. L. C. Cork *et al.*, GM2 ganglioside lysosomal storage disease in cats with beta-hexosaminidase deficiency. *Science* **196**, 1014 (May, 1977).

88. H. J. Baker, G. D. Reynolds, S. U. Walkley, N. R. Cox, G. H. Baker, The gangliosidoses: comparative features and research applications. *Veterinary Pathology* **16**, 635 (Nov, 1979).
89. D. R. Martin *et al.*, An inversion of 25 base pairs causes feline GM2 gangliosidosis variant 0. *Exp.Neurol.* **187**, 30 (2004).
90. M. C. Rattazzi, A. M. Appel, H. J. Baker, Enzyme replacement in feline GM2 gangliosidosis: catabolic effects of human beta-hexosaminidase A. *Prog.Clin.Biol.Res.* **94**, 213 (1982).
91. M. C. Rattazzi, A. M. Appel, H. J. Baker, J. A. Nester, in *Lysosomes and Lysosomal Storage Diseases*, J. W. Callahan, J. A. Lowden, Eds. (Raven Press, New York, NY, 1981).
92. S. U. Walkley, H. J. Baker, M. C. Rattazzi, M. E. Haskins, J. Y. Wu, Neuroaxonal dystrophy in neuronal storage disorders: evidence for major GABAergic neuron involvement. *J Neurol Sci* **104**, 1 (Jul, 1991).
93. P. A. Wood, M. R. McBride, H. J. Baker, S. T. Christian, Fluorescence polarization analysis, lipid composition, and Na⁺, K⁺-ATPase kinetics of synaptosomal membranes in feline GM1 and GM2 gangliosidosis. *Journal of Neurochemistry* **44**, 947 (Mar, 1985).
94. S. U. Walkley, H. J. Baker, M. C. Rattazzi, Initiation and growth of ectopic neurites and meganeurites during postnatal cortical development in ganglioside storage disease. *Brain Res Dev Brain Res* **51**, 167 (Feb, 1990).
95. S. U. Walkley, S. Wurzelmann, M. C. Rattazzi, H. J. Baker, Distribution of ectopic neurite growth and other geometrical distortions of CNS neurons in feline GM2 gangliosidosis. *Brain Res* **510**, 63 (Feb, 1990).
96. R. C. Baek, D. R. Martin, N. R. Cox, T. N. Seyfried, Comparative analysis of brain lipids in mice, cats, and humans with Sandhoff disease. *Lipids* **44**, 197 (Mar, 2009).
97. M. A. Passini *et al.*, Combination brain and systemic injections of AAV provide maximal functional and survival benefits in the Niemann-Pick mouse. *Proc Natl Acad Sci U S A* **104**, 9505 (May, 2007).
98. F. Jacobs *et al.*, Direct comparison of hepatocyte-specific expression cassettes following adenoviral and nonviral hydrodynamic gene transfer. *Gene Therapy* **15**, 594 (Apr, 2008).
99. N. R. Cox *et al.*, Thymic alterations in feline GM1 gangliosidosis. *Veterinary Immunology & Immunopathology* **63**, 335 (Jun, 1998).

100. J. Zhou, N. R. Cox, S. J. Ewald, N. E. Morrison, H. J. Basker, Evaluation of GM1 ganglioside-mediated apoptosis in feline thymocytes. *Vet Immunol Immunopathol* **66**, 25 (Nov, 1998).
101. J. Zhou, H. Shao, N. R. Cox, H. J. Baker, S. J. Ewald, Gangliosides enhance apoptosis of thymocytes. *Cell.Immunol.* **183**, 90 (Feb, 1998).
102. S. Kanzaki *et al.*, Thymic alterations in GM2 gangliosidosis model mice. *PLoS One* **5**, e12105 (2010).
103. K. Matsuoka, D. Tsuji, T. Taki, K. Itoh, Thymic involution and corticosterone level in Sandhoff disease model mice: new aspects the pathogenesis of GM2 gangliosidosis. *J Inherit Metab Dis* **34**, 1061 (Oct, 2011).
104. C. Ciron *et al.*, Human alpha-iduronidase gene transfer mediated by adeno-associated virus types 1, 2, and 5 in the brain of nonhuman primates: vector diffusion and biodistribution. *Human gene therapy* **20**, 350 (Apr, 2009).
105. D. Sondhi *et al.*, Enhanced survival of the LINCL mouse following CLN2 gene transfer using the rh.10 rhesus macaque-derived adeno-associated virus vector. *Molecular therapy : the journal of the American Society of Gene Therapy* **15**, 481 (Mar, 2007).
106. M. A. Cabrera-Salazar *et al.*, Timing of therapeutic intervention determines functional and survival outcomes in a mouse model of late infantile batten disease. *Mol Ther* **15**, 1782 (Oct, 2007).
107. C. H. Vite *et al.*, Effective gene therapy for an inherited CNS disease in a large animal model. *Annals of Neurology* **57**, 355 (2005/03//, 2005).
108. L. E. Mays, J. M. Wilson, The complex and evolving story of T cell activation to AAV vector-encoded transgene products. *Mol Ther* **19**, 16 (Jan, 2011).
109. R. L. Klein *et al.*, Efficient neuronal gene transfer with AAV8 leads to neurotoxic levels of tau or green fluorescent proteins. *Mol Ther* **13**, 517 (Mar, 2006).
110. B. Georgievska, D. Kirik, A. Bjorklund, Aberrant sprouting and downregulation of tyrosine hydroxylase in lesioned nigrostriatal dopamine neurons induced by long-lasting overexpression of glial cell line derived neurotrophic factor in the striatum by lentiviral gene transfer. *Exp Neurol* **177**, 461 (Oct, 2002).
111. B. E. Shapiro, E. L. Logigian, E. H. Kolodny, G. M. Pastores, Late-onset Tay-Sachs disease: the spectrum of peripheral neuropathy in 30 affected patients. *Muscle Nerve* **38**, 1012 (Aug, 2008).

112. L. L. Muldoon, E. A. Neuwelt, M. A. Pagel, D. L. Weiss, Characterization of the molecular defect in a feline model for type II GM2-gangliosidosis (Sandhoff disease). *American Journal of Pathology* **144**, 1109 (May, 1994).
113. D. M. Hoover, J. Lubkowski, DNAWorks: an automated method for designing oligonucleotides for PCR-based gene synthesis. *Nucleic Acids Res* **30**, e43 (May, 2002).
114. F. Jacobs *et al.*, Direct comparison of hepatocyte-specific expression cassettes following adenoviral and nonviral hydrodynamic gene transfer. *Gene Ther* **15**, 594 (Apr, 2008).
115. M. L. Broekman *et al.*, Complete correction of enzymatic deficiency and neurochemistry in the GM1-gangliosidosis mouse brain by neonatal adeno-associated virus-mediated gene delivery. *Mol Ther* **15**, 30 (Jan, 2007).
116. R. Matalon *et al.*, Adeno-associated virus-mediated aspartoacylase gene transfer to the brain of knockout mouse for canavan disease. *Molecular therapy : the journal of the American Society of Gene Therapy* **7**, 580 (May, 2003).
117. M. L. Broekman, L. A. Comer, B. T. Hyman, M. Sena-Esteves, Adeno-associated virus vectors serotyped with AAV8 capsid are more efficient than AAV-1 or -2 serotypes for widespread gene delivery to the neonatal mouse brain. *Neuroscience* **138**, 501 (2006).
118. R. C. Baek, J. L. Kasperzyk, F. M. Platt, T. N. Seyfried, N-butyldeoxygalactonojirimycin reduces brain ganglioside and GM2 content in neonatal Sandhoff disease mice. *Neurochemistry international* **52**, 1125 (May, 2008).
119. T. N. Seyfried, R. K. Yu, N. Miyazawa, Differential cellular enrichment of gangliosides in the mouse cerebellum: analysis using neurological mutants. *J Neurochem* **38**, 551 (Feb, 1982).
120. J. L. Kasperzyk *et al.*, N-butyldeoxygalactonojirimycin reduces neonatal brain ganglioside content in a mouse model of GM1 gangliosidosis. *J Neurochem* **89**, 645 (May, 2004).
121. L. J. Macala, R. K. Yu, S. Ando, Analysis of brain lipids by high performance thin-layer chromatography and densitometry. *J Lipid Res* **24**, 1243 (Sep, 1983).
122. T. N. Seyfried, G. H. Glaser, R. K. Yu, Cerebral, cerebellar, and brain stem gangliosides in mice susceptible to audiogenic seizures. *J Neurochem* **31**, 21 (Jul, 1978).
123. J. Folch, M. Lees, G. H. Sloane Stanley, A simple method for the isolation and purification of total lipides from animal tissues. *The Journal of biological chemistry* **226**, 497 (May, 1957).

124. J. L. Kasperzyk, A. d'Azzo, F. M. Platt, J. Alroy, T. N. Seyfried, Substrate reduction reduces gangliosides in postnatal cerebrum-brainstem and cerebellum in GM1 gangliosidosis mice. *J Lipid Res* **46**, 744 (Apr, 2005).
125. S. Ando, N. C. Chang, R. K. Yu, High-performance thin-layer chromatography and densitometric determination of brain ganglioside compositions of several species. *Anal Biochem* **89**, 437 (Sep, 1978).
126. D. R. Martin *et al.*, Molecular consequences of the pathogenic mutation in feline GM1 gangliosidosis. *Mol Genet Metab* **94**, 212 (Jun, 2008).
127. H. D. Lacorazza, M. Jendoubi, In situ assessment of beta-hexosaminidase activity. *Biotechniques* **19**, 434 (Sep, 1995).
128. J. Q. Huang *et al.*, Apoptotic cell death in mouse models of GM2 gangliosidosis and observations on human Tay-Sachs and Sandhoff diseases. *Human molecular genetics* **6**, 1879 (Oct, 1997).
129. R. Myerowitz *et al.*, Molecular pathophysiology in Tay-Sachs and Sandhoff diseases as revealed by gene expression profiling. *Human molecular genetics* **11**, 1343 (May, 2002).
130. Y. P. Wu, R. L. Proia, Deletion of macrophage-inflammatory protein 1 alpha retards neurodegeneration in Sandhoff disease mice. *Proceedings of the National Academy of Sciences of the United States of America* **101**, 8425 (Jun, 2004).
131. D. Tsuji *et al.*, Specific induction of macrophage inflammatory protein 1-alpha in glial cells of Sandhoff disease model mice associated with accumulation of N-acetylhexosaminyl glycoconjugates. *Journal of neurochemistry* **92**, 1497 (Mar, 2005).
132. S. Kyrkanides *et al.*, Peripheral blood mononuclear cell infiltration and neuroinflammation in the HexB^{-/-} mouse model of neurodegeneration. *Journal of neuroimmunology* **203**, 50 (Oct, 2008).
133. A. M. Bradbury *et al.*, Therapeutic response in feline sandhoff disease despite immunity to intracranial gene therapy. *Molecular therapy : the journal of the American Society of Gene Therapy* **21**, 1306 (Jul, 2013).
134. E. Kawashita *et al.*, Abnormal production of macrophage inflammatory protein-1alpha by microglial cell lines derived from neonatal brains of Sandhoff disease model mice. *Journal of neurochemistry* **109**, 1215 (Jun, 2009).
135. S. Kyrkanides *et al.*, Conditional expression of human beta-hexosaminidase in the neurons of Sandhoff disease rescues mice from neurodegeneration but not neuroinflammation. *Journal of neuroinflammation* **9**, 186 (2012).

136. J. H. Wolfe *et al.*, Reversal of pathology in murine mucopolysaccharidosis type VII by somatic cell gene transfer. *Nature* **360**, 749 (Dec, 1992).
137. M. Cucchiaroni, X. L. Ren, G. Perides, E. F. Terwilliger, Selective gene expression in brain microglia mediated via adeno-associated virus type 2 and type 5 vectors. *Gene therapy* **10**, 657 (Apr, 2003).
138. L. S. Pike *et al.*, Imaging gene delivery in a mouse model of congenital neuronal ceroid lipofuscinosis. *Gene therapy* **18**, 1173 (Dec, 2011).
139. L. Wang *et al.*, Systematic Evaluation of AAV Vectors for Liver directed Gene Transfer in Murine Models. *Molecular Therapy* **18**, 118 (2009).
140. T. Ohshima *et al.*, alpha-Galactosidase A deficient mice: a model of Fabry disease. *Proc Natl Acad Sci U S A* **94**, 2540 (Mar, 1997).
141. M. Casal, M. Haskins, Large animal models and gene therapy. *European journal of human genetics : EJHG* **14**, 266 (Mar, 2006).
142. M. M. Aye *et al.*, Histopathological and ultrastructural features of feline hereditary cerebellar cortical atrophy: a novel animal model of human spinocerebellar degeneration. *Acta neuropathologica* **96**, 379 (Oct, 1998).
143. M. Podell, P. A. March, W. R. Buck, L. E. Mathes, The feline model of neuroAIDS: understanding the progression towards AIDS dementia. *J Psychopharmacol* **14**, 205 (2000).
144. L. C. Cork, J. F. Munnell, M. D. Lorenz, The pathology of feline GM2 gangliosidosis. *The American journal of pathology* **90**, 723 (Mar, 1978).
145. H. J. Baker, Jr., J. R. Lindsey, G. M. McKhann, D. F. Farrell, Neuronal GM1 gangliosidosis in a Siamese cat with beta-galactosidase deficiency. *Science (New York, N.Y.)* **174**, 838 (Nov, 1971).
146. W. R. Hein, P. J. Griebel, A road less travelled: large animal models in immunological research. *Nature reviews. Immunology* **3**, 79 (Jan, 2003).
147. L. F. Costa, T. A. Paixao, R. M. Tsohis, A. J. Baumler, R. L. Santos, Salmonellosis in cattle: advantages of being an experimental model. *Research in veterinary science* **93**, 1 (Aug, 2012).
148. F. Meurens, A. Summerfield, H. Nauwynck, L. Saif, V. Gerdtts, The pig: a model for human infectious diseases. *Trends in microbiology* **20**, 50 (Jan, 2012).

149. C. H. Vite, M. A. Passini, M. E. Haskins, J. H. Wolfe, Adeno-associated virus vector-mediated transduction in the cat brain. *Gene therapy* **10**, 1874 (Oct, 2003).
150. V. J. H. I. G.-E. McCurdy, Ashley N. Randle, Allison M. Bradbury, Aime K. Johnson, Patricia M. Beadlescomb, Nancy Morrison, Misako Hwang, Miguel Sena-Esteves, Douglas R Martin, Dramatic Phenotypic Improvement after Adeno-Associated Virus Gene Therapy in a Feline Model of Sandhoff Disease. *Molecular Therapy* **21**, 15 (2013).
151. A. K. Johnson, V.J. McCurdy, A.M. Bradbury, H. Gray-Edwards, A.N. Randle, M. Huang, N.R. Cox, S.G. Leroy, M. Sena-Esteves, D.R. Martin, AAV Gene therapy Normalizes Disease Phenotype and Extends Lifespan >4 fold in Feline GM1 Gangliosidosis. *Molecular Therapy* **21**, 226 (2013).
152. A. M. Bradbury, V.J. McCurdy, A.K. Johnson, H. Gray-Edwards, B.L. Brunson, A.N. Randle, N.R. Cox, M. Sena-Esteves, D.R. Martin, Intracranial AAV Gene Therapy Extends the Life Span of GM2 Gangliosidosis Cats >4 Four-Fold with No Clinical Evidence of Vector Toxicity. *Molecular Therapy* **21**, 226 (2013).
153. T. Kodama *et al.*, Lyso-GM2 ganglioside: a possible biomarker of Tay-Sachs disease and Sandhoff disease. *PLoS One* **6**, e29074 (2011).
154. S. M. Aronson, A. Saifer, G. Perle, B. W. Volk, Cerebrospinal fluid enzymes in central nervous system lipidoses (with particular reference to amaurotic family idiocy). *Proc Soc Exp Biol Med* **97**, 331 (Feb, 1958).
155. S. M. Aronson, A. Saifer, A. Kanof, B. W. Volk, Progression of amaurotic family idiocy as reflected by serum and cerebrospinal fluid changes. *The American journal of medicine* **24**, 390 (Mar, 1958).
156. H. Satoh *et al.*, Cerebrospinal fluid biomarkers showing neurodegeneration in dogs with GM1 gangliosidosis: possible use for assessment of a therapeutic regimen. *Brain Res* **1133**, 200 (Feb 16, 2007).
157. R. H. Lachmann *et al.*, Treatment with miglustat reverses the lipid-trafficking defect in Niemann-Pick disease type C. *Neurobiology of disease* **16**, 654 (Aug, 2004).
158. D. Te Vruchte *et al.*, Relative acidic compartment volume as a lysosomal storage disorder-associated biomarker. *The Journal of clinical investigation*, (Feb 3, 2014).
159. E. Raniierri, R. L. Gerace, E. M. Ravenscroft, J. J. Hopwood, P. J. Meikle, Pilot neonatal screening program for lysosomal storage disorders, using lamp-1. *Southeast Asian J Trop Med Public Health* **30 Suppl 2**, 111 (1999).
160. N. Parakh, H. L. Gupta, A. Jain, Evaluation of enzymes in serum and cerebrospinal fluid in cases of stroke. *Neurology India* **50**, 518 (Dec, 2002).

161. E. Osuna, M. D. Perez-Carceles, A. Luna, D. J. Pounder, Efficacy of cerebro-spinal fluid biochemistry in the diagnosis of brain insult. *Forensic science international* **52**, 193 (Jan, 1992).
162. K. O'Neill, S. Chen, R. Diaz Brinton, Impact of the selective estrogen receptor modulator, tamoxifen, on neuronal outgrowth and survival following toxic insults associated with aging and Alzheimer's disease. *Exp Neurol* **188**, 268 (Aug, 2004).
163. A. Quaglia *et al.*, Total Lactate dehydrogenase in Cerebrospinal fluid for identification of bacterial meningitis. *Journal of medical microbiology*, (Aug, 2013).
164. H. Schmidt *et al.*, CSF lactate dehydrogenase activity in patients with Creutzfeldt-Jakob disease exceeds that in other dementias. *Dementia and geriatric cognitive disorders* **17**, 204 (2004).
165. D. Rao, V. S. Ghalaut, P. S. Ghalaut, S. Rao, Case series: CSF LDH, proteins and electrolyte levels in patients of acute lymphocytic leukemia. *Clinica chimica acta; international journal of clinical chemistry* **413**, 1045 (Jul, 2012).
166. J. A. Vazquez, C. Adducci Mdel, D. Godoy Monzon, K. V. Iserson, Lactic dehydrogenase in cerebrospinal fluid may differentiate between structural and non-structural central nervous system lesions in patients with diminished levels of consciousness. *The Journal of emergency medicine* **37**, 93 (Jul, 2009).
167. M. Nussinovitch, D. Harel, T. Eidlitz-Markus, J. Amir, B. Volovitz, Lactic dehydrogenase isoenzyme in cerebrospinal fluid of children with infantile spasms. *European neurology* **49**, 231 (2003).
168. D. V. Kamat, B. P. Chakravorty, Comparative values of CSF-LDH isoenzymes in neurological disorders. *Indian journal of medical sciences* **53**, 1 (Jan, 1999).
169. E. Lloyd-Evans, F. M. Platt, Lysosomal Ca(2+) homeostasis: role in pathogenesis of lysosomal storage diseases. *Cell calcium* **50**, 200 (Aug, 2011).
170. M. L. Koenig, R. S. Jope, H. J. Baker, K. M. Lally, Reduced Ca²⁺ flux in synaptosomes from cats with GM1 gangliosidosis. *Brain research* **424**, 169 (Oct, 1987).
171. D. Pelled *et al.*, Inhibition of calcium uptake via the sarco/endoplasmic reticulum Ca²⁺-ATPase in a mouse model of Sandhoff disease and prevention by treatment with N-butyldeoxynojirimycin. *The Journal of biological chemistry* **278**, 29496 (Aug, 2003).
172. R. M. Norman, H. Urich, A. H. Tingey, R. A. Goodbody, Tay-Sachs' disease with visceral involvement and its relationship to Niemann-Pick's disease. *The Journal of pathology and bacteriology* **78**, 409 (Oct, 1959).

173. A. Taberero *et al.*, Albumin promotes neuronal survival by increasing the synthesis and release of glutamate. *Journal of neurochemistry* **81**, 881 (May, 2002).
174. M. Algamal, J. Milojevic, N. Jafari, W. Zhang, G. Melacini, Mapping the Interactions between the Alzheimer's Abeta-Peptide and Human Serum Albumin beyond Domain Resolution. *Biophysical journal* **105**, 1700 (Oct, 2013).
175. L. Belayev, R. Busto, W. Zhao, J. A. Clemens, M. D. Ginsberg, Effect of delayed albumin hemodilution on infarction volume and brain edema after transient middle cerebral artery occlusion in rats. *Journal of neurosurgery* **87**, 595 (Oct, 1997).
176. L. Belayev *et al.*, Diffusion-weighted magnetic resonance imaging confirms marked neuroprotective efficacy of albumin therapy in focal cerebral ischemia. *Stroke; a journal of cerebral circulation* **29**, 2587 (Dec, 1998).
177. P. W. Huh *et al.*, The effect of high-dose albumin therapy on local cerebral perfusion after transient focal cerebral ischemia in rats. *Brain research* **804**, 105 (Aug 31, 1998).
178. C. P. Cavender, S. D. Turley, J. M. Dietschy, Sterol metabolism in fetal, newborn, and suckled lambs and their response to cholesterol after weaning. *The American journal of physiology* **269**, E331 (Aug, 1995).
179. G. Quan, C. Xie, J. M. Dietschy, S. D. Turley, Ontogenesis and regulation of cholesterol metabolism in the central nervous system of the mouse. *Brain Res Dev Brain Res* **146**, 87 (Dec, 2003).
180. P. Kaplan, H. C. Andersson, K. A. Kacena, J. D. Yee, The clinical and demographic characteristics of nonneuronopathic Gaucher disease in 887 children at diagnosis. *Archives of pediatrics & adolescent medicine* **160**, 603 (Jun, 2006).
181. P. Kaplan *et al.*, Revised recommendations for the management of Gaucher disease in children. *Eur J Pediatr* **172**, 447 (Apr, 2013).
182. S. M. Chung *et al.*, Lysophosphatidic acid induces thrombogenic activity through phosphatidylserine exposure and procoagulant microvesicle generation in human erythrocytes. *Arteriosclerosis, thrombosis, and vascular biology* **27**, 414 (Feb, 2007).
183. J. A. Balint, H. L. Spitzer, E. C. Kyriakides, Studies of Red-Cell Stromal Lipids in Tay-Sachs Disease and Other Lipidoses. *The Journal of clinical investigation* **42**, 1661 (Nov, 1963).
184. D. A. Booth, Erythrocyte lipids in Tay-Sachs disease. *Lancet* **1**, 626 (Mar 18, 1967).

185. J. A. Balint, E. C. Kyriakides, Studies of red cell stromal proteins in Tay-Sachs disease. *The Journal of clinical investigation* **47**, 1858 (Aug, 1968).
186. M. Pourfar, S. Levy, Effect of Triton X-100 on electrophoretic mobility of red blood cell ghosts from normal individuals and patients with Tay-Sachs disease. *Clinical chemistry* **17**, 332 (Apr, 1971).
187. L. Massaccesi, A. Lombardo, B. Venerando, G. Tettamanti, G. Goi, Isoenzyme pattern and partial characterization of hexosaminidases in the membrane and cytosol of human erythrocytes. *Clinical biochemistry* **40**, 467 (Apr, 2007).
188. J. van der Zee, T. M. Dubbelman, J. van Steveninck, Peroxide-induced membrane damage in human erythrocytes. *Biochim Biophys Acta* **818**, 38 (Aug, 1985).
189. A. Lopez-Revuelta, J. I. Sanchez-Gallego, A. Hernandez-Hernandez, J. Sanchez-Yague, M. Llanillo, Increase in vulnerability to oxidative damage in cholesterol-modified erythrocytes exposed to t-BuOOH. *Biochim Biophys Acta* **1734**, 74 (May, 2005).
190. E. Colombo, B. Borgiani, C. Verderio, R. Furlan, Microvesicles: novel biomarkers for neurological disorders. *Frontiers in physiology* **3**, 63 (2012).
191. R. J. Nilsson *et al.*, Blood platelets contain tumor-derived RNA biomarkers. *Blood* **118**, 3680 (Sep, 2011).
192. M. K. Pandey *et al.*, Gaucher disease: Chemotactic factors and immunological cell invasion in a mouse model. *Molecular genetics and metabolism*, (Sep, 2013).
193. V. Haurigot *et al.*, Whole body correction of mucopolysaccharidosis IIIA by intracerebrospinal fluid gene therapy. *The Journal of clinical investigation*, (Jul, 2013).
194. M. Fukumizu, H. Yoshikawa, S. Takashima, N. Sakuragawa, T. Kurokawa, Tay-Sachs disease: progression of changes on neuroimaging in four cases. *Neuroradiology* **34**, 483 (1992).
195. S. Mugikura *et al.*, MR findings in Tay-Sachs disease. *J Comput Assist Tomogr* **20**, 551 (Jul-Aug, 1996).
196. R. A. Kroll *et al.*, White matter changes associated with feline GM2 gangliosidosis (Sandhoff disease): correlation of MR findings with pathologic and ultrastructural abnormalities. *AJNR Am J Neuroradiol* **16**, 1219 (Jun-Jul, 1995).
197. G. H. Maegawa *et al.*, The natural history of juvenile or subacute GM2 gangliosidosis: 21 new cases and literature review of 134 previously reported. *Pediatrics* **118**, e1550 (Nov, 2006).

198. D. L. Jewett, Volume-conducted potentials in response to auditory stimuli as detected by averaging in the cat. *Electroencephalography and clinical neurophysiology* **28**, 609 (Jun, 1970).
199. J. S. Buchwald, C. Huang, Far-field acoustic response: origins in the cat. *Science* **189**, 382 (Aug, 1975).
200. G. Pampiglione, A. Harden, Neurophysiological investigations in GM1 and GM2 gangliosidoses. *Neuropediatrics* **15 Suppl**, 74 (Sep, 1984).
201. T. M. Cox, in *Fabry Disease: Perspectives from 5 Years of FOS*, A. Mehta, M. Beck, G. Sunder-Plassmann, Eds. (Oxford, 2006).
202. J. R. Cook, Jr., D. B. DeNicola, Cerebrospinal fluid. *The Veterinary clinics of North America. Small animal practice* **18**, 475 (May, 1988).
203. J. E. Steiss, H. J. Baker, K. G. Braund, N. R. Cox, J. C. Wright, Profile of electrodiagnostic abnormalities in cats with GM1 gangliosidosis. *American journal of veterinary research* **58**, 706 (Jul, 1997).
204. M. H. Sims, Electrodiagnostic evaluation of auditory function. *The Veterinary clinics of North America. Small animal practice* **18**, 913 (Jul, 1988).
205. T. Friedmann, R. Roblin, Gene therapy for human genetic disease? *Science (New York, N.Y.)* **175**, 949 (Mar, 1972).
206. R. M. Blaese *et al.*, T lymphocyte-directed gene therapy for ADA- SCID: initial trial results after 4 years. *Science (New York, N.Y.)* **270**, 475 (Oct, 1995).
207. D. Teichler Zallen, US gene therapy in crisis. *Trends in genetics : TIG* **16**, 272 (Jun, 2000).
208. S. Hacein-Bey-Abina *et al.*, A serious adverse event after successful gene therapy for X-linked severe combined immunodeficiency. *The New England journal of medicine* **348**, 255 (Jan, 2003).
209. S. L. Ginn, I. E. Alexander, M. L. Edelstein, M. R. Abedi, J. Wixon, Gene therapy clinical trials worldwide to 2012 - an update. *The journal of gene medicine* **15**, 65 (Feb, 2013).